SIMULATION OF SEISMICITY PATTERN AND RECURRENCE BEHAVIOR ON A HETEROGENEOUS FAULT USING LABORATORY FRICTION LAWS

BY

TIANQING CAO

B.S., CHINESE UNIVERSITY OF SCIENCE AND TECHNOLOGY AT PEKING
NUCLEAR PHYSICS (1965)

SUBMITTED TO THE DEPARTMENT OF
EARTH, ATMOSPHERIC, AND PLANETARY SCIENCES
IN PARTIAL FULFILLMENT OF THE REQUIREMENTS
FOR THE DEGREE OF

DOCTOR OF PHILOSOPHY

IN

GEOPHYSICS

AT THE
MASSACHUSETTS INSTITUTE OF TECHNOLOGY
MARCH, 1986

Signature of Author: _____
Department of Earth, Atmospheric, and Planetary Sciences

Certified by: _____
Keiiti Aki
Thesis Advisor

Accepted by: _____
William F. Brace

Chairman, Department of Earth, Atmospheric, and Planetary Sciences

WITHDRAWN FROM MIT LIBRARIES

MASS. INST. TECH. JUN 17 1986 LIBRARIES

Lindgren

Simulation of Seismicity Pattern and Recurrence Behavior on a Heterogeneous Fault Using Laboratory Friction Laws

by

Tianqing Cao

Submitted to the

Department of Earth, Atmospheric, and Planetary Sciences

in March, 1986, in Partial Fulfillment of the Requirements for

the Degree of Doctor of Philosophy

Abstract

This thesis aims at using laboratory friction laws to explain observed seismicity patterns and earthquake recurrence behavior of heterogeneous faults. We adopted Burridge and Knopoff's one-dimensional mass-spring model configuration and solved its motion dynamically using different constitutive relations for the frictional slip of a fault. We found that some of the important features about seismicity patterns and recurrence processes can be explained by the constitutive relations applied to a heterogeneous fault.

The first major feature of seismicity we studied is the occurrence of precursory quiescence before large earthquakes. We compared the seismicity simulations using a simple friction law characterized by static friction and dynamic friction and a displacement hardening-softening friction law proposed by Stuart respectively, and demonstrated that a seismicity pattern which consists of recurrent major earthquakes, enough small events consistant with the observed magnitude-frequency relation, and seismic quiescence before major events can be reproduced if we use the displacement hardening-softening friction law. It was necessary to choose its critical softening displacement of the same order of magnitude as estimated from observed strong motion spectra by Papageorgiou and Aki using a specific barrier model. If the adopted critical displacement is much larger than the above value, we get a recurrent sequence of aseismic slip followed by major earthquake

without small earthquakes; if it is much smaller than the above value, we get a seismicity pattern, which consists of recurrent major events and many small events but no seismic quiescence as in the case of the simple friction law.

Our explanation for the cause of seismic quiescence is the stress smoothing due to preseismic slip which is predicted by the displacement hardening-softening friction law. This explanation is different from Kanamori's in which a bimodal distribution of fault strength is assumed in an ad-hoc manner. Our model results point to a promising approach for the simultaneous interpretation of recurrence phenomenon and rupture process on a heterogeneous fault.

The second major feature of seismicity we studied is the observed stationary magnitude-frequency relation. In order to explain this relation, a stress deficit roughening process is needed to counter the smoothing process due to the interactions between fault segments. Here, the stress deficit is defined as the fault strength minus the stress. This is the amount of stress needed to be increased in order to initiate a rupture. The smoothing process, by which the number of small events decreases with time and is in contradiction with the stationarity of the observed magnitude-frequency relation, was encountered in many numerical experiments and also showed in our simulations with the simple friction law and the displacement hardening-softening friction law. By introducing a laboratory inferred friction law called the rate and state dependent friction law to the one-dimensional mass-spring model, we found that this model predicts non-uniform slip and stress drop on a heterogeneous fault and each major rupture becomes a stress deficit roughening process instead of a smoothing process.

The simulations with the rate and state dependent friction law also indicate that the existence of strong patches with higher effective stresses on a fault is needed for the occurrence of large earthquakes. The creeping section of a fault such as the one along the San Andreas fault, on the other hand, can be simulated by the rate and state dependent friction law with certain model parameters which, however, must not include strong patches. In this case, small earthquakes and aseismic slip relieve the accumulating strain without any major events.

The third feature of seismicity we studied is the effect of slip rate on stress drop. Kanamori and Allen's observational results showed that a earthquakes with longer recurrence times have higher average stress drops. In order to explain this result in terms of the healing effect, which is included in the rate and state dependent friction law, we first calculated the stress drop and recurrence time as functions of loading rate for a homogeneous fault model. We found that in general the stress drop increases with the decreasing loading rate in agreement with the observation. But the observed great variability of stress drop from a few to a

few hundred bars cannot be attributed to the healing effect alone at least for the simple strike-slip. Our simulation showed that the variability may be due primarily to the different distribution of fault strength.

Our simulation also suggests that among two empirical laws, which were inferred from the same laboratory friction data and called the power law and the logarithmic law by Shimamoto and Logan, the former can explain the observed stress drop vs. slip rate relation better than the latter which is an earlier and simpler version of the rate and state dependent friction law.

From our simulations, we can conclude that many observed features of seismicity pattern and recurrence behavior can be attributed to the constitutive relations of fault slip and the fault heterogeneity.

Thesis Supervisor: K. Aki
Title: Professor of Geophysics

Acknowledgements

After being sent to Inner Mongolia for ten years without doing anything scientific, I was lucky that I got the opportunity to study at MIT and work with Professor Keiiti Aki. I would like to express my deepest gratitude to him for accepting me as a student and supervising me for the past five years. During these years Kei not only taught me advanced seismology, but also showed me many basic skills for doing scientific research. His broad interest and inexhaustable enthusiasm in seeking truth of nature influenced me a lot. He is also such a renaissance man, well read in world history, nature, sports, cooking, etc. He made me believe that a good scientist does not have to be a nerd as MIT people usually are described. I do appreciate his criticism and patience in supervising me. I owe him a great deal for his time and effort in improving my English and scientific logic. To be Kei's student is not time limited, his influence will last for my entire life.

Among the other faculty members, I extend special thanks to Ted Madden and Nafi Toksoz. When I was leaving MIT to be a non-resident student at USC, Ted kindly accepted my request to be my academic advisor. His quick comments (always with physical insight) and questions on seminars always amazed me. Part of my thesis done after my qualifying examination is due to his questioning. Nafi gave many Chinese visitors and students, I am among them, help, encouragement, and advice. I also would like to thank him for being interested in my work.

I am grateful to Professor Francis Wu and his wife Miriam Wu. My good fortune to study with Kei started from their suggestion and recommendation. I also would like to thank professors Gu and Cheng at Geophysical Institute, Peking, China for their recommendations.

Kei brought many seismologists all over the world to us, I benefitted a great deal from discussions with them. We spent happy times together during holidays that I will often recall. Among them I would like to express my special thanks to Dr. Haruo Sato, Dr. Moo-Young Song, Dr. Francisco Sanchez-Sesma, and Dr. Kojiro Irikura. Among those seismologists whom Kei introduced me to, I want to thank Professors T. Mikumo, J. Rice, R. Dmowska, V. Li, N. Biswas, H. Kanamori, K. Mogi, T. Teng, T. Henyey, S. Das, B. Evans, and B. Tucker for their helpful suggestions and discussions.

Dr. Steve Ellis, Dr. Teng-Fong Wong, Dr. Ru-Shan Wu, Dr. Paul Huang, and my officemate Rafael Benites helped me tremendously in science and daily life, special thanks should be given to them. Rina Rubenstien and Yehuda Ben-Zion are also among them, they helped me and my family during some difficult times.

I was lucky that many Chinese visiting scientists (many were my friends even before I came to MIT) offered me a lot of help. Ye Huong, Qian Jia-Dong, Gu Ji-Cheng, Wang Qi-Ming, Wang Bi-Quan, and Jin An-Shu are among those I would like to thank.

My fellow students, many of them are excellent examples for me to learn from, offered all the help I asked for. Among them I want to express my gratitude to Scott Phillips, Pei-Zhen Zhang, Tien-When

Lo, John Nabelek, Peter Roberts, Kaye Shedlock, Helene Lyon-Caen, Roger Buck, Jack Jemsek, Joao Rosa, Kiyoshi Yomogida at MIT , Simon Tse at Harvard University, and Syhhong Chang, Jenn-yin Peng, Hung-Chie Chiu, Valerie Ferrazzini, and John Faulkner at USC.

Debby Roecker took care of all the paper work needed for me to be a visitor and a graduate student at MIT. Sharon Feldstein, Donna Martel, Jan Nattier-Barbaro helped me in different respects. I would like to extend special thanks to them.

Half of my thesis was written after I moved to USC as a MIT non-resident student. During this time period, John McRaney offered me tremendous help especially for my research work. I will never be able to thank him enough.

I also want to take this opportunity to extend special thanks to my colleagues at the seismological Bureau of Liaoming Province and at the Education Division of State Seismological Bureau, China. Their help made my voyage to U.S. possible. Mr. Guang-Yu Gao and other teachers at the No. 1 high school, my alma mater at my hometown Wu Xi, China, are unforgetable. I would like to express my gratitude to them and report my progress to them.

Dorothy Frank at MIT and Susan Turnbow at USC typed most of my papers and thesis. I would like to thank them for their kindness and patience.

Finally, I would like to thank my mother, my wife, my son and daughter for many sacrifices they have made for me. I cannot find words to adequately convey my thanks.

I am grateful to the U.S. Geological Survey for supporting this research under contract numbers 14-08-0001-21280, 14-08-0001-G-885 and G-990.

January, 1986

(When Halley's Comet is visiting us.)

Table of Contents

		Page
Title Page		1
Abstract		2
Acknowledgements		5
Table of Contents		9
Chapter 1.	Introduction	11
	References	23
Chapter 2.	Seismicity Simulation with a Displacement Hardening-Softening Friction Law	26
	2.1 Precursory Quiescence of Seismicity	26
	2.2 Numerical Modeling With Friction Laws	34
	2.3 Friction and Fault Model	35
	2.4 Model Parameters and Results	41
	2.5 Critical Slip-Weakening Displacement	47
	2.6 Discussion and Conclusions	49
	Figure Captions	52
	References	54
	Figures	60
Chapter 3.	Seismicity Simulation with a Rate and State Dependent friction Law	65
	3.1 Introduction	65
	3.2 Model Parameters Affecting the Spatial Smoothing of Stress Deficit	67

Page

3.3 Rate and State Dependent Friction Law 72

3.4 Comparison of Dynamic Motions of a Single Block-Spring System 80

3.5 Dynamic Solution of a Multiple Block-Spring System 88

3.6 Discussion and Conclusions 100

References 104

Figure Captions 109

Figures 114

Chapter 4. Effect of Slip Rate on Stress Drop 130

4.1 Introduction 130

4.2 Fault Model and Friction Law 131

4.3 Homogeneous Fault Model 135

4.4 Heterogeneous Fault Model 139

4.5 Discussion and Conclusions 142

Figure Captions 144

References 147

Table 149

Figures 150

Chapter 5. Summary and Proposed Future Research Directions 159

References 166

Appendix: Assigning Probability Gain for Precursors of Four Large Chinese Earthquakes 168

Chapter 1

Introduction

In this introduction, I shall try to explain: (1) why we have chosen numerical simulations with a one-dimensional mass-spring model characterized by different friction laws to study the observed precursory quiescence of seismicity before major earthquakes and other seismic phenomena; (2) what approach we have taken in our study; (3) how can we be sure that our formulation and calculation are correct; (4) the contents of the following chapters.

The starting point of this thesis was the question if we can explain the precursory quiescence of seismicity, often observed before major earthquakes, using the new laboratory-developed constitutive relations for frictional slip. Since seismic source and its response are indirectly studied by laboratory experiments and field observations respectively (Brace and Byerlee, 1966), one approach to the understanding of earthquake process is to relate the experimental results to the field observations by numerical modeling or computer simulation. There are some features which make the computer simulation an important and unreplaceable method in seismic studies. First, the great span of seismic events in time and space prohibits most of the simulations being performed in laboratories. However, computer simulations can deal with problems in which the events may span many hundred years and kilometers and simulate them possibly in a few seconds to a few hours. Second, the numerical simulations give us all the details about fault motion and with

this it is very convenient to test our different hypotheses. Third, the problem we are dealing with involves friction and is nonlinear, thus the solution is in general very difficult to obtain unless we solve it numerically with a computer. Therefore, numerical simulation seems one of the most natural approaches for studying seismic phenomena including quiescence along a heterogeneous fault.

As indicated by Aki (1985), the modeling of seismicity should include three equally important elements (1) the tectonic loading (2) the friction law governing fault slip (3) the structural heterogeneity of earthquake source region. Ideally, a three-dimensional dynamic solution of a heterogenous fault should be obtained for a self-generating, propagating, and stopping fault problem in which only the initial and boundary conditions and the fault properties are given (Israel and Nur, 1979). This is a difficult mathematical problem. Usually, the fault geometry and boundary and inital conditions are simplified or idealized in order to make the problem more tractable. We shall follow Burridge and Knopoff's (1967) one-dimensional model, which has been adopted by many authors under different circumstances (King and Knopoff, 1968; Otsuka, 1972; Dieterich, 1972; King, 1975; Yamashita, 1976; Cohen, 1977,b; Rundle and Jackson, 1977; Cohen, 1978; Israel and Nur, 1979, among others). This one-dimensional model (see Chapters 2 and 3 for details) is composed of blocks which slide on a frictional surface and therefore is a mechanical analog of an earthquake fault. The blocks are connected to each other by coil springs and to a moving slab by leaf springs. Here the moving slab represents the tectonic loading; the distributions of frictional strength and stress between

block and frictional surface represent the heterogeneities of seismic source region; and the constitutive relation between fault slip and frictional stress governs the fault motion.

With this simple model configuration many observed seismic phenomena, such as the stationary magnitude-frequency relation of seismicity, the occurrence of foreshocks and aftershocks, the occurrence of pre and postseismic slip, and the occurrence of fault stable sliding and long-term aseismic creep, have been related to certain physical characteristics of the source. The magnitude-frequency relation is due to the heterogeneity of a fault (Burride and Knopoff, 1967; Israel and Nur, 1978); the occurrence of foreshocks and aftershocks is due to the viscoelasticity of rocks (Burridge and Knopoff, 1967; Cohen, 1978) or the stress-induced crack nucleation (Rundle and Jackson, 1977) or the viscoelasticity and the time dependent friction law (Dietrich, 1972); the stable sliding and aseismic creep are due to the viscoelasticity (Cohen, 1978) or a rate and state dependent friction law (Dietrich, 1979 a,b).

Here, the possible mechanism for each phenomenon may relate to all three imporant elements in seismicity modeling. Among these elements the fault heterogeneity has been most intensively studied to explain many seismic phenomena; the effects from constitutive relations (friction laws), which govern the fault slip, could not be properly determined until a quantitative description of the relation was recently established; the tectonic loadiong, which may be simply represented by a constant rate as usually assumed, is closely

related to the constitutive relation and only can be evaluated with such a relation as we will show in Chapter 4. Therefore, we decided to concentrate ourselves in the studies of comparing different friction laws and their applications.

A constitutive relation should tell the frictional strength of an existing fault and its variation with slip deformation and the stability of motion. The fault strength is well defined by Coulomb's law and Byerlee's (1978) law. Coulonmb's law states that the shear stress required to cause slip is proportional to the normal stress and Byerlee's law gives the following relations:

$$\tau = 0.85\sigma_n \qquad \sigma_n < 2Kb$$

$$\tau = 0.5 + 0.6\sigma_n \qquad \sigma_n > 2Kb$$

where τ is frictional resistance and σ_n is normal stress. It is very interesting to note that Byerlee's law means that the initial surface roughness and rock types having little or no effect on friction (Byerlee, 1978). For the variation of friction with slip motion, a simple friction law which includes dynamic and static friction is commonly used. The quantitative relation between static and dynamic friction is also given by Byerlee (1970), who finds that their ratio is about 1.2-1.3 from laboratory stick-slip experiments. In this simple friction law the details of friction variations during the transition of motion from static to dynamic or dynamic to static are ignored. One obvious deficiency of this simple friction law is that slip initiation is always unstable because dynamic friction is always smaller than static friction and this is in

contradiction with field and laboratory observations which showed that in certain cases the slip is stable (creep).

In order to obtain a quantitative constitutive relation, numerous laboratory experiments were performed, especially after Brace and Byerlee (1966) proposed stick-slip as a mechanism for earthquakes. Among those experimental results, as indicated by Dieterich (1978), there were three puzzling characteristics of rock friction phenomenology: (1) dependence of the transition between stick-slip and stable sliding on normal stress; (2) dependence of stick-slip on stiffness of the test system; (3) surface roughness effects. These problems were resolved by introducing rate dependence of dynamic friction and time dependence of static friction and a critical displacement which is needed for the friction to change from one stable value to another when the slip rate changes (Dieterich, 1978b). In Dieterich's constitutive relation, the time dependence of friction is represented by a variable θ called the average contact time which is equal to the critical displacement divided by the slip velocity and the friction depends on slip rate and the average contact time. Later, Ruina (1980, 1983) found that θ is not equal to time for stationary contact and generalized it as an internal variable which is defined abstractly without regard to a particular experiment or microscopic interpretation as Dieterich did (Ruina, 1984).

The constitutive relation developed by Dieterich and Ruina can describe many kinds of fault behavior including preseismic slip,

critical displacement, stable sliding, and healing process. This seems to be the most up-to-date version as compared with the slip weakening friction law (Rice, 1980, Stuart, 1979) or the rate dependent friction law. Hence, we choose Ruina's constitutive relation as one of the physical basis for our study but also compare with other constitutive relations in order to find the real physical mechanisms for some seismic phenomena. We will see in Chapter 4 that Dieterich and Ruina's rate and state dependent friction law is still not perfect.

In modeling seismicity, we can use either dynamic or static solution. Since we are studying a complex aggregate of seismic events and not simple earthquakes, the simple static modeling which neglects inertial forces is not suitable. The static solution cannot include dynamic healing process and thus cannot be used to evaluate the final state of stress on a fault after an earthquake (Israel and Nur, 1979). In Chapter 3 we will see that healing process is most important in affecting non-uniform slip and stress drop, and may be related to the observed magnitude-frequency relation.

In this thesis, we follow the general approach of science, namely, starting with an initial guess, we later support or correct it after testing its consequences against the observation. We made a few guesses in this thesis for the physical mechanisms of some seismic phenomena. For example, one guess is about the mechanism of seismic quiescence that is different from Kanamori's (1981). Kanamori assumed a bi-modal Weibull distribution of the

fault strength and qualitatively explained how the quiescence occurs. Later, this distribution was adopted in Mikumo and Miyatake's numerical simulations (1978, 1979, 1983). However, quiescence is such a commonly observed phenomenon at many differenct fault regions (Kanamori, 1981), a special strength distribution looked too arbitrary to us. We guessed that some more basic features included in some friction laws may be responsible for the quiescence. Therefore, we decided to simulate seismicities with differenct friction laws to see if some features in these friction laws are responsible for the precursory quiescence of seismicity.

In looking for physical explanations for the observed phenomena by numerical modeling, we tried to use parameters and boundary conditions appropriate to the real field, and varied few parameters or boundary conditions at a time to isolate their effect. For example, in Chapter 3, we studied the effect of spring constant ratio between coil and leaf springs on the simulated seismicity. By changing the spring constant ratio and fixing the initial and boundary conditions, the fault heterogeneity and the friction law (in this case, the simple friction law specified by dynamic and static frictions), we found that the simulated seismicity changes significantly when the ratio changes from 1 to 5. One outstanding difference is about the magnitude frequency relation of the simulated seismicity. When the ratio is 1, small earthquakes were simulated but no major event was simulated (also see Dieterich, 1972; Cohen, 1977 a,b); when the ratio is 5, we found a smoothing effect in the simulated seismicity and the number of small earthquakes gradually decreased with the recurrence of major

earthquakes.

The smoothing effect means that the spatial distribution of the difference between strength and stress along the fault becomes smoother after the occurrence of earthquakes. With this effect, the simulated small events become too few for explaining the observed magnitude-frequency relation. Dieterich (personal communication, 1985) considers only the case in which the coil spring constant is low and concludes that the simple friction law and heterogeneity of frictional strength can explain the observed magnitude frequency relation. We argue that for a more proper choice of the ratio, the simple friction law cannot explain the observation (Yamashita, 1976; Dieterich 1972; Cohen, 1977 a,b). We believe that a roughening process countering the smoothing process is needed in order to explain the observed stationary magnitude-frequency relation. This is our major subject discussed in Chapter 3.

Since this thesis involves a large amount of computer programming, it is important to make sure that there are no errors in the program. One way to check this is to calculate some special cases of our programming that have been done by other people. If we get the same results, we are probably right. In Chapter 2, we simulated seismicity with the simple friction law, and got the same results as Dieterich (1972) and Cohen (1977, a,b) for the same choice of parameters. The formulation and calculation for a single block-spring system controlled by the rate and state dependent friction law in Chapter 3 were done independently by Rice and Tse

(1985). Their results are exactly the same as ours. This consistency encouraged us to extend the solution to a multiple block-spring system which is necessary to simulate a heterogenous fault.

Let us now summarize the contents of the following chapters.

In Chapter 2, we first give a special review about seismicity quiescence because it is important for earthquake predition and it is an observational basis to start our study. Then we compare the simulated seismicities for two different friction laws, the simple friction law which is specified by static friction and dynamic friction and the slip weakening friction law. We found that the precursory phenonmenon "quiescence" before major earthquakes can be simulated if we use the displacement hardening-softening friction law and choose a critical displacement, which is the fault displacement between the initiations of hardening and instability, at the same order of magnitude as estimated from strong motion data. The simulated seismicity also looks satisfactory in terms of the observed magnitude-frequency relation at least for a limited time period. From our modeling, the quiescence is explained by the interaction between fault segments due to their preseismic slip when the average stress is high before major earthquakes. This explanation is supported by some observations of fault preseismic slip (Dieterich, 1978a) and does not need any ad-hoc assumption like the biomodal distribution of frictional strength on the fault introduced by Kanamori (1981). The consistency of critical displacements obtained from our numerical experiment and strong

motion data indicates that our approach may be also good for studying certain aspects of the rupture process as we will show in Chapter 3. Another important result of this Chapter is that the simulated seismicity suffers from a smoothing effect. The number of small events decreases with increasing time and fails to explain the observed magnitude-frequency relation.

In Chapter 3, we addressed the problem raised in Chapter 2. First, we confirmed that the smoothing effect is not due to errors in our calculation. Actually it appeared in many other simulations, such as Andrews (1975, 1978), Mikumo and Miyatake (1978, 1979), and Israel and Nur (1979). However, Dieterich (1972) and Cohen's (1976 b, 1979) simulations did not show the smoothing effect although they used the same model configuration, boundary conditions, fault strength distribution, and friction law as we used. We found this discrepancy is due to the difference of the spring constant ratio as we mentioned earlier. This spring constant ratio represents the ratio of two interactions: One is between fault segments and the other is between fault and driving mechanism. According to Yamashita's (1976) formula for the choice of parameters, Dieterich and Cohen used a ratio too small to simulate a real fault. Thus, we suspected that the smoothing effect may be inherent in the simple friction law used in the simulation. We then introduced the laboratory inferred so-called rate and state dependent friction law into the simulation. We found that the smoothing effect is removed because of the time dependent healing which is predicted by

this new friction law. We physically explained how a roughening process of the difference between fault strength and stress can be introduced to a major fault rupture process. The time dependent healing elongates the time duration for stopping fault rupture or the interaction time among fault segments during the stopping. Thus, the interaction among fault segments, which causes the smoothing process, is reduced and a major rupture of a heterogeneous fault becomes a roughening process. This explanation is consistent with Israel and Nur's (1979) work. They found that variations in the absorbed energy of fault rupture causes discontinuities in the healing process and is necessary for the heterogeneous nature of earthquake faulting.

In Chapter 4, we applied the simulation with the rate and state dependent friction law to a discussion of recurrence process of large earthquakes. The important parameters involved in recurrence process are the recurrence time, long term slip rate (tectonic loading rate), stress drop, and the relations among them. We directed our modeling effort to explain Kananmori and Allen's (1985) observational result that the earthquakes with longer recurrence times have higher average stress drops. We found the increase of stress drop due to the decrease of long term slip rate is in agreement with the observations which showed a negative correlation between stress drop and slip rate. However, the observed great variability of stress drop from a few to a few hundred bars may not be attributed to the variation of slip rate as Kanamori and Allen (1985) suggested. We showed that the variability may be due

primarily to the different distribution of fault strength. In this simulation, we had to extrapolate to much lower slip rates beyound the range studied in the laboratory experiments. We found that an empirical law, called the power law can explain the observed stress drop vs. slip rate relation better than the logarithmic law at least for strike-slip faults, although both of them fit laboratory friction data equally well. The power law says that the stress drop in frictional experiments is proportional to t^b , where t is the contact time and b is a constant; the logarithmic law says that the stress drop increases with contact time logarithmically. The logarithmic law is an earlier and simpler version of the rate and state dependent friction law used in most of our simulations, so that the above result may be very important for revising friction laws for the very low slip rate.

In the final chapter, we summarize our results and indicate some of the weak points in our simulations that need to be improved in the future studies. The numerical simulation discussed in this thesis is a theoretical deterministic approach for earthquake predetion. We also studied the empirical statistical approach by assigning probabilities of earthquake occurrence according to observed precursors (Cao and Aki, 1983, see appendix). A method which can combine the two different approaches is proposed at the end of this thesis.

REFERENCES:

Aki, K., Theory of earthquake prediction with special reference to Monitoring of the quality factor of lithosphere by the Coda method, Earthq. Predict. Res., 3, 219-230. 1985.

Aki, K., P. G. Richards, Quantitative Seismology: Theory and Methods, 932 pp., W. H. Freeman and Company, 1980.

Andrews, D. J., From antimoment to moment: Plane-strain models of earthquakes that stop, Bull. Seismol. Soc. Am., 65, 163-182, 1975.

Andrews, D. J. Coupling of energy beteween tectonic processes and earthquakes, J. Geophys. Res., 83, 2259-2264, 1978.

Brace, W. F., and D. Byerlee, Stick-slip as a mechanism for earthquakes, science, 153, 990, 1966.

Burridge, R., and L. Knopoff, Model and theortical seismicity, Bull. Seismol. Soc. Am., 57, 341-371, 1967.

Byerlee, J. D., Static and kinetic friction of granite at high normal stress, Int. J. Rock Mech. Mineral. Soc., 7, 577-582, 1970.

Cohen, S. C., Faulting parameters derived from computer simulation of earthquakes, NASA/GSFC X Doc. 921-77-142, 1977a.

Cohen, S. C., Computer simulation of earthquakes, J. Geophys. Res., 82, 3781-3796, 1977b.

Cohen, S. C., The visco elastic stiffness model of seismicity, J. Geophys. Res., 83, 5425-5431, 1978.

Cohen, S. C., Numerical and laboratory simulation of fault motion and earthquake occurrence, J. Geophys. Res., 17, 61-72, 1979.

Dieterich, J. H., Time-dependent friction as a possible mechanism for aftershocks, J. Geophys., Res., 77, 2771-3781, 1972.

Dieterich, J. H., Preseismic fault slip and earthquake prediction, J. Geophys. Res., 83, 3940-3948, 1978a.

Dieterich, J. H., Time dependent friction and the mechanics of stick slip, PAGEOPH, 116, 790-806, 1978b.

Dieterich, J. H., Modeling of rock friction, 1, Experimental results and constitutive equations, J. Geophys. Res., 84, 2161-2168, 1979a.

Dietrich, J. H., Modeling of Rock Friction, 2, Simulation of pre-seismic slip, J. Geophys. Res., 84, 2169-2175, 1979b.

Israel, M., and A. Nur, A complete solution of a one-dimensional propagating fault with Nonumiform stress and strength, J. Geophys. Res., 84, 2223-2234, 1979.

Kanamori, H., The nature of seismicity patterns before large earthquakes in Earthquake Prediction: An International Review, Maurice Ewing Series, 4, D. Simpson and P. Richards, Editors, Amer. Geophys. Union publ., Washington, D. C., 1-19, 1981.

Kamamori, H., and C. R. Allen, Earthquake repeat time and average stress drop, manuscript for the 5th Ewing Symposium on Earthquake Source Mechanics, 1985.

King, C. Y. Model seismicity and faulting parameters, Bull. Seismol. Soc. Am., 65, 245-259, 1975.

King, C. Y., and L. Knopoff, Model Seismicity: Rupture parameters, stress and energy relations, J. Geophys. Res., 73, 1399-1406, 1968.

Mikumo, T., and Miyatake, T., Dynamical rupture process on a three-dimensional fault with non-uniform frictions, and near-field seismic waves, Geophys. J. R. Astr. Soc., 54, 417-438, 1978.

Mikumo, T., and Miyatake, T., Earthquake sequences on a frictional fault model with non-uniform strengths and relaxation times, Geophys. J. R. Astr. Soc., 59, 497-522, 1979.

Mikumo, T., and Miyatake, Numerical modeling of space and time variations of seismic activity before major earthquakes, Geophys. J. R. Astr. Soc. 74, 559-583, 1983.

Otsuka, M., A simulation of earthquake occurrence, Phys. Earth Planet Interiors, 6, 311-315, 1972.

Papageorgiou, A. S., and K. Aki, A specific barrier model for the quantitative description of inhomogeneous faulting and the prediction of strong motion: Part II, Applications of the model, Bull. Seismol. Soc. Am., 73, 953-978, 1983.

Rice, J. R., the mechanics of earthquake rupture, Proc. Intern School of physics "Enrico Fermi", Italian Physical Society, Course LXXVIII (1979, Varenna on Lake Como, Italy) on Physics of the Earth's Interior, E. Boschi and A.M. Dziewonski, Editors, North-Holland Publishing Co., Amsterdam, 555-649, 1980.

Rice, J. R., and S. T. Tse, Dynamic motion of a single degree of freedom system following a rate and state dependent friction law, J. Geophys. Res., impress, 1985.

Ruina, A. L., Friction laws and instabilities: A quasistatic analysis of some dry frictional behavior, Ph.D. Thesis, Brown University, 1980.

Ruina, A. L., Slip instability and state variable friction laws, J. Geophys. Res., 88, 10359-10370, 1983.

Ruina, A. L., Constitutive relations for frictional slip, Mechanics in Geomaterials, Edited by F. P. Bazant, John Wiley Publishing Co., New York, 1984.

Rundle, J. B., and D. D. Jackson, Numerical simulation of earthquake sequences, Bull. Seismol. Soc. Am., 67, 1363-1377, 1977.

Stuart, W. D., Strain softening prior to two-diomensional strike-slip earthquakes, J. Geophys. Res., 84, 1063-1070, 1979,

Stuart, W. D., Instability model for recurring large and great earth-quakes in Southern California, PAGEOPH, in press, 1985.

Yamashita, T., On the dynamical processes of fault motion in the presence of friction and inhomogeneous initial stress, I, Rupture propagation, J. Phys. Earth, 24, 417-444, 1976.

Chapter 2

Seismicity Simulation With a Displacement Hardening-Softening Friction Law

2.1 PRECURSORY QUIESCENCE OF SEISMICITY

As we mentioned in Chapter 1 that seismic quiescence is the observational basis to start our study, here we introduce its definition, properties as a precursor, proposed explanations, and methods for identifying it in some detail.

A period of quiescence of seismicity lasting for a few years has been proposed as a precursor to many large earthquakes (Inouye, 1965; Mogi, 1969, Kanamori, 1981; Fedotov, 1982). Because seismic quiescence is sometimes called temporal gap as compared with spatial gap and is an important part to make up a doughnut pattern (Mogi, 1969), it is desirable to define seismic quiescence together with the spatial gap and doughnut pattern. A spatial seismic gap is a segment of plate boundary which has not experienced a large earthquake for a long time compared with its neighboring segments. In such a gap, the rate of occurrence of small to moderate earthquakes is usually stationary for most of the time between major earthquakes. If the rate decreases to a level significantly lower than the stationary rate before the occurrence of a major earthquake for certain time period, such a quiet period is called precursory quiescence of seismicity. Hence, a spatial gap is defined by large earthquakes and a temporal gap is defined by small to moderate earthquakes. Sometimes changes include not only the seismicity

rate but also fault stress or strength (Wyss and Habermann, 1979). On the other hand a complete doughnut pattern consists of a quiet focal region surrounded by an active region and foreshocks. Usually only a part of this pattern appears.

The seismicity quiescence as a precursor for earthquake prediction has received increasing attention because of the following features: (1) short precursory time; (2) high success rate for earthquake prediction; (3) the possible relations with fault heterogeneity such as asperities; (4) easy to observe.

First, the precursory time of seismicity quiescence is usually a few years (Mogi, 1969; Haberman, 1981; Kanamori, 1981; Wyss et al., 1983), which is now called an intermediate-term precursor (McNally, 1982). Seismic quiescence could be one of the signs of the maturity of a seismic gap (Habermann, 1981).

Second, although we still do not know the reliable estimate of success rate of quiescence in earthquake prediction, the following facts may give us some idea. At least four successful predictions have been made based on the observed seismic quiescence (McNally, 1982). The first was the Oaxaca, Mexico, earthquake (Ms=7.8) of 29 November 1978. Ohtake et al. (1977, a,b) predicted the location and magnitude of this coming up earthquake according to the seismic gap method and the time of its occurrence according to the observed seismic quiescence. They estimated that the earthquake may occur within 1.5 years following a resumption of activity. The real earthquake occurred 0.9 yr following the resumption of activity

(Ohtake, et al., 1981; McNally, 1982). The second successful prediction was made by Ryall and Ryall for the Mammoth Lake, California, earthquake on 25 May 1980. The third prediction was made by Guendel and McNally (1981) for an earthquake (M_S=5.6) at Costa Rica on 17 August 1982 and the fourth was made by McNally et al (1980) for the Imperial Valley, California, earthquake (M_L=6.6) of 15 October 1979. More detailed descriptions about the above predictions can be found in McNally's paper (1982).

One thing which seems common to the above four regions was that the seismicity pattern observed in the same region repeated itself very well, so that we may expect very high success rate in these regions. For other regions, Keilis-Borok et al. (1982) reported that about 75% of the events with M>6.4 in South California were preceded by several years of relative quiescence; Kanamori (1981) made space-time plots of seismicity for many large earthquakes by using NOAA and JMA catalogs and concluded that among various seismicity patterns preseismic quiescence appears most common; Habermann (1981) examined eleven large events using the normal deviate test for defining seismic quiescence and other seismic patterns quantitatively and found that among seven events, for which the data were good enough for statistical test, three were preceded by temporally and spatially unique seismic quiescence, three preceded by clusters and one was not preceded by a recognizable seismicity anomaly; Liu et al (1984) studied ten intraplate earthquakes (M>7.0) in China from 1966 to 1976 and found that all of them were preceded by quiescence periods lasting 2 to 36

months. From the above examples it is convincing enough that quiescence as a precursor has very high success rate compared with other precursors (Cao and Aki, 1983, see appendix).

The third feature of quiescence is its possible relations with fault heterogeneities. Habermann (1984) and Wyss et al. (1984) proposed a way to relate asperities on a fault to seismicities. This method includes two steps: First, seismic quiescence and clusters are statistically identified for some segments along a fault where asperities can be located according to various characteristics. These characteristics include rupture initiation and stopping for large earthquakes (Aki, 1979; Kanamori, 1981; Wyss et al., 1981) and clusters of aftershocks (Aki, 1979; Ruff and Kanamori, 1983) and many others (Habermann, 1984). Second, statistically relate the idenfified seismic quiescence and clusters to those asperities. They found that asperities and active regions are related directly and that asperities and quiet areas are not related. This seems inconsistent with Kanamori's explanation about quiescence in terms of asperity and the corresponding seismicity (Kanamori, 1981). We will discuss this later.

The fourth unique feature of quiescence is the ease in monitoring and identification. By "easy to observe" we mean that only a catalogue of earthquakes, sometimes a teleseismic seismicity data, and simple statistical test are needed to identify seismic quiescence. Of course a complete catalogue is always difficult to get and the statistical test usually involves many complex problems,

such as the fluctuation of seismicity which is not related to the impending earthquake and the existence of permanently quiet fault segments (Wyss et al, 1984).

The identification of seismic quiescence is easy but still involves many complex problems as we mentioned above. Usually this is done by comparing seismicity maps for consecutive time intervals and magnitude threshold for a fault segment at plate boundary or a specific seismic region, and results from this method are qualitative and sometimes subjective. On the other hand, Habermann (1981, 1984) and Wyss et al. (1984) are pursuing a statistical method called Z test, a standard deviate test as we mentioned before. The significance of the difference between two seismicity rates, such as the rate in some segment of a plate boundary and the mean rate of the entire boundary, can be tested. In order to detect a small difference we need data for a long time period. This is difficult to meet for many seismic regions. Another difficulty with the statistical approach is that the stationary rate of occurrence must be assumed. Also, subjective choice must be made about two magnitude thresholds which are needed for determining the seismicity rates. One threshold is the maximum magnitude below which the data are complete, and the other is the minimum magnitude above which the seismic detection is uniform through the time span of the data set (Wyss et al., 1984).

The physical explanation of temporal seismic quiescence can be divided into three categories. The first attributes to a heterogeneous distribution of stress (Mogi, 1977) or strength

(Tsumura, 1979; Kanamori, 1981); the second to precursory or aseismic slip (Habermann, 1981; later in this chapter); the third to stress corrosion accompanied with precursory aseismic fault slip (Ohnaka, 1985). According to Mogi (1977) the focal region becomes seismically quiet when most of the high stress spots are broken in the form of small earthquakes; Tsumura (1979) argued that certain strength distributions on fault surfaces may explain different seismicity patterns including quiescence. Actually, both Mogi's stress model and Tsumura's strength model need some special assumptions about the fault stress or strength disbributions. This was clearly stated in Kanamori's (1981) qualitative explanation of quiescence using an asperity model.

Kamamori divided a fault surface into many subfaults and assumed that the number of subfaults have a bi-modal Weibull distribution of their strength, in other words, the subfault number vs. strength curve has two peaks. When the linearly increasing load exceeds the strength of the first peak, less small earthquakes will occur. This explains the seismic quiescence. Mikumo and Miyatake (1983) numerically simulated seismic quiescence using the bi-modal Weibull distribution of strength. From Kanamori's bi-modal assumption for strength, we can see that Mogi's stress model needs a similar assumption for the distribution of stress of the subfaults on a fault surface. This explanation of quiescence by bi-modal distribution of strength is ad-hoc, because there is no explanation why the distribution should be bi-modal.

Another interpretation of seismic quiescence was made by Wyss and Habermann (1979), Wyss et al. (1981), Haberman (1981), and us (later in this chapter) in terms of stress smoothing by aseismic slip. The preparatory process of the Kalapana, Hawaii earthquake of November 1975 (M=7.2) was attributed (Wyss et al., 1981) to strong asperities on a strain softening fault surface. The precursory aseismic slip or stress release on softening part of a fault surface is responsible for the seismic quiescence. By introducing Stuart's (1974, 1979a) slip weakening friction law to numerical modeling, we will show that seismic quiescence can be simulated without assuming bi-modal distribution of strength on the fault. Interestingly, we found that the crital displacement, which characterizes the slip weakening failure process, is consistent with the result obtained from observed strong motion spectra by Papageorgiou and Aki (1983) using a specific barrier model. We believe that seismic quiescence occurs because when the average fault stress is high enough before a large earthquake, many parts of the fault are aseismically slipping and this process smooths out stress concentration on the whole fault area and results in less small events or quiescence.

The third explanation (Ohnaka, 1985) also depends on the precursory aseismic slip which causes the stress to level off. Ohnaka proposed that a stress corrosion process which starts with the initiation of aseismic slip and the decay rate of acoustic emission observed from laboratory experiment due to the stress corrosion can explain the seismic quiescence. This explanation has the following difficulty. The stress corrosion effect has been

studied under the loading history that a sustained constant stress is suddenly applied. This kind of loading history may be applicable to an aftershock area but probably not before a main shock.

From the discussion above, we see that seismic quiescence is explained by different mechanisms which include a spacial distribution of fault heterogeneity, preseimic slip, and stress corrosion. In order to find which mechanism is more reasonable, we need to study seismic quiescence together with fault heterogeneity, fault displacement, and fault stress. As a first step, we try numerical simulations of seismicity to see if we can reproduce seismic quiescence with certain friction law and a heterogeneious fault.

2.2 Numericl modeling with friction laws

Numerous numerical models have been used to simulate the spatial and temporal patterns of seismicity and its statistical feature. Burridge and Knopoff (1967) constructed a 1-D model in which the frictional force was assumed to be a function of the sliding velocity. Dieterich (1972) extended Burridge and Knopoff's model by using a time-dependent friction law inferred from laboratory experiments. He found that aftershocks can be generated by the inclusion of viscoelastic elements and time-dependent fault friction.

Mikumo and Miyatake (1978, 1979, 1983) published a series of papers about numerical modeling of spatial and temporal patterns of seismicity. They investigated a 3-D frictional fault model with non-uniform distribution of strength and relaxation time, in which the fault is subjected to a time-dependent shear stress. Their model simulated many precursory changes reported for actual earthquakes, including precursory earthquake swarms, clustering, pre-seismic quiescence, foreshocks, and doughnut patterns. However, the simulation of pre-seismic quiescence was only possible by assuming a bimodal Weibull distribution of the fault strength following Kanamori's (1981) assumption.

Stuart (1979a,b) and Stuart and Mavko (1979), on the other hand, obtained numerical solutions for slip hardening-weakening models corresponding to strike-slip faults (mode-III slip). The friction law assumed in their models is displacement hardening up to a peak stress, followed smoothly by a displacement softening.

Such a friction law permits a variety of seismic and aseismic phenomena to occur over a range of space and time scales (Stuart, 1979a,b). The model predicts extensive stable slip on a fault, terminated by an instability (earthquake). The instability is preceded by a rapidly accelerating, but still quasi-static, rate of slip. For other parameter values, the stress on the entire fault can also drop to the residual friction level without instability.

We are most interested in whether we can simulate the pre-seismic quiescence by a friction law without requiring a bimodal distribution of the fault strength. Thus, Stuart's friction law is used in simulating precursory seismic activities.

According to Mikumo and Miyatake (1983) the main physical parameters in their model that influenced precursory seismicity patterns are the loading rate of tectonic stress and the static and sliding frictional strength and their spatial variation on the fault. The other parameters of their model, the rate of recovery of fault strength, the relaxation time, and relaxed elastic modulus of fault materials, have been simplified in our simulation to the case of instant recovery and pure elasticity. We therefore do not expect the post-seismic behavior (for example, aftershocks).

2.3 Friction and Fault Model

The friction law introduced by Stuart (1979a,b) and Stuart and Mavko (1979) can be simplified as

$$\tau = S \exp\left[- \left(\frac{\omega - \omega_o}{a} \right)^2 \right] \qquad (1)$$

where τ is the frictional stress; ω is the fault slip; and S, ω_o and a are constants. The material constant S is the largest peak stress obtained when $\omega = \omega_o$; it is also called the upper yield stress (Andrews, 1976). The constant ω_o is the value of the fault slip at the peak stress. Constant a measures the range of slip over which hardening and weakening occur. The exponential term describes the displacement hardening and softening response. This equation intends to approximate the constitutive response of fault materials associated with a single brittle failure (Stuart and Mavko, 1979). We shall define the fault stiffness K_f as the rate of change of stress with respect to fault displacement,

$$K_f = \frac{\partial \tau}{\partial \omega} = -2 \frac{s(\omega - \omega_o)}{a^2} \exp\left[- \left(\frac{\omega - \omega_o}{a} \right)^2 \right] \qquad (2)$$

The conditions for the occurrence of instability will be discussed latter.

The numerical model used in the computation is similar to that of Burridge and Knopoff (1967) as shown in Figure 1. This is a 1-D mechanical analog of an active earthquake fault. In this model, the material adjacent to the fault is represented as an array of discrete elements or blocks which are in frictional contact with the fault. These blocks are connected to each other by coil springs and to a common driving block by leaf springs. The driving block represents material far from the fault. In our case the springs are perfectly elastic.

Following Dieterich's (1972) notations the ith block is connected to the driving block by leaf spring L_i and to the blocks i-1 and i+1 by coil springs C_{i-1} and C_i, respectively (Figure 2). The displacement of each block is specified by d_i. The driving block moves at a constant velocity V (say, 5.0 cm/yr for the San Andreas fault) and at time T undergoes a total displacement VT. The static force F_i acting on block i at time T arises from the displacements of the frictional elements and the driving block. It is given by Dieterich (1972)

$$F_i = L_i(VT-d_i) + C_{i-1}(d_{i-1} - d_i) + C_i(d_{i+1} - d_i) \qquad (3)$$

or

$$F_i = \sum_{j=i-1}^{i+1} K_{ij}d_j + L_iVT \qquad (4)$$

where K_{ij} is a stiffness matrix that relates the forces acting on the friction blocks to displacements, and

$$K_{i\ i-1} = C_{i-1}$$

$$K_{ii} = -(L_i + C_{i-1} + C_i)$$

$$K_{i\ i+1} = C_i$$

We also adopte the periodicity of the block elements along the fault (Dieterich, 1972) to avoid abnormal conditions at the ends. Therefore we have

$$K_{1\ 0} = C_n$$

$$d_0 = d_n$$

and

$$K_{n\ n+1} = C_1$$

$$d_{n+1} = d_1$$

where n is the total number of blocks. In a simulation, when T reaches a certain value, the block i will start to move slowly (creep). From (1), the motion is resisted by frictional stress

$$\tau_i = S_i \exp\left[-\left(\frac{\omega_i-\omega_o^i}{a_i}\right)^2\right] \tag{5}$$

where the superscript and subscript i's denote the ith block. From equations (4) and (5), the quasistatic force equilibrium condition is

$$\sum_{j=i-1}^{i+1} K_{ij}d_j + L_iVT = A_iS_i \exp\left[-\left(\frac{\omega_i-\omega_o^i}{a_i}\right)^2\right] \tag{6}$$

where both d_i and ω_i are displacements of block i, but the origin of coordinates of ω_i is chosen at the point at which the block starts to creep. A_i is the area of the side face of block i which is in contact with the fault. Equation (6) is solved as a quasi-static elastic problem (Stuart, 1979). The fault is hardening until the stress reaches the peak at $\omega_i = \omega_o^i$. After this peak, the fault weakens. If the fault weakens faster than the elastic stress of the driving block is relieved, instability will take place. In addition to the fault stiffness K_f of block i

$$K_f^i = \frac{\partial\tau_i}{\partial\omega_i} = -2S_i \frac{\omega_i-\omega_o^i}{a_i^2} \exp\left[-\left(\frac{\omega_i-\omega_o^i}{a_i}\right)^2\right] \tag{7}$$

we shall define the minimum stiffness of the surrounding elastic earth corresponding to one block as

$$K_p^i = \frac{\partial(F_i/A_i)}{\partial\omega_i} = \frac{\partial(F_i/A_i)}{\partial d_i} = K_{ii}/A_i \tag{8}$$

In terms of K_f^i and K_p^i, the instability of block i occurs when $K_f^i < K_p^i$ which is equivalent to the condition that $[\partial\omega_i/\partial(VT)] \to \infty$. Figure 3 shows the fault stress τ_i versus ω_i and the driving stress F_i/A_i versus d_i. The solution ω_i for $K_f^i = K_p^i$ is denoted ω_u^i and called the critical displacement in the friction law. Because more than one neighbouring blocks may turn to unstable together, K_{ii} will be different from what is defined above. In this case, the simulated seismicity pattern will be different too. This points out some inconsistancy. It is due to the discrete model and the approximation we made here in which we take K_{ii} as constant.

When a block i goes beyond the instability point ($\omega_i > \omega_u^i$), we take the frictional stress as the residual frictional stress or the sliding friction R_i for block i. According to Byerlee (1970), 1/1.25 of the static friction is assigned to R_i. In our case the static friction is equal to $A_i S_i \exp[-(\omega_o^i/a_i)^2]$. Therefore, the equation of motion of the slipping block i (not creeping) is given for acceleration b_i as

$$m_i b_i = \sum_{j=i-1}^{i+1} K_{ij} d_j + L_i VT - R_i \tag{9}$$

where m_i is the mass of block i.

To solve equations (6) and (9), we use an iterative procedure and a stepwise forward integration (Wilson and Clough, 1962), respectively. It is assumed that the acceleration varies linearly within the time step Δt. At the end of each time step a direct integration yields the following equations for the velocities

$V_i^{t+\Delta t}$ and the displacements $d_i^{t+\Delta t}$ for the slipping elements.

$$V_i^{t+\Delta t} = V_i^t + (\Delta t/2)\, b_i^t + (\Delta t/2) b_i^{t+\Delta t}$$
$$d_i^{t+\Delta t} = d_i^t + \Delta t V_i^t + (\Delta t^2/3) b_i^t + (\Delta t^2/6) b_i^{t+\Delta t} \tag{10}$$

Substituting (10) into (9) yields

$$m_i b_i^{t+\Delta t} = \sum_{j=i-1}^{i+1} K_{ij} \left[d_j^t + \Delta t V_j^t + (\Delta t^2/3) b_j^t + (\Delta t^2/6) b_j^{t+\Delta t} \right] + L_i V(T+\Delta t) - R_i \tag{11}$$

where i ranges over the slipping elements.

Substituting (10) into (6) we obtain similar equations for creeping elements:

$$\sum_{j=i-1}^{i+1} K_{ij} d_j^{t+\Delta t} + L_i V(T+\Delta t) = A_i S_i \exp\left[- \frac{(\omega_i^{t+\Delta t} - \omega_o^i)^2}{a_i^2} \right] \tag{12}$$

where $\omega_i^{t+\Delta t} = \omega_i^t + d_i^{t+\Delta t} - d_i^t$. In (11), the unknown is $b_j^{t+\Delta t}$; in (12) the unknown is $d_j^{t+\Delta t}$. Solving all the simultaneous equations of moving blocks and creeping blocks according to (11) and (12) yields accelerations for slipping blocks and displacements for creeping blocks at the end of time step Δt. After each step the velocities and displacements for slipping blocks are calculated according to (10). In (11) and (12), when the blocks of $j = i+1$, $i-1$ are slipping or creeping, then V_j (and in general b_j too) $\neq 0$ or V_j, $b_j = 0$, respectively. During each step, we use the iterative procedure because equation (12) is nonlinear.

The force acting on a stationary element i is determined

from (4). If it exceeds $A_i S_i \exp\left[-\left(\frac{\omega_o^i}{a_i}\right)^2\right]$, the element is allowed to creep during the next time step. The critical displacement ω_u^i for a creeping block i for which it becomes unstable can be calculated from $K_f^i = K_p^i$ according to (7) and (8). At the end of each step, if the displacement ω_i of a creeping block i reaches ω_u^i, it is allowed to slip during the next step according to equation (9). If the velocity of a slipping block has become 0 during the preceding time step, the block i is held stationary until the force again exceeds the static friction $A_i S_i \exp\left[-(\omega_o^i / a_i)^2\right]$. If the given initial conditions do not allow instability to take place for some blocks, they will simply creep to residual friction level without instability (Rice, 1980, pp. 600-603).

2.4 MODEL PARAMETERS AND RESULTS

Now that formulas are ready for our simulation, we must choose model parameters. We need to choose the time step Δt, the block mass, leaf and coil spring constants, constants ω_o^i and a_i in the friction law, and the fault strength. Fifty blocks are used in the present model to simulate a 50 km long strike-slip fault. For simplicity, common values for elastic and mass parameters are used; that is $m_i = m$, $L_i = L$, $C_i = C$, $A_i = A$ for all blocks. Only the friction parameters are varied from block to block.

According to the stability discussion in numerical calculation, Δt should be less than the time needed for an elastic wave travelling across the block spacing. In the solution of simultaneous equations (6) and (9), if at least one block is slipping (not creeping), the time step Δt is then set at one-fifth the time required to propagate a seismic disturbance between adjacent blocks; if no block is slipping but at least one block is creeping which is the quasi-static case, we used 1000 seconds as the time step; if no block is slipping or creeping, we can easily find the time T for the first block to creep again using equation (4).

Yamashita (1976) extended the mechanical model of Burridge and Knopoff (1967) to a case in which the driving slab has non-uniform velocity distribution. He derived formulas for block mass m and spring constants L and C by comparing equation (9) with a finite difference equation which is an approximation of a 2-D wave equation in the neighborhood of a fault surface. His formulas for a block with a unit height are

$$m = \rho \Delta y \Delta z \ ,$$

$$C = [2(\lambda+\mu)(V_s/V_p)^2+\mu](\Delta z/\Delta y) \ , \qquad (15)$$

$$L = \mu \Delta y/\Delta z$$

where ρ is density, λ and μ are elastic constants, and V_s and V_p are S- and P-wave velocities, respectively. In our modelling we have chosen $\rho = 2.8$ g/cm^3, $\lambda = \mu = 3 \times 10^{11}$ dyne/cm^2, $V_s = 3.55$ km/sec, and $V_p = 6.15$ km/sec. The following is the physical meaning of Δz. If a pulse propagates in a direction perpendicular to the fault

surface at a veloctiy V_s, the side, which is perpendicular to the fault surface, of the volume contributing to the mass of inertia for the fault motion can be estimated by $V_s t_o$, where t_o is the average rise time when the fault is dislocated. In our computation $t_o = 1$ sec is used. Here Δy is the length of the block along the fault strike direction. We have chosen $\Delta y = 1$ km. The side area A of a block with unit height is equal to Δy.

Usually ω_o^i and a_i are different among blocks. In order to simplify the simulation and to emphasize the effects of strength distribution and critical displacement on the simulated seismicity patterns, we assume that ω_o^i and a_i are proportional to S_i. In order to keep the upper yield stress S_i within 10% higher than the static frictional stress τ_i (ω_i=0), in accordance with the experimental results, we further fix the ratio ω_o^i/a_i to be 1/5. Because S_i, ω_o^i and a_i together define the friction law (Figure 3) completely, our assumptions simplify the relations among blocks and leave the critical displacement ω_u^i and S_i to be the main characteristic parameters which vary among all blocks. With all these assumptions we then have only two independent parameters to specify the friction law completely, namely the fault strength S_i and the critical displacement ω_u^i, which is determined from given a_i and ω_o^i according to the condition $K_f^i = K_p^i$. Their effects on the simulated seismicity patterns are easily distinguished by assigning different ranges of S_i and a_i (or ω_o^i). For the same reason -emphasizing the effects of strength distribution and critical displacement on the simulated seismicity patterns - we assume that the initial shear stresses

applied on each block are 0. The results for three different cases of simulation are shown in the following.

(A) Weakly heterogeneous distribution of the fault strength (S_i ranges from 100 to 300 bars)

We first use the simple friction law in the simulation which is special case of Stuart's friction law when $\omega_o^i \to 0$ and $a_i \to 0$. The simulated seismicity is shown in Figure 4. In this figure the horizontal axis gives the location of the block along the fault and vertical axis indicates the time. Time increases downward. The symbol "+" means the occurrence of instability of a particular block; the horizontally connected symbol "+" represents a single seismic event extended over the connected blocks during a few seconds . The figure shows that only a few small shocks occur as the tectonic stress increases, and a large event suddenly occurs, rupturing the entire fault plane without any obvious precursory events. After the first main rupture, similar large events repeat at almost the same time intervals. The recurrence time is controlled by the driving velocity V and the range of fault strength. These results are in agreement with Mikumo and Miyatake's (1983) A1 model with relatively homogeneous fault properties. When we use Stuart's friction law for the same strength range but different ranges of ω_o^i and a_i, we obtain almost the same seismicity patterns as in the case of the simple friction law. The slight differences are that (1) the recurrence times of the major events are longer under the same driving velocity V, (2) every block creeps

before it undergoes the instability, and (3) only creep events occur between major seismic events unless a_i and ω_o^i are as small as the orders of 0.015 cm and 0.003 cm, respectively.

(B) Moderately to strongly heterogeneous distribution of fault strength (S_i ranges from 100 to 800 bars)

When we use the simple friction law, the simulated seismicity (Figure 5) tends to increase over a long period of time prior to a major event. There is no quiescence before the major event. These results indicate that as fault heterogeneities increase, small to moderate size shocks tend to occur prior to a large event. All of these results are similar to Mikumo and Miyatake's (1983) A4 model in which the strength distribution is assumed to be widely spread over 200-1180 bars.

When we use the displacement hardening-softening friction law and set ω_o^i = (0.03-1.3 cm) and a_i = (0.15-6.5 cm), howere, keep the same fault strength distribution and the same initial stresses, the simulated seismicity becomes very different (Figure 6). The symbols of "O" in Figure 6 indicate the starting times of creep for the particular block. Once a block has started to creep, it will follow the frictional curve in Figure 3 until reaching the point B and turn into instability. If we look at a single block's behavior along the direction of time axis in the figure , creep should always precede instability. However, when a creep event is followed by instability in few seconds, the creep symbol is eliminated. An example is shown in Figure 6, before the major earthquake, which occurs at T = 55

years. Many blocks are not preceded by the creep symbol "O" before this earthquake. In this case, there is a precursory accelerating deformation just before the mainshock. Differences between Figures 5 and 6 are as follows.

(1) In Figure 6, there is a ten year long quiescence period from T = 45 years to T = 55 years before the major earthquake which ruptures the entire fault. Obviously, quiescence is not determined by the behavior of any individual block but by the global behavior of all blocks. In Figure 5 there is no quiescence at all but enhanced seismicity before the similar major earthquakes (T = 28 years).

(2) In Figure 5, after the major earthquake there is a quiescence period without any events; but in Figure 6, immediately after the major earthquake, many blocks start to creep or slip again, that last about two years.

(3) Under the same driving velocity V, it takes about twice as much time in Figure 6 as in Figure 5 to get to the first major earthquake.

(C) The same strengh S_i as in (B), but a_i and ω_o^i are 10 times larger than in (B).

In this case, only creep events but no small earthquakes occur between major earthquakes. A similar seismicity pattern has appeared in simulation (A), in which we used Stuart's friction law with a_i and ω_o^i two orders of magnitude smaller than the present case but S_i ranges from 100 to 300 bars.

From the above simulation, we found that the important

precursory phenomenon called "quiescence" may be produced by introducing the displacement hardening-softening friction law. The reason why the quiescence period is produced by this friction law may be explained as follows. When the stress level is low, small events and creep can occur at low strength blocks along the fault (Figure 6). When the stress along the fault reaches a certain high level, but still lower than the highest level at which the mainshock will occur, most blocks can creep at this level. Because a creeping block can release a part of the concentrated stress at its neighbors, the pre-seismic creep will reduce the possibility of small events. Then very few (or no) small events will occur at this stress level. In other words, quiescence, a global behavior of a fault, is produced by the interaction between the increasing stress along the fault and all blocks that obey the displacement hardening-softening friction law.

After a systematic search of the changes in seismic occurrence rate for the segment of the Kurile Island arc and eleven other areas with large earthquakes, Wyss and Habermann (1979) and Habermann (1981) found many examples of precursory seismic quiescence in which the rate was lowered by 50% at the 99% confidence level. They suggested a similar explanation, namely the precursory displacement and aseismic stress release on some portion of the future rupture surfaces.

2.5 CRITICAL SLIP-WEAKENING DISPLACEMENT

As demonstrated in the examples above, a key parameter

controlling the seismicity pattern is the critical slip-weakening displacement ω_u^i. The average values of ω_u^i for simulations (A), (B), and (C) are 0.006, 0.8, and 11 cm, respectively, covering three orders of magnitude. The first value is of the same order of magnitude as found in Dieterich's (1981) experiments on a large rock sample. The values for cases (B) and (C) happened to be of the same orders as Mavko's one-dimensional and two-dimentional models (1984), respectively. Mavko did not explain why he used these critical displacements a few orders of magnitude larger than Dieterich's laboratory results. However, by noticing that a long fault has greater roughness than a short fault and that, as the experiments show, the rough fault has larger critical displacement than a smooth fault (Dieterich, 1981), and by then assuming that the critical displacement is roughly proportional to the fault length, we can extrapolate the experimental results to fault of an in-situ scale. Another similar consideration leads to the same conclusion. If we consider interaction of larger earthquakes, we may want to increase the block length. Then in order to generate the same seismicity pattern, the critical displacement should also be increased proportionally to the block length to preserve the physical similarity. In Okubo and Dieterich's (1984) recent experiment the fault length is 2 m. The critical displacements are 5μm-25μm. Then, for a 1 km long block the average critical displacement $\bar{\omega}_u^i$ = 0.8 cm in simulation (B) may be a reasonable extrapolation of the experimental results. If we extrapolate further from simulation (B) to earthquakes with fault lengths 10 km and 100 km, blocks with

these lengths would require the critical displacement of 10 cm and 1 m, respectively.

This result is in a good agreement with the estimates of slip-weakening displacement from totally independent observations of an earthquake fault. The independent estimate comes from the interpretation of strong motion acceleration spectra made by Papageorgiou and Aki (1983) on the basis of a specific barrier model (Das and Aki,1977; Aki,1979). The critical displacement is derived from acceleration spectra by the following steps. First the barrier interval $2\rho_o$, local stress drop $\Delta\sigma$, and cut-off frequency f_{max} are determined from the observed acceleration power spectra. From ρ_o and $\Delta\sigma$, the apparent Griffith energy G is estimated. From f_{max} the length d of the cohesive zone is estimated. From G and d we find the cohesive stress σ_c, and from G and σ_c we finally obtain the critical displacement D (noted as ω_u^i in this paper). The resultant values of D for several California earthquakes are of the order of 10 cm to 1 m in agreement with the values inferred from our seismicity simulation experiment.

2.6 DISCUSSION AND CONCLUSIONS

In order to simulate the seismicity along a fault (like the San Andreas fault) in which the seismicity pattern varies greatly from one segment to another, we need to assign different ranges of S_i, a_i and ω_o^i for different segments. For example, if we assign small ω_o^i and a large ratio of ω_o^i/a_i to one segment, then the peak of the friction law curve (Figure 3) will become narrower or sharper to favor the instability, the critical displacements will be small, and

we shall expect frequent small seismic events on this fault segment. On the other hand, if we assign large ω_o^i and a small ratio of ω_o^i/a_i to a fault segment, the peak of the friction law curve will become flatter, and we shall then expect fewer small seismic events. If the curve is flat enough, the condition $K_f^i < K_p^i$ will never be satisfied. Then we shall have only creep and no earthquakes.

In the simulations above, we showed more than one cycle of repeated major events only for case (A), because the simulated seismicity pattern before the first major event in case (B), as in case (A), was not repetitive, whatever the friction law used. For all the simulations, after the first major event, small events between sucessive major events gradually decreased to a level at which no quiescence or enhancement of seismicity patterns could be identified, even for the case with strongly heterogeneous distribution of fault strength and small critical displacements. The same difficulty was encountered early by Andrews (1975, 1978). He pointed out, from energy considerations, that the stationary occurrence of a large number of small earthquakes cannot be explained by the load of smoothly varying tectonic stress alone, but require a generation of short wavelength self stress by a large earthquake, unless fault creep, varying in amplitude of all length scales, prepares the fault for small earthquakes. This difficulty indicates that the earthquake phenomena may consist of two distinct processes. One of the process is the coupling between tectonic driving and large earthquakes. The other process is the generation

of "self stress", as it is called by Andrews (1978), which originates from earthquakes themselves. According to this idea, not only the immediate aftershocks of a large earthquake but also earthquakes in the normal period may be caused by irregular slip of large earthquakes. Such a theory may lead to a better understanding of the physical basis of the well-known Gutenberg and Richter empirical relation for the frequencies of earthquakes of various magnitudes, and Andrews (1978) proposed that friction which changes with displacement may be essential to fault mechanism. Our simulation showed, however, that the displacement hardening-softening friction law does not seem to be capable of a sustained generation of small earthquakes. On the other hand, the barrier model (Aki, 1979) offers a physical mechanism for such a roughening of self stress in the fault zone after a major earthquake. In our future simulation, we shall incorparate such a stress roughening process. In spite of the above problems encountered in our simulation the following conclusions may be drawn.

(1) From the above simulation we found that the important precursory phenomenon called "quiescence" may be accounted by introducing the displacement hardening-softening friction law.

(2) Only when we choose an average critical displacement $\overline{\omega}_u^i$ with the scale-dependent slip-weakening critical displacement D as obtained by Papageorgiou and Aki (1983) do we obtain the seismicity pattern that includes creep, small events, main events, and quiescence before major events.

FIGURE CAPTIONS

Figure 1. Schematic diagram of the fault model (after Burridge and Knopoff, 1967). The blocks represent friction elements in contact with the fault. The friction elements are connected by the elastic elements represented as coil springs. Leaf springs connect the fault elements to the driving block.

Figure 2. Indexing and notation for numerical analysis of the fault model (after Dieterich, 1972). Indexing is done with respect to the friction elements of mass m_i. The stiffness of the coil springs adjacent to the element i are denoted by C_{i-1} and C_i, and the stiffness of the leaf spring connecting element i to the driving block is L_i. Displacements of the elements are denoted by d_i. The driving block moves at a uniform velocity V.

Figure 3. Postulated friction law with a_i = 0.3 cm, ω_o^i = 0.1 cm, and S_i = 300 bars (heavy line). Instability occurs at point B. After point B friction drops to sliding friction R_i. Before point B the friction versus displacement is the displacement hardening-softening friction law introduced by Stuart.

Figure 4. Simulated seismicity using the simple friction law for the weakly heterogeneous distribution of the fault strengh (100 - 300 bars). The symbol (or symbols) of "+" represents individual earthquakes. The locations

of events on the fault are shown with the horizontal axis. The occurrence times of events are shown with the vertical axis. The connected symbols of "+" in horizontial direction represent a single seismic event extended over the connected blocks.

Figure 5. Simulated seismicity in the model with the simple friction law and moderately to heavily heterogeneous fault strength (100 ~ 800 bars).

Figure 6. Simulated seismicity in the model with the displacement hardening-softening friction law and the same fault strength distribution as in Figure (5). The symbols of "o" indicate the starting times of block creep for the particular blocks. The quiescence period is between time T = 45 years and T = 55 years.

REFERENCES

Aki,K., (1979), Charaterization of barriers on an earthquake fault J. Geophys. Res., 84, 6140-6148.

Andrews, D.J. (1975), From antimoment to moment: Plane-strain models of earthquakes that stop, Bull. Seis. Soc. Am., 65,163-182.

Andrews, D.J. (1978), Coupling of energy between tectonic processes and earthquakes, J. Geophys. Res., 83,2259-2264.

Andrews, D.J. (1976), Rupture velocity of plane strain shear cracks, J. Geophys. Res., 81, 5679-5687.

Burridge, R., and Knopoff, L. (1967), Model and theoretical seismicity, Bull. Seis. Soc. Am., 57, 341-371.

Byerlee, J.D. (1970), Static and kinetic friction of granite at high normal stress, Int. J. Rock Mech. Mineral. Soc., 7, 577-582.

Das, S and Aki, K. (1977), Fault planes with barriers: A versatile earthquake model, J. Geophys. Res., 82, 5648-5670.

Dieterich, J.H. (1972), Time-dependent friction as a possible mechanism for aftershocks, J. Geophys. Res., 77, 3771-3781.

Dietrich, J. (1981), Constitutive properties of faults with simulated gauge, Mechanical Behavior of Crustal Rocks, Monograph 24, eds. N.L. Carter, M. Friedman, J.M. Logan, and D.W. Stearns, Amer. Geophys. Un., 103-120.

Fedotov, S. A., S.D. Chernyshew, and G. V. Chernysheva, The improved determination of the source boundaries for earthquakes of $M^{>}7$ $^{3}/_{4}$, of the properties of the seismic cycle and of long-term seismic prediction for the Kurile-Kamchatka arc, Earthquake Pred. Res. 1, 153-171, 1982.

Guendel, F. And K. C. McNally, The foreshock-mainshock sequence of the 1978 (M_s=7.0) Samara, Costa Rica earthquake: a unique data set, Earthquake Notee 53, 81, 1982.

Habermann, R.E. (1981), Precursory seismicity patterns: Stalking the mature seismic gap, in Earthquake Prediction -An International Review, Maurice Ewing Series 4, American Geophysical Union, 680pp.

Habermann, R. E., Spatial Seismicity variations and asperities in the New Hebrides seismic zone, J. Geophys. Res., 89, 5891-5903, 1984.

Inouye, W., On the seismicity in the epicentral region and its neighborhood before the Niigata earthquake, Kenshin Jiho, 29, 31-36, 1965 (in Japanese).

Kanamori, H. (1981), The nature of seismicity patterns before large earthquakes, in Earthquake Prediction -An International Review, Maurice Ewing Series 4, American Geophysical Union, 680pp.

Keilis-Borok, V.I., R. Lamoreaux, C. Johnson and B. Minster, Swarms of the main shocks in Southern California, preprint, 1982.

Liu, P., D. Huang, L. Wang, Z. Wang, D. Zheng, H. Feng, Seismicity pattern over the perparatory process of strong earthquakes, ISCSEP Seismological Press, Beijing, China, 100-110, 1984.

Mavko, G. (1984), Large-scale earthquakes from a laboratory friction law, J. Geophys. Res., in press.

McNally, K. C., Variations in seismicity as a fundamental tool in earthquake prediction, Bull. Seism. Soc. Am. 72, 5351-5366, 1982

McNally, K. C., F. Richter, B. J. Leitner, and H. Kanamori, Aftershock sequences and minor seismicity in Southern California and Mexico: Relationship to the Mexicali earthquake (M_L=6.6,M_S=6.8) of 15 October 1979, Earthquake Notes 50, 52, 1980.

Mikumo, T., and Miyatake, T. (1978), Dynamical rupture process on a three-dimensional fault with non-uniform frictions, and near-field seismic waves, Geophys. J. R. Astr. Soc., 54, 417-438.

Mikumo, T., and Miyatake, T. (1979), Earthquake sequences on a frictional fault model with non-uniform strengths and relaxation times, Geophys. J. R. Astr. Soc., 59, 497-522.

Mikumo, T., and Miyatake, (1983), Numerical modelling of space and time variations of seismic activity before major earth-quakes, Geophys. J. R. Astr. Soc. 74, 559-583.

Mogi, K., Some features of recent seismic activity in and near Japan (2) activity before and after great earthquakes, Bull. Earthquake Res. Ins., Tokyo Univ. 47, 395-417, 1969.

Mogi, K., Seismic activity and earthquake predictions, in Proceedings of the symposium on Earthquake Prediction Research, 203-214, 1977 (in Japanese).

Ohnaka, M., A sequence of seismic activity in the Kanto Area precursory to the 1923 Kanto Earthquake, PAGEOPH, 122, 848-862, 1985.

Ohtake, M. T. Matumoto, and G. Latham, Seismicity gap near Oaxaca, Southern Mexico as a probable precursor to a large earthquake PAGEOPH 115, 375, 1977a

Ohtake, M., T. Matumoto, and G. Latham, Temporal changes in seismicity preceding some shallow earthquakes in Mexico and Central America, Bull, Int. Inst. Seism. Earthquake Eng., 15, 105, 1977b

Ohtake, M., T. Matumoto, and G. Latham, Evaluation of the forecoast of the 1978 Oaxaca, Southern Mexico earthquake based on a precursory seismic quiescence, in Earthquake Prediction, An International Review, D. W. Simpson and P.G. Richards, Editors, American Geophysical Union, Washington D. C., 53-61 1981.

Okubo, P.G., and Dieterich, J.H. (1983), Effects of physical fault properties on frictional instabilities, produced on simulated faults, J. Geophys. Res., 89, 5815-5827, 1984.

Papageorgiou, A. S. and K. Aki, A specific barrier model for the quantitative description of inhomogeneous faulting and the prediction of strong gound motion: Part II, Applications of the model, Bull. Seism. Soc. Am. 73, 953-978, 1983

Rice, J.R., (1980), The mechanics of earthquake rupture, in Physics of the Earth's Interior, ed. by A.M. Dziewonsky and E. Baschi, Italian Physical Society, printed by North Holland Publ. Co., pp. 555-649.

Ruff, L., and H. Kanamori, The rupture process and asperity distribution of three great earthquakes from long-period diffracted P-waves, Phys. Earth Planet. Inter., 31, 202-230, 1983.

Ryall, A., and F. Ryall, Spatial-temporal variations in seismicity preceding the May 1980, Mammoth Lakes, Calfiornia earthquakes, Bull, Seism. Soc. Am., 71, 747-760, 1981.

Stuart, W. D., Diffusionless dilatancy model for earthquake precursors, Geoph. Res. Let., 1, 261-264,1974.

Stuart, W.D., (1979a), Strain softening prior to two-dimensional strike-slip earthquakes, J. Geophys. Res., 84, 1063-1070.

Stuart, W.D., (1979b), Aging and strain softening model for episodic faulting, Tectonophysics, 52, 613-626.

Stuart, W.D., and Mavko, G.M. (1979), Earthquake instability on a strike-slip fault, J. Geophys. Res., 84, 2153-2160.

Tsujiura, M., The difference between foreshocks and earthquake swarms, as inferred from the similarity of seismic waveform, Bull Earthquake Res. Inst. Tokyo Univ., 54, 309-315, 1979 (in Japanese).

Wilson, E.L., and Clough, R.W. (1962), Dynamic response by step-by-step matrix analysis, in Symposium on the Use of Computers in Civil Engineering, Lisbon, October 1962, paper 45, pp. 1-14, Laboratorio National de Engenharia Civil, Lisbon, Portugal.

Wyss, M., F. W. Klein, and A. C. Johnston, Precursors to the Kalapana M=7.2 earthquakes, J. Geophys. Res., 86, 3881-3900, 1981.

Wyss, M., and R. E. Habermann, Seismic quiescence precursory to a past and a future Kuriles islands earthquake, PAGEOPH, 117, 1195, 1979.

Wyss, M., R. E. Habermann, and C. Heiniger, Seismic quiescence, stress drops and asperities in the New Hebrides Arc, Bull. Seism. Soc. Am., 73, 219-236-1983.

Wyss, M., R. E. Habermann, and J. C., Griesser, Seismic quiescence and asperities in the Tonga-Kermadec Arc, J. Geophys, Res., 89, 9293-9304, 1984.

Yamashita, T., (1976), On the dynamical process of fault motion in the presence of friction and inhomogeneous initial stress. Part I. Rupture propagation, J. Phys. Earth, 24, 417-444.

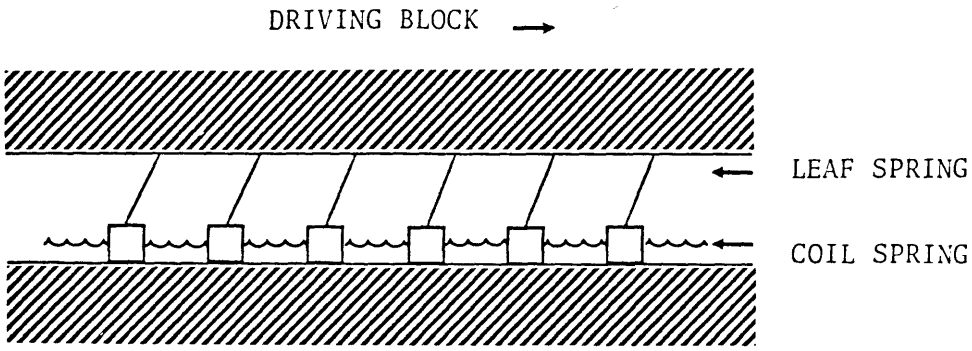

Figure 1

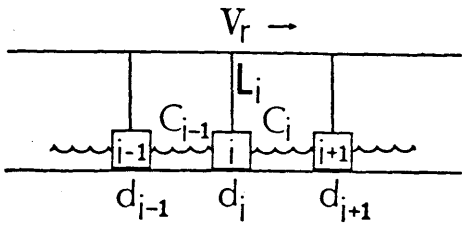

Figure 2

FRICTION LAW

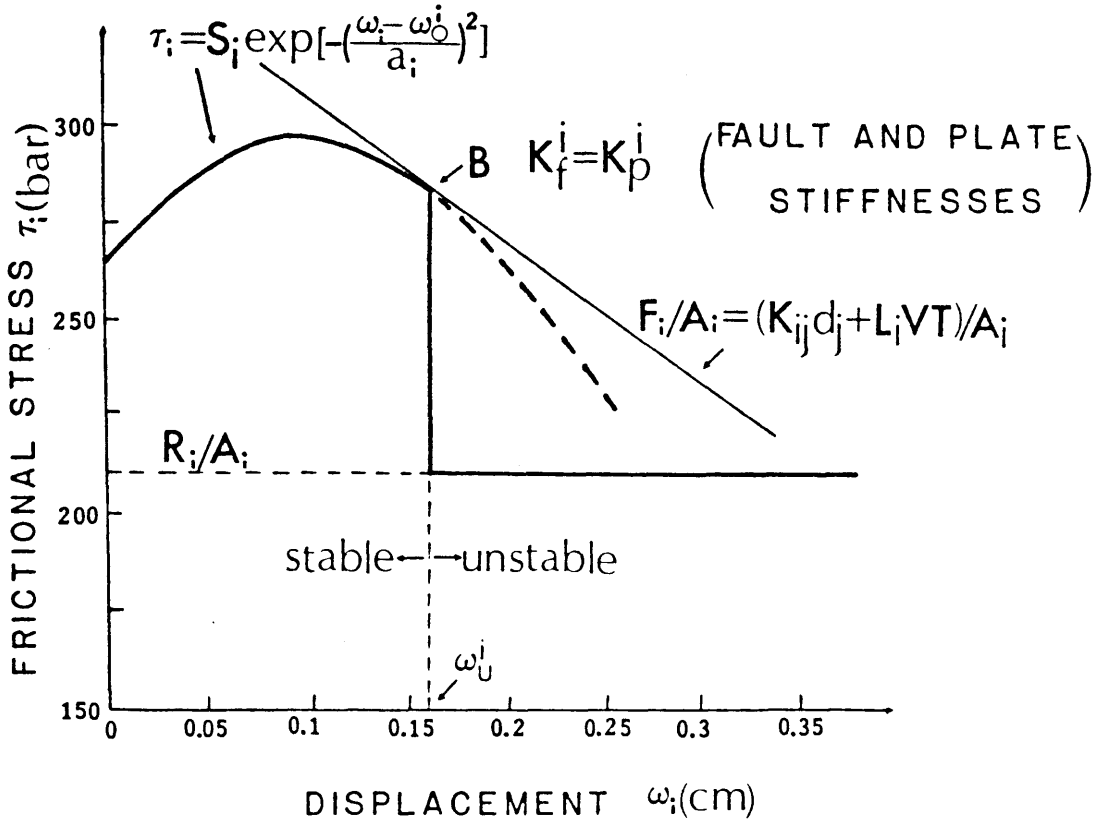

A_i: CONTACT AREA
R_i: SLIDING FRICTION
S_i: PEAK STRESS

$$\left.\begin{array}{l}\tau_i = F_i/A_i \\ m_i b_i = F_i - R_i\end{array}\right\} \text{EQUATIONS OF MOTION}$$

Fig. 3

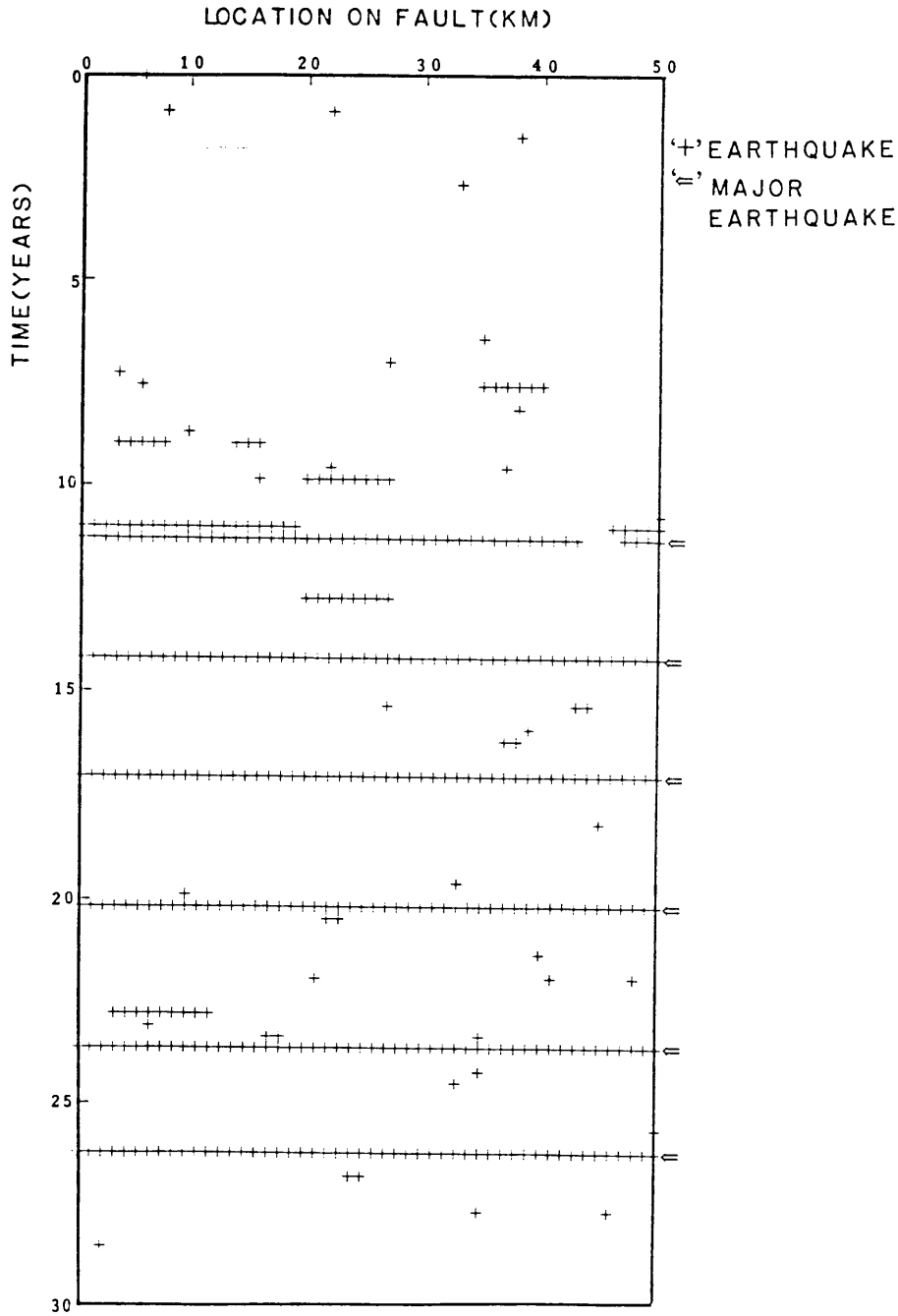

SEISMICITY PATTERN

Fig.4

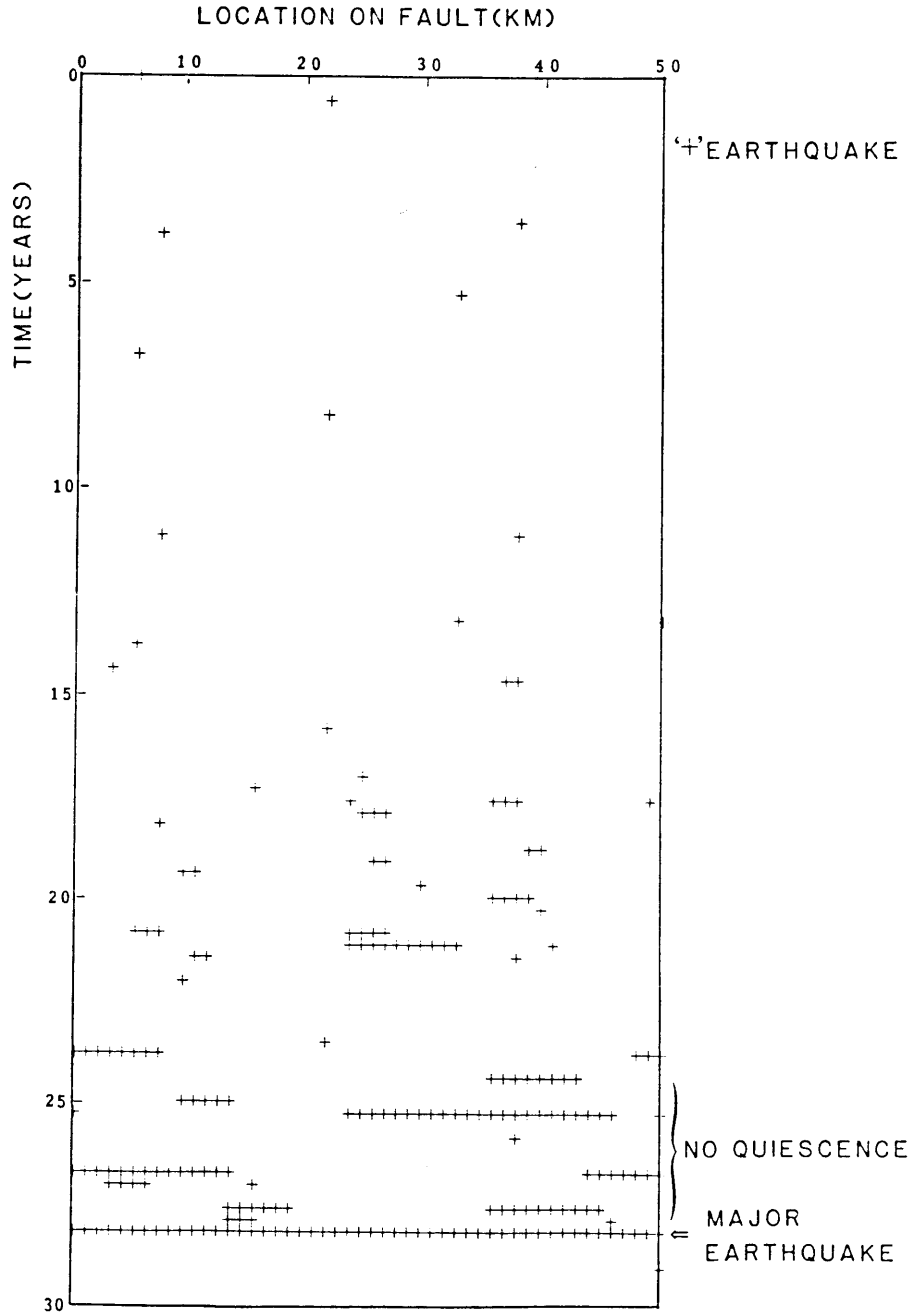

SEISMICITY PATTERN

Fig.5

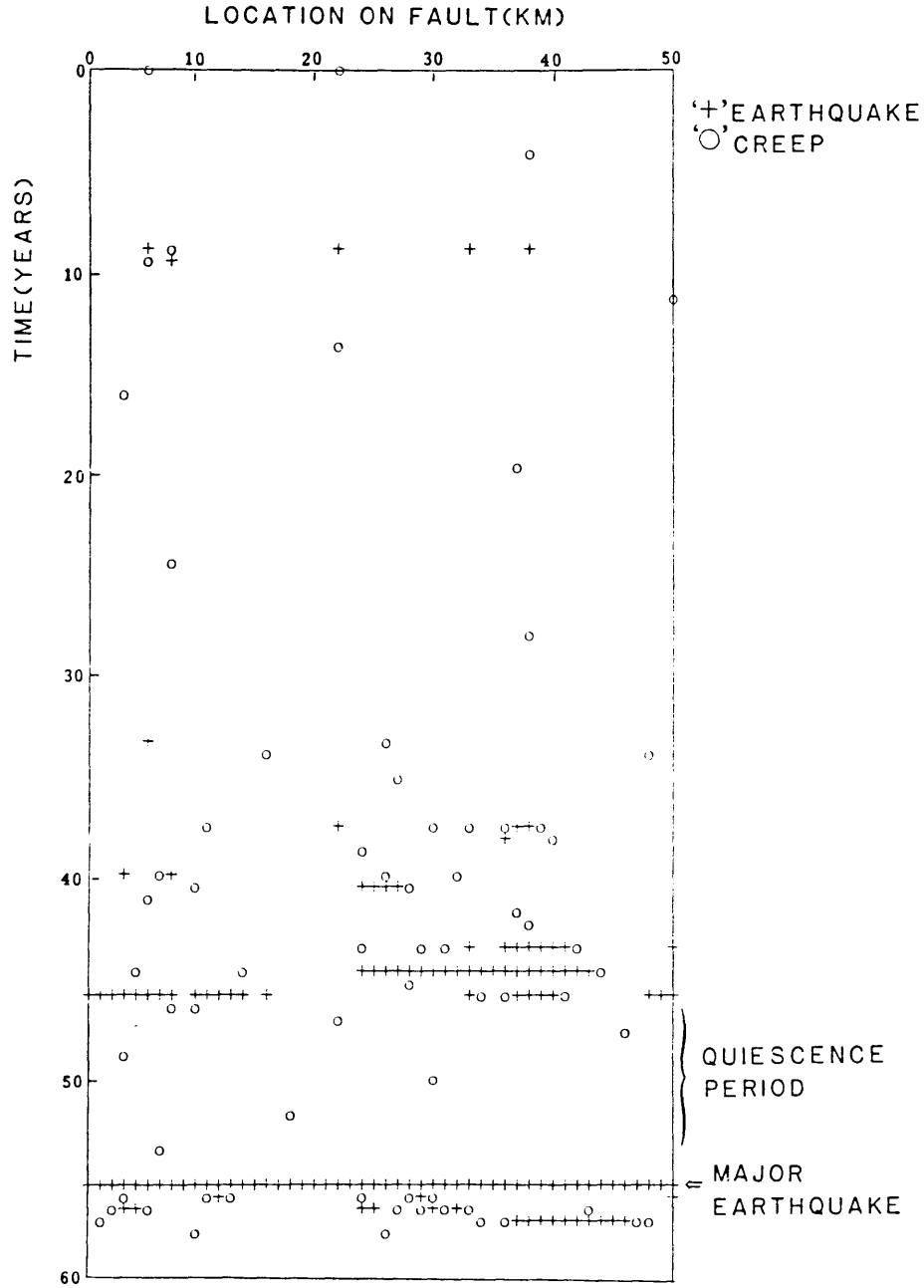

SEISMICITY PATTERN

Fig.6

Chapter 3

Seismicity Simulation With a Rate and State Dependent Friction Law

3.1 Introduction

Numerical simulations of fault motion and earthquake occurrence provide a convenient test-bed for examining models of earthquake source mechanisms and for exploring their dynamic consequences. Three equally important elements of earthquake phenomena (Aki, 1983), namely, (1) the loading of tectonic stress, (2) the friction law governing fault slip, and (3) the structural heterogeneity of the earthquake source region, can be taken into account in the simulation. Many of the observed large-scale phenomena associated with earthquakes and fault motions have been reproduced by such simulations (Burridge and Knopoff,1967; Dieterich, 1972; Cohen, 1977; Mikumo and Miyatake, 1978, 1979, 1983; Cao and Aki, 1984), including the occurrence of foreshocks, mainshocks, and aftershocks, correlation among various source parameters, and the occurrence of stable, preseismic and postseismic slips.

However, there is a discrepancy about the stationarity of the magnitude-frequency relation among some of these simulations. Some of them (Dieterich, Cohen) simulated the stable magnitude-frequency relation without suffering from a smoothing effect, although no major events were simulated. By the smoothing effect, we mean that the relative rate of occurrence of small to moderate events in the simulated seismicity decrease with the recurrence of major events.

The others suffered from this smoothing effect, even when they used the same friction law as the former. Andrews (1975, 1978) found that the smoothing effect is existing because tectonic loading cannot change the fault's self-energy (Eshelby, 1957). He also indicated that this difficulty is not removed by letting friction be a function of position because the difference between fault strength and stress will tend to become spatially smoother after each major event. (In the following, we will call this difference the stress deficit because it is the amount of stress needed to be increased in order to initiate a rupture.) Cao and Aki's (1984) simulations with a simple friction law and a slip-weakening friction law confirmed Andrews' conclusions. Therefore, it is interesting and important to clear up this discrepancy. We will show that this discrepancy results from the difference of model parameters, which, however, cannot be arbitrarily chosen in order to remove the smoothing effect. The stress deficit roughening merits furture studies.

The barrier model (Das and Aki, 1977; Aki, 1979) was proposed to offer a physical mechanism for the stress deficit roughening process. In contrast to the barrier model is the asperity model (Kanamori and Stewart, 1978) in which a major earthquake is a stress deficit smoothing process. Obviously, without referring to a particular friction law, we cannot define the role of strong and weak patches on the fault plane. Only after we define a specific friction law, tectonic loading condition, and heterogeneous distributions of parameters in the friction law over the fault

plane, may we determine if strong patches act as barriers or asperities. The same is also for the roughening or smoothing process.

In the present paper, we are mostly interested in seismicity simulations using the state of the art laboratory inferred friction law called the rate and state dependent friction law (Dieterich, 1979, 1980, 1981; Ruina, 1980, 1983). We shall show that the stress deficit roughening process could be simulated by introducing this friction law to a discrete one-dimensional mass-spring model.

In the following, we first describe Andrews' smoothing process precisely, and discuss the choice of relevant model parameters which is responsible for the discrepancy about the smoothing effect. Then, we compare the dynamic solutions of a single block-spring system governed by the rate and state dependent friction law (Rice and Tse, 1983) and the simple friction law. By this comparison, we learn how to specify and simulate a heterogeneous fault. Finally, we extend the dynamic solution to a multiple block-spring system governed by the rate and state dependent friction law.

3.2 Model Parameters Affecting The Spatial Smoothing of Stress Deficit

Wesson and Ellsworth (1973) qualitatively discussed the smoothing process in which the difference between fault strength and stress become spatially smoothed with each event. In order to explain observed seismicity preceding moderate earthquakes in California, they considered that the difference between strength and

stress are inhomogeneous along a fault. Small earthquakes occur on patches where the failure criterion is met locally. Individual small earthquakes will lead to a spatial smoothing of the difference between strength and stress, that we have defined as the stress deficit. As the stress deficit becomes smoother in space, the failure will occur simultaneously over a large area, resulting in an occurrence of a large earthquake. Wesson and Ellsworth, however, did not consider the undesirable consequence of spatial smoothing of the stress deficit on the magnitude-frequency relation. Andrews (1975) also showed that the faulting process in an initially heterogeneous stress environment tends to smooth out the irregularities; after sufficient slip has occurred, the difference between strength and stress becomes less and less along the fault, and the heterogeneity in stress deficit disappears or decreases.

A numerical experiment which dramatically shows this smoothing effect is Mikumo and Miyatake's simulation (1979, 1983). Their frictional fault models have non-uniform distributions of strength and relaxation time and the fault is subjected to a time-dependent shear stress. They concluded that the main physical parameters that control seismicity patterns are the forms of distributions of static and sliding frictional strength and their spatial variations over a fault and also the rate of increase of tectonic stress. Figure 1 shows their case B1 in which non-uniformity of the strength distribution is classified as moderate to heavy (200~408 bars). The smoothing effect is very obvious. After the major event which occurs on the 2700th day of the simulation, we rarely see small

events. All their simulations from weakly to heavily non-uniform fault strength distributions showed this effect although the smoothing process takes a longer time for an initially more heterogeneous fault. In Cao and Aki's (1984) one-dimensional mass-spring model simulations, this effect also appeared when they used both the simple friction law and the slip weakening friction law (Stuart, 1979a,b).

On the other hand, the one-dimensional mass-spring model simulations by Dieterich (1972) and Cohen (1977) apparently did not generate the smoothing effect when the simple friction law was used, but their simulations also did not produce major earthquakes. Therefore, there is a discrepancy between simulated seismicities with the same one-dimensional mass-spring model configuration and the same simple friction law. This discrepancy implies that the model parameters could affect the simulated seismicity significantly. Actually, in Cao and Aki's (1984) simulation with the simple friction law, they used exactly the same strength distribution along the simulated fault, periodic boundary condition, and loading as Dieterich's (1972) except a different spring constant ratio was employed. This ratio will be discussed after we briefly introduce the model configuration.

The schematic diagram of a one-dimensional mass-spring fault model originally due to Burridge and Knopoff (1967) is shown in Figure 2. In this model, an array of discrete equal mass (m) elements connected to each other by coil springs is in frictional contact with a surface, which simulates a fault. Each element is

also connected with a moving slab by leaf spring to simulate the tectonic loading. Numerical solutions are obtained by a stepwise forward integration (Wilson and Clough, 1962) as used in Dieterich (1972) and Cao and Aki's (1984) simulations.

In order to simulate a real fault using such a one-dimensional discrete model we must specify block masses, leaf and coil spring constants, and the fault strength which is the static frictional stress between model elements and the contacting surface. First, following Burridge and Knopoff (1967), common values of coil and leaf spring constants C and L are used for all blocks, only the static friction or fault strength is varied from block to block. To specify other parameters, we use Yamashita's formulas (1976) which give appropriate block mass m and spring constants L and C by comparing the equation of motion of a block-spring system with a finite difference approximation of a two-dimensional wave equation in the neighborhood of a vertical fault surface. His formulas for a block with a height Δx in the vertical direction and an effective horizontal extent specified by Δy along the fault and Δz in the direction perpendicular to the fault surface are

$$m = \rho \Delta x \Delta y \Delta z, \tag{1a}$$

$$C = [2(\lambda+\mu)(V_s/V_p)^2+\mu](\Delta x \Delta z/\Delta y), \tag{1b}$$

$$L = \mu \Delta x \Delta y/\Delta z \tag{1c}$$

where ρ is density, λ and μ are elastic constants, and V_s and V_p are S-and P-wave velocities, respectively. In the following modeling we have chosen ρ = 2.8 g/cm^3, $\lambda=\mu=3 \times 10^{11}$ dyne/cm^2, V_s = 3.55 km/sec, and V_p = 6.15 km/sec. In Yamashita's discretization from a

continuum to a block spring model, Δz has the following physical meaning: if a pulse propagates in a direction normal to the fault surface with the shear velocity V_s, the side Δz, which is perpendicular to the fault surface, of the volume contributing to the mass of inertia for the fault motion can be estimated by $V_s t_o$, where t_o is the average rise time during which the fault is dislocated. We have chosen $t_o = 1$ sec. Soon we will show that t_o does not affect the ratio L/C. Following Ohnaka (1973, 1974), the block length Δy along the fault strike direction is chosen equal to vt_o, where v is an average propagating velocity of dislocation in the direction of the fault strike. Here, v = 2.5 km/sec is used. Accordingly, the appropriate value of L/C is about 1/5. From (1b) and (1c) we have $L/C \sim (\Delta y/\Delta z)^2 = (v/V_s)^2$, so that it is an important physical constant instead of a parameter depending on the choices of t_o or Δy and Δz.

Fault strength distribution in the following simulation is the static friction assigned to each block range from 100 to 300 bars, the distribution of assigned values between these limits is uniform for the entire model, and the location on the fault of a specific value within this distribution is random. The ratio between static friction and dynamic friction is 1.25 (Byerlee, 1970; Dieterich, 1972). These, except the L/C ratio, are similar to the simulation of Dieterich (1972). The simulated seismicity pattern with the above ratio of L/C is shown in Figure 3 for block number n=50. In this figure the horizontal scale gives the locations of events on the fault, and the vertical scale indicates the times of occurrence of the events. Time increases downward. A series of horizontally

connected solid diamonds represents a single seismic event extended over the connected blocks. Because we set a stress free initial condition, there is a 17 years long charging period at the beginning of the simulation. After the charging period, large events repeatedly occur with intervals shorter than ten years and very few small events occur between these large events. We could not remove this stress deficit smoothing effect by adding some strong patches (Cao and Aki, 1984). But when we change the L/C ratio from 1/5 to 1 and keep all other parameters and initial conditions the same as in Figure 3, the simulated seismicity pattern is totally changed as shown in Figure 4. This result is very similar to those of Dieterich (1972) and Cohen (1977) who used the same friction law and L/C ratio as the case shown in Figure 4. In this case, the smoothing effect does not occur but no major earthquakes, which break the entire fault segment simulated, are simulated.

From the above examples, we see that the stress deficit smoothing effect is affected by different L/C ratios. The choice of smaller C reduces the interaction among blocks and then removes the smoothing effect but excludes simulating major events as well. In order to keep the simulation applicable to actual fault, we cannot make C too small without violating the assumption of equation (1). Thus, we have to look for other ways to solve the problem. One purpose of the present study is to check if the stress deficit smoothing effect during major events can be removed by introducing a proper friction law to the mass-spring model.

3.3 Rate and State Dependent Friction Law

Before we explain why the rate and state dependent friction law is chosen for our simulation, it is convenient to introduce the dynamic solution of a single block-spring system (Figure 5a) controlled by the simple friction law. In the absence of any initial motion of a block the frictional resistance prevents sliding until the stress rises to the value $\sigma_n f_s$, where f_s is the coefficient of static friction and σ_n is the normal stress. Once sliding has begun, the frictional resistance drops to the dynamic value $\sigma_n f_d$, where f_d is the coefficient of dynamic friction. In this case, it is not difficult to obtain an analytic solution of the motion for such a single block spring system (for example, Cohen, 1979). The total displacement Δd and the frictional stress drop $\Delta\tau$ in a slip event are

$$\Delta d = 2\sigma_n(f_s - f_d)/K \qquad (2)$$

and

$$\Delta\tau = 2\sigma_n(f_s - f_d)$$
$$= \Delta d/K \qquad (3)$$

where K is the stiffness of the spring. Here, we have implicitly assumed $f_d > 0.5f_s$, which makes sure that the slip velocity never changes direction (Cohen, 1977).

If we have a chain of blocks connected by springs to simulate a fault (Figure 2) which has a heterogeneous distribution of (f_s-f_d) values, the strong fault segments with relatively large (f_s-f_d) tend to slip more than the weak neighbors and will be arrested or decelerated by the weak neighbors which stop earlier and recover their frictional strength instantaneously to a static friction. Because of this interaction between neighboring blocks, the strong

blocks cannot release as much stress as predicted by (3) for the case of a single block. Then, higher stress is left at strong segments, so that after a major slip event the difference between strength and stress along the fault becomes spatially smoother than before the slip and thus the major event itself is a smoothing process. Of course, the interaction is weak when the coil spring constant which defines the connection between blocks is small and will disappear when the spring constant is zero. For the small spring constant case as we showed in the preceding section, the smoothing effect does not appear but no major events can be simulated. In order to simulate a real fault with major events, however, we cannot have coil spring constant too small. Thus, the smoothing effect seems unavoidable.

Actually, it can be avoided. From the analysis described earlier we found that the interaction between blocks depends upon not only the connecting spring constant but also the relative motion of blocks and the time duration of the interaction. With the same connecting spring constant, two blocks having more different speeds will have stronger interaction than those having less different speeds, especially when the interaction finishes in a short time; here, the finishing time is affected by the friction between blocks and the contracting surface. One extreme case is that two blocks moving at same speed have no interaction at all even if they are connected by a strong but unstressed spring. Because the relative motion between blocks and the interacting time also affect their final interaction, it becomes apparent that during a major event the

first stopped weak segment (relatively small f_s-f_d) will have different interactions with the further moving strong segment due to the different healing processes of the frictional strength. The further moving strong fault segment will be arrested or decelerated sooner by the weak segment with a instantaneous healing than with a time dependent healing or the weak segment with a time dependent healing will accommodate itself to the further moving strong segment easier than with a instantaneous healing. Starting from the same relative velocity the interaction time or the time for reaching final stop is longer for the time dependent healing than that for the instantaneous healing, so that the interaction in the case of instantaneous healing is stronger than in the case of time dependent healing.

The interaction between fault segments is important mainly at the stages of slip initiation and termination, because between these two stages, fault segments have similar velocities or small velocity difference and their interaction is small. For the slip initiation stage, small difference exists among different friction laws in terms of interaction among fault segments. Thus, in order to remove the smoothing effect or more precisely to introduce a stress deficit roughening process but still keep the connection (represented by coil spring in our modeling) between fault segments strong enough to produce major events, we need to introduce a friction law which defines a time dependent healing. Such a fault zone constitutive law was developed by Dieterich (1979, 1980, 1981) and Ruina (1980, 1983) to explain a number of laboratory friction experiments on both

clean and gouge-filled sawcuts in granite. One or more state variables are introduced, which evolve with slip or time in such a way that the effects in various experiments can be predicted. This will result in the new friction law having the feature for a time dependent healing. Mikumo and Miyatake (1978, 1979, 1983) included a time dependent healing in their seismicity simulation, but they assumed a spatially homogeneous dynamic friction and a common renewed static friction during the arresting stage of fault slip. The homogeneity of these parameters apparently results in the stress deficit smoothing effect as found in all of their simulations mentioned earlier.

One of the simplest forms of the new rate and state dependent friction law (Ruina, 1980, 1983) describes the fault strength in terms of the coefficient f of friction (see Mavko, 1983):

$$f = A_1+\theta+A_2\ln(V/V_o) \qquad (4a)$$

$$\dot{\theta} = -[V/D][\theta+A_3\ln(V/V_o)] \qquad (4b)$$

Where V and θ are the sliding rate and state variable respectively (thus the name of the friction law), the others, including A_1, A_2, A_3 and D are material constants; V_o is an arbitrary constant with the dimension of velocity. Later, we shall see that A_1 is a nominal value of friction which does not affect the dynamic solution of a system and D the characteristic sliding distance is similar to the critical displacement in the slip-weakening friction law. Some of the important features about this friction law, useful for the further discussions, can be summarized as follows (Ruina, 1984; Mavko, 1983).

1. The coefficient f is determined by two competing effects (Figure 5). First, f has a positive viscous-like dependence on instaneous changes of slip velocity ($V_1 \rightarrow V_2$, $V_2 > V_1$ in Figure 5) as described by the last terms on the right side of (4a). Second, f has a negative dependence on non-instantaneous changes of slip velocity (V_2 is kept for a finite duration) as described by θ in (4). The curve in Figure 5b shows these two effects. The coefficient increase due to the positive viscous-like dependence is $\Delta f = A_2 \ln(V_2/V_1)$; the coefficient decays to a low value $f_2 = (A_3 - A_2)\ln(V_2/V_1)$ due to the negative dependence (Mavko, 1983).

2. The concept of steady sliding has a central role in the rate and state dependent friction law proposed by Dieterich (1979, 1980, 1981) and Ruina (1980, 1983, 1984). In those experiments which led to the rate and state dependent friction law sliding is steady or perturbed from the steady state. As shown by Mavko (1983) for a constant driving velocity V_{ss}, the steady slip velocity is also V_{ss} and the steady value of the state variable θ is:

$$\theta_{ss} = -A_3 \ln(V_{ss}/V_o) \qquad (5)$$

and the steady state coefficient of friction is

$$f_{ss} = A_1 + (A_2 - A_3)\ln(V_{ss}/V_o) \qquad (6)$$

3. The stability criterion for a steady state has been found by Ruina (1980, 1983), Rice and Ruina (1983), and Gu et al. (1984) using linearized analysis that small perturbations about a steady solution for the hypothetical sliding experiment (Figure 5) are neutrally stable if

$$\beta = \frac{(A_3-A_2)\sigma_n}{KD} = 1 \qquad (7)$$

unstable if $\beta>1$, and stable if $\beta<1$, where σ_n is the normal stress. For convenience in the following, the stiffness K is defined as the rate of change of stress with respect to fault displacement. $(A_3-A_2)<0$ is a special case which makes a block creeping without instability. This kind of sliding may exist at the creeping sections of the San Andreas fault and below the depth (~15 km) for the brittle-ductile transition (Mavko, 1983; Tse and Rice, 1985).

From Yamashita's (1976) formula (1) and the above stability criterion (7), we can estimate the maximum characteristic sliding displacement D of a fault segment represented by a block for having instability in the one-dimensional modeling (Figure 2). The stiffness K in (7), defined as the rate of change of stress with respect to fault displacement for the surrounding elastic earth of block i is given by Cao and Aki (1984)

$$K_i = -\frac{\partial(F_i/A_i)}{\partial d_i} = (2C_i+L_i)/A_i \qquad (8)$$

where F_i is the static force acting on block i due to displacements of neighboring blocks i-1 and i+1 and the driving slab, d_i is the displacement of block i, C_i and L_i are coil and leaf spring constants respectively, A_i is the area of the side face of block i. If we assume $A_i=A=\Delta x\Delta y$, $m_i=m$, $L_i=L$, $C_i=C$ and $K_i=K_o$ for all blocks, then we have

$$K_o = [(14/3)\mu\Delta z\Delta x/\Delta y + \mu\Delta y\Delta x/\Delta z]/(\Delta x\Delta y)$$
$$= (14/3)\mu\Delta z/(\Delta y)^2 + \mu/\Delta z$$

where $\mu=\lambda$ and $(V_s/V_p)^2 = 1/3$ have been assumed. If we further choose Δz and Δy the same as in the previous section, then we obtain $K_o \simeq 8.7 \times 10^6$ (dyne/cm^3). For (A_3-A_2) and σ_n we use the same values as used in Mavko's (1983) one-dimensional modeling ($A_3-A_2=0.002$, σ_n = 3 kbar). We find that the instability criterion ($\beta>1$) for a block in Figure 2 is $D<0.68$ cm. Because K_o is rise time dependent through Δy and Δz, D is also rise time dependent. When we choose a longer rise time and simulate a larger event, K_o will be smaller and D will be larger. This is consistent with observations and theoretical results (Papageorgiou and Aki, 1983).

This result on the upper limit of D for the unstable behavior is remarkably close to the slip-weakening critical displacement (0.8 cm) obtained according to seismicity simulations using a displacement hardening-softening friction law (Cao and Aki, 1984). In that study, they used the same model configuration and same rise time as in the example above and found if a critical displacement was chosen at the same order of magnitude as the slip-weakening critical displacement estimated by Papageorgiou and Aki (1983) from strong motion data, the simulation of a heterogeneous fault can produce a normal seismicity pattern which includes small to large earthquakes and even a quiescence period before large earthquakes. The above correspondence between slip-weakening critical displacement and characteristic sliding displacement suggests that

at least for the part before instability, the slip weakening is an approximation of the stress-slip relation observed with the rate and state dependent friction law.

Before we can use the rate and state dependent friction law for seismicity simulation, we need to clear up certain things which are important for modeling heterogenous faults. This can be done by comparing the dynamic solution of a single block-spring system controlled by the rate and state dependent friction law (Rice and Tse, 1985) with the solution of the same system controlled by the simple friction law.

3.4 Comparison of dynamic motions of a single block-spring system

A fairly comprehensive analysis of quasi-static slip motion and its possible instabilities has been done for one state and two state variable laws with a single spring-block system (Rice and Ruina, 1983; Rice and Gu, 1983; Gu et al., 1984). The equation of motion for such a system in a quasi-static condition is an equilibrium equation between driving force and friction

$$\sigma_n f = K(U_r - U) \qquad (9)$$

where U_r is the displacement of driving plate and U is the block displacement (Figure 5). According to (4), the sliding velocity will increase as an instantaneous response to keep the balance of (9). This process will eventually lead to the violation of quasi-static assumptions because the velocity increases too rapidly. In treating this problem, Dieterich (1981) suggested an approximate method in which a cut-off velocity V_{max}, independent of equilibrium

equation (9), is introduced. By limiting the maximum sliding velocity to V_{max}, the computation can be continued through the instability until the spring force is relaxed enough for the quasi-static condition to be once again satisfied. This method was also adopted in Mavko's (1983) simulation. Clearly, this method will introduce unpredictable distortion to the final solution, especially a common cut-off velocity may introduce artificial smoothing effect during a slip event, and may not be suitable for the purpose of the present study. A more rigorous treatment is to include inertia effects in (9). Such a problem has been solved by Rice and Tse (1985). For the convenience of later description, we write down the basic formulas in our own notation and the parameters we used. Then, the equation of motion is given by

$$m \frac{d^2U}{dt^2} + A\sigma_n f = AK(U_r - U) \qquad (10)$$

where m is the block mass, t is time and A is the area of the block side face. Here, we first assume that the direction of slip velocity will not change ($dU/dt>0$), the corresponding criterion will be given later. Thus, the sign before the second term on the left side of (10) does not change. If we take the time derivative of (10) and (4a), then by using (4b) and collecting terms we obtain the following three simultaneous ordinary differential equations which govern the system,

$$\frac{dV}{dt} = a \tag{11a}$$

$$\frac{d\theta}{dt} = -\frac{V}{D}[\theta + A_3 \ln(V/V_o)] \tag{11b}$$

$$\frac{da}{dt} = \frac{AK}{m}(V_r - V) + \frac{AV\sigma_n}{mD}[\theta + A_3 \ln(V/V_o)] - \frac{AA_2 a\sigma_n}{mV} \tag{11c}$$

where a is the acceleration, V_r is the driving velocity and V is the block slip velocity. These simultaneous equations can be easily solved by using the Runge-Kutta method as shown by Rice and Tse (1985). Of course, when the acceleration is very low we still can perform the calculation in a quasi-static regime. In this regime, equation (11) reduce to two equations:

$$\frac{dV}{dt} = \frac{K}{A_2\sigma_n}V(V_r - V) + \frac{V^2}{A_2 D}[\theta + A_3 \ln(V/V_o)] \tag{12a}$$

$$\frac{d\theta}{dt} = -\frac{V}{D}[\theta + A_3 \ln(V/V_o)] \tag{12b}$$

In the actual calculations, we switch from (11) to (12) when the inertia force (the first term on the left side of (10)) becomes smaller than one thousandth of the friction force (the second term on the left side of (10)); then switch back to (11) when the inertia term becomes larger than one thousandth of the friction force. Here, one thousandth is arbitrarily chosen but small enough to keep the transition smooth. Since A_1 does not appear in (11) and (12) and will not affect the solution, we will use the relative friction

coefficient ($f-A_1$) and the corresponding relative fault friction in the following discussion without specifying "relative" again.

The time step Δt used in the calculation is adjusted automatically. From (11) and (12), as indicated by Rice and Tse (1985), there exists two characteristic time scales in the problem. One is characterized by the ratio of the characteristic slip displacement of the friction law to the block velocity, D/V. Another is characterized by the ratio of velocity to the acceleration, V/a. In the calculations of this section and the next section, $\Delta t = 0.1$ D/V and $\Delta t = 0.1$ V/a are used for dynamic and quasi-static cases, respectively.

Other parameters and constants in equations (11) and (12) are chosen as $\Delta x = 10$ km, $\Delta y = 2.5$ km, $\Delta z = 3.55$ km, $\rho = 2.8$ g/cm^3, $V_r = 3.5$ cm/yr, $V_o = 3.5$ cm/yr, $\sigma_n = 3$ kbar, $A_2 = 0.002$, $A_3 = 0.004$ and $K = 3.7 \times 10^6$ dyne/cm^3. By changing D in (7), we can simulate a stable ($\beta<1$), unstable ($\beta>1$) or neutrally stable ($\beta=1$) system. The initial conditions of acceleration, and state variable θ are set equal to the exact values for the steady-state sliding at slip velocity V_r at which $\theta(t=0) = 0$, $a(t=0) = 0$. The system is perturbed by setting the initial slip velocity V = 4.7 cm/yr which is larger than the steady value $V = V_r = 3.5$ cm/yr.

The numerical solutions show that the perturbation to a neutrally stable (D = 1.624 cm, $\beta = 1$) system causes steady oscillations in slip velocity and friction at constant amplitude; the perturbation to a stable (D = 1.8 cm, $\beta = 0.9$) system damps out

and all variables tend toward the steady solution. These results are exactly the same as Mavko's (1983) because the solutions still belong to the quasi-static case. The solution for an unstable (D = 1.476 cm, β = 1.1, A_3-A_2>0) system is described in detail as follows.

As shown in Figure 6, the initial perturbation in velocity causes oscillations in slip velocity and friction that grow in amplitude until the instability. The welding points between quasi-static and dynamic calculations are idicated by W_1 and W_2 in Figure 6a. This figure was first got by Rice and Tse (1985). After W_1, the slip velocity quickly reaches a maximum value at point S and starts to decrease. Point S must be on the steady state line because the acceleration is close to zero for an extended slip distance around this point. Shortly before and after S, the system slides under a nearly steady state condition until further shortening of the spring is hampered at R. Then, as indicated by Rice and Tse (1985), the block is "arrested" within an extremely short displacement (Figure 6b, R~W_2) and the slope of line RW_2 in Figure 6a is $\sigma_n A_2$. This means that during the "arrest" the state variable does not change or the state is frozen. At the end of the "arrest" (W_2), the inertial force is negligible again and quasi-static calculation is resumed. During this quasi-static stage (W_2 to W_1 on left side of Figure 6a), the friction increases to a maximum value τ_p at P and then decreases rapidly so that the block is accelerated again leading to another unstable slip event, and the cycles of the system motion are repeated exactly.

This solution is very different from using the simple friction law, especially at points P and W_2 (Figure 6b). Figure 7 shows a schematic comparison between these two friction laws. The shaded area on the left side of point S represents the block kinetic energy which is obtained from the excess of spring force over the friction after the instability. Around point P, the rate and state dependent friction law predicts hardening followed by softening; The simple friction law predicts an instantaneous change of motion from static to dynamic when the stress reaches a threshold τ_s (static friction). After point W_2, the simple friction law assumes an instant healing to τ_s, while the new friction law involves a non-instantaneous healing. Another difference is about the relation between friction strength and stress. In the case of the simple friction law, the frictional stress is not always balanced with the friction strength. The strength can only have two values, the static friction τ_s and dynamic friction τ_d, but according to Cohen (1979) the frictional stress could be any value between τ_s and $(\tau_d-(\tau_s-\tau_d))$ (Figure 7). In the case of the rate and state dependent friction law, the frictional stress is always balanced with the frictional strength, the minimum strength τ_{w_2} reached at point point W_2 is much lower than the value τ_{ss} at the steady sliding point S. These differences are important in explaining the seismicity simulation results in the following sections. By the comparison in Figure 7, we also can find the criterion for $dU/dt>0$

in (10) where the new friction law is used. It is $\tau_{ss}>0.5\tau_p$, which is similar to $f_d>0.5f_s$ for the case of the simple friction law (Cohen, 1979).

The velocity measure $\ln(V/V_o)$ vs. time curve (Figure 6c) shows that before the unstable slip the velocity has increased to a value higher than the driving velocity and after the unstable slip the velocity decreases to a value much lower than the driving velocity. Figures 6d and 6e are the time changes of frictional stress (relative to the nominal value $\sigma_n A_1$) due to changes of $(\Theta+A_2\ln(V/V_o))$ and Θ respectively in (4a). A comparison between these two curves shows that the change of frictional stress before and after an unstable event is mainly due to the change of state variable θ not the change of velocity through term $A_2\ln(V/V_o)$. According to (4b), θ evolves very slowly right after the event because slip velocity changes very slowly. This is the non-instantaneous healing.

From Figure 6b, we can define a frictional strength drop by the difference between maximum strength τ_p at P and minimum strength τ_{w_2} at W_2. In the case of the simple friction law, we can define a frictional strength drop by the difference between static and dynamic friction (Mikumo and Miyatake, 1978). For the rate and state dependent friction law, the frictional stress drop is proportional to (A_3-A_2) (Mavko, 1983). The frictional stress drop

for A_3-A_2=0.002 in Figure 6b is 220 bars. Figure 6f is for a system in which only A_3-A_2 = 0.0022 is larger than in Figure 6b, the stress drop for this system is 250 bars. Therefore, a larger difference of A_3-A_2 means a higher stress drop or a higher effective stress (Kasahara, p. 139, 1981) if we borrow this name for the rate and state dependent friction law. As indicated by Brune (1970), Kanamori (1972) and Yamashita (1976) among others, dynamics of fault rupture are determined by the effective stress. In other words, the absolute stress is irrelevant to the dynamic fault motion and we cannot use a heterogeneous distribution of the nominal parameter A_1 in (4a) to specify a heterogenous fault. From the above comparison between Figures 7b and 7f, we see that we can use a heterogeneous distribution of (A_3-A_2) values along a fault to specify a heterogeneous fault model. In the dynamic meaning, a fault segment with larger (A_3-A_2) value or larger effective stress will behavior stronger than the segment with lower (A_3-A_2) value. For example, the displacement in each unstable event is larger for a single block spring system with larger (A_3-A_2) value when the system is driven by the same constant velocity; a larger displacement in each event means fewer events in a fixed time period but each event is larger. Therefore, in the case of the simple friction law, a fault rupture process is completely specified by the distributions of static and dynamic frictions and the initial stress along the fault (Mikumo and Miyatake, 1978); now, for the new friction law a rupture process of

a heterogeneous fault is determined by a heterogeneous distribution of (A_3-A_2) values and a set of initial conditions along the fault. In the following, for the convenience of descripton we will use "strong or weak" to mean the fault segments with larger or smaller (A_3-A_2) values as well as their effective stresses.

So far, we have shown how to build up a heterogeneous fault model controlled by the rate and state dependent friction law, so we are ready to apply the rate and state dependent friction law to a multiple block-spring system.

3.5 Dynamic solution of a multiple block-spring system

Now, we use the schematic model shown in Figure 2 to simulate a fault which is governed by the rate and state dependent friction law. The calculation is performed dynamically as for a single block-spring system.

The equation of motion for block i is derived by calculating the friction force from (4), we have

$$ma_i = \sum_{j=i-1}^{i+1} K_{ij}d_j + LV_r t - A\sigma_n[A_1^i + \theta_i + A_2^i \ln(V_i/V_o)] \qquad (13)$$

where the common values of m, C, L and A have been used, the superscript and subscript i's denote ith block, K_{ij} is a stiffness matrix, $K_{ij} = C$ for $i \neq j$ and $K_{ij} = -(L+2C)$ for $i=j$. By taking the time derivative of (13) and combining the equation for θ, we obtain

the simultaneous equations of motion of block i as

$$\frac{da_i}{dt} = \sum_{j=i-1}^{i+1} \frac{K_{ij}}{m} V_j + \frac{LV_r}{m} - \frac{A\sigma_n}{m}\{- \frac{V_i}{D_i}[\theta_i + A_3^i \ln(V_i/V_o)] + A_2^i \frac{a_i}{V_i}\} \tag{14a}$$

$$\frac{d\theta_i}{dt} = - \frac{V_i}{D_i}[\theta_i + A_3^i \ln(V_i/V_o)] \tag{14b}$$

$$\frac{dV_i}{dt} = a_i \tag{14c}$$

where the unknown variables are a_i, V_i and θ_i. When the inertial force become smaller than one thousandth of the friction, we switch to the following equations

$$\frac{dV_i}{dt} = \sum_{j=i-1}^{i+1} \frac{K_{ij}}{A_2^i} V_i V_j + \frac{LV_r}{A_2^i} V_i + \frac{A\sigma_n}{A_2^i D_i} V_i^2 [\theta_i + A_3^i \ln[V_i/V_o)] \tag{15a}$$

$$\frac{d\theta_i}{dt} = - \frac{Vi}{D_i}[\theta_i + A_3^i \ln(V_i/V_o)] \tag{15b}$$

where the unknown variables are only V_i and θ_i. If a fault is simulated by a model with n blocks, i in (14) or (15) or in (14) and (15) together ranges from 1 to n. For example, if all the blocks are slipping dynamically, the system is described by 3n equations from (14); if all the n blocks are moving quasistatically, the system is described by 2n equations from (15); if n_1 blocks are slipping dynamically and n_2 blocks are moving quasistatically ($n_1+n_2=n$), the system is described by $3n_1+2n_2$ equations in which $3n_1$

equations are from (14) and $3n_2$ equations are from (15). All these $3n_1+2n_2$ simultaneous equations are ordinary differential equations and can be solved using Runge-Kutta method.

The time step Δt is self-adjustable as in the case of a single block-spring system in the previous section. After each step, we can obtain a suitable Δt for each block, $\Delta t = 0.1\ D/V$ or $\Delta t = 0.1\ V/a$, where D, V and a are the characteristic sliding displacement, sliding velocity and acceleration of that block. The minimum Δt among all blocks will be the one for the next step. Indeed, near the end of the "arrest" the velocity has reduced to a low value but the deceleration may still be high; or during the nearly steady state slip around S (Figure 6b), the slip velocity is very high. Both of the cases will limit Δt as short as 10^{-3} sec to 10^{-5} sec and make the numerical calculation very time consuming when n is large. We have chosen n=10, much smaller than in Figures 3 and 4, in the following simulations.

For the boundary conditions, we also introduce a periodicity of the block elements along the fault to avoid anomalous conditions at the ends of the model (Dieterich, 1972). We have

$$d_o = d_n$$

$$V_o = V_n$$

$$a_o = a_n$$

and

$$d_{n+1} = d_1$$

$$V_{n+1} = V_1$$

$$a_{n+1} = a_1$$

The initial conditions of slip velocity, acceleration and state variable for each block are set equal to the exact values for steady sliding at driving velocity V_r = 3.5 cm/yr, except for one block (i=8) which is the block to be perturbed. These values are $\theta_i = 0$ (i=1-10), $a_i = 0$ (i=1-10), V_i = 3.5 cm/yr (i=1-7, 9-10) and V_8 = 4.5 cm/yr. Obviously, a successful modeling in seismicity simulation should not be initial-condition dependent, especially for the study of a stationary magnitude-frequency relation. In practice the system we are simulating may never undergo a state of motion defined by the assigned initial conditions above, but after sufficient time the effect from initial conditions should die out. It is safe to choose those initial values to be uniform along the fault for the study of stress deficit roughening. Conversely, results from a heterogeneous distribution of initial values may mainly reflect the influences from the initial conditions if the simulation time is not long enough to reach a steady state.

The model parameters of m, L, C and A for each block are chosen to be the same as in simulations of Figures 3 and 4. Thus far, parameters which have not been chosen are A_2^i, A_3^i and D_i (i=1-10) in the friction law. A heterogeneous fault is simulated by setting

heterogeneous distributions of these values along the fault. Parameter A_1^i, the nominal value of friction coefficient, again does not affect the solution. The difference $(A_3^i-A_2^i)$, which compares the inverse and direct velocity dependences, defines the effective stress of block i as discussed in the previous section for a single block-spring system. Hence, we have assigned $(A_3^i-A_2^i)$ values along a fault by the following steps. First, a set of 10 basic $(A_3^i-A_2^i)$ values, which range from 0.0002 to 0.0012, are assigned to 10 blocks. The values, which are uniformly distributed between these limits, are randomly assigned to all blocks. Second, we change some of the $(A_3^i-A_2^i)$ values to let some blocks have much higher (A_3-A_2) values and some blocks have negative (A_3-A_2) values.

According to the results described in the previous section, a block i with a positive $(A_3^i-A_2^i)$ value much larger than other blocks is dynamically a strong patch and a block with a negative $(A_3^i-A_2^i)$ value is a creeping patch. For convenience, A_2^i is fixed to be 0.002 for all blocks and for all simulations and only A_3^i is changeable from block to block and from simulation to simulation. For simplicity, β is fixed at 1.7 for all blocks in all simulations, except for those blocks with $(A_3^i-A_2^i)<0$. In the following simulations, we have chosen $(A_3^i-A_2^i)=-0.001$ for all the creeping blocks. Basically, we can try four kinds of fault models, although we do not know if the simulated seismicities are qualitatively different. They are (1) a fault with strong patches but no creeping patches; (2) a fault with strong and creeping patches; (3) a fault

with creeping patches but no strong patches; (4) a fault without strong and creeping patches. With the assigned model and material constants above, we can calculate the frictional strength drop for each block according to the solution of a single block-spring system. Then, we can get four distributions of the strength drop along a fault for these four fault models as shown in Figure 8. The simulated four seismicity patterns are shown in Figure 9, which is plotted in the same way as in Figures 3 and 4.

Simulation (a) in Figure 9 is for the case of a fault with strong patches (blocks 6 and 7) but no creeping patches. The basic features of this simulation are (1) major events which rupture the entire fault occur in about every sixty years time interval, (2) during the ten years before and twenty years after the major events (A and B), the level of seismicity is very low, (3) between major events, there are many small events, (4) no aftershocks are simulated after major events, (5) small events between major events tend to occur in clusters in space and time but outside the strong patches. In Chapter 4, which is for studying slip rate and stress drop, we simulate seismicity for more than 200 years in which more major events were simulated. These simulations also confirm the results above.

Simulation (b) in Figure 9 is for the case of a fault with strong patches (same as in simulation (a)) and creeping patches (blocks 1, 3 and 9). The simulated seismicity is very similar to

that of (a). The differences are (1) time interval between major events is slightly shorter than in (a), (2) the quiescence periods of small events before and after the major events are about 5 years which is much shorter than in simulation (a), (3) small events between major events tend to occur very uniformly in space and time.

Model (c) in Figure 8 is for the case of a fault with creeping patches as in (b) but no strong patches. The simulated seismicity (Figure 9c) is very different from models (a) and (b). The features of this simulation are (1) there are no major events but many small events that occur uniformly in space and time, (2) the uniform initial conditions in velocity and state variable cause clustering of small events in a shorter time period along the major part of the fault, but the effect of the initial conditions dies out very quickly.

Simulation (d) in Figure 9 is for the case of a fault without strong and creeping patches. No major events but many small events are produced by this model. The small events do not occur uniformly in space and time but tend to occur as a swarm over the entire fault in a short time period (1-2 years).

These four simulations above are all different. However, they do have one thing in common which is that none of them show the tendency toward declining number of small events. Thus, an observed stationary magnitude-frequency relation may be simulated by using the rate and state dependent friction law to a heterogeneous fault

even with a low L/C ratio that was found to cause smoothing in the similar models. This result does not depend on the level of fault heterogeneity or initial conditions, so it is encouraging because of the fact that the stationarity of magnitude-frequency relation holds commonly (such as discussed by Schwartz and Coppersmith, 1984).

The four simulations, in which only two kinds of significantly different seismicity patterns were obtained, also suggest some interesting relations. First, by comparing simulations (a) and (b) with simulations (C) and (d) we see that strong patches may be necessary for having major events on a fault. Second, when a fault has creeping patches small events do not occur in clusters in space and time as shown in simulations (b) and (c). Of course, these relations are preliminary because we tried only a few examples.

Fault sections, which showed either high creep rate and low level seismicity or low creep rate and high level seismicity have been observed along the San Andreas fault. In the former case small earthquakes and aseismic creep relieve at least a fraction of the accumulating strain (Wesson et al., 1973). Therefore, according to simulation (c), it is also suggested that strong patches may not exist on a creeping section and no large earthquakes are expected there. If this is finally true, it will be very useful for earthquake prediction. These are interesting topics to be further studied.

An observed stationary magnitude-frequency relation is related

to a stress deficit roughening process (Andrews, 1978; Aki, 1984). In the section of "the rate and state dependent friction law", we have discussed that this friction law may offer a physical mechanism for such a process because of the introduction of a rate dependent state variable. Now, we can study the changes of stress and stress deficit along a fault for the above simulations (Figure 9). Here, the stress deficit is defined as the difference (τ_p-τ_{w_2}). In cases (c) and (d), no major events occur, so that they are not good examples for studying the roughening process. We choose simulation (a) as an example. The distribution of stress deficit along the fault simulated at three times, 0.1 year before and 0.1 year after the major events and 19 years after the major events, are plotted in Figures 10 and 11.

From these curves, one can find (1) 0.1 year before major events (A) and (B) in simulation (a) , the difference between maximum fault strength and current stress has become very smooth along the fault because the smoothing effect of small events as discussed by Wesson and Ellsworth (1973); (2) 0.1 year after the major events (A) and (B), the above difference has been roughened by the major events themselves, the fault no longer shows the smoothing effect discussed by Andrews (1975, 1978); (3) Figures 10b and 11b show the difference between maximum fault strength and current stress due to the state variable θ. A comparison between these curves and the curves in Figures 10a and 11a suggests that the change in θ is responsible for the features described in (1) and (2); (4) because almost no small events occur before and after the

major events for a time period longer than a few years, the difference between curves of 0.1 year after and 0.1 year before the major event gives an approximation of the stress drop along the fault, which is much larger at strong patches than at weak patches; (5) 19 years after the major events, the difference between maximum fault strength and current stress has decreased from 0.1 year after the major events because of the increase of tectonic stress, but the heterogeneity of this difference along the fault does not change because within 19 years no small events have occurred; (6) after those small events which occur between major events (A) and (B), the stress deficit along the fault becomes homogeneous again before event (B), so that the smoothing process caused by small events and the roughening process caused by major events are happening interchangeably which may offer a mechanism for the observed stationary magnitude-frequency relation.

It is necessary to indicate that the stress and frictional strength here are relative values to $\sigma_n A_1$ as mentioned before. This means that we are not using absolute stress or strength, which do not determine the dynamics of fault slip, but we are using the parts of stress and strength which determine the fault dynamics. Thus, the above results are not changed by adding an arbitrary function of position to the coefficient of friction. The roughening process appeared in the simulations above for the fault models with strong patches is also unchanged in the limiting case of a continuous fault. Such a limiting case happens when the spacing between blocks vanishes. According to Knopoff et al. (1973), the coil spring

constant does not vanish in such a limiting case. Therefore, the interaction between blocks still exists and our analysis about the roughening process still holds.

The fault slip as a function of location for event (B) is shown in Figure 12. Similar to the stress drop, which can be derived from the stress deficit curves in Figure 11, the strong patches slip more than the weak patches during a major event. When the simple friction law is used, both the stress drop and slip of a major event are very uniform along the fault after a sufficiently long time even if the fault strength and initial stress distributions are very heterogeneous (Andrews, 1975, 1978; Cao and Aki, 1984).

Our numerical simulations also give all the details of unstable slip for each major event. Figure 13 includes ten slip curves for ten blocks of event (B) in simulation (a) of Figure 9. Each curve represents the value of $\ln(V/V_0+1)$ as a function of time. The area under each curve is a monotonic function of the slip distance of each block. This figure shows that the strong patches (blocks 6 and 7) slip more than the weak patches.

The whole slip process can be approximately divided into three stages according to the relative velocities between neighboring blocks. The first stage is the slip initiation. During this stage, block slips are initiated and accelerated nearly to a common upper limit V_{max} by their first moving neighbors. The velocity change of each block from a small value near zero to V_{max} is accomplished in a very short time duration as compared with what we will see at third stage. According to Newton's second law, large forces or strong

interactions are involved in this stage.

In the second stage, all the blocks slip approximately with a common high velocity. This stage lasts about two thirds of the entire slip duration. During this stage, we see that some blocks slow down or stop but speed up again without affecting their neighboring blocks significantly. This is because the time dependent healing. After the slip initiation every block is easy to be moved and weak interaction exists among blocks.

Following the second stage is the arresting stage. At the beginning of this stage, many weak blocks start to decelerate. In this stage, all blocks slip with velocities different from each other, but most of these velocities are much lower than the high velocities in the second stage. Therefore, the relative velocities between neighboring blocks are much smaller than in the first stage ($\sim V_{max}$) and the interactions are much smaller too. In fact, the velocity change of each block from its highest value ($\sim V_{max}$) to near zero in this stage takes a much longer time as compared with the same amount of velocity change (absolute value) in the first stage. According to Newton's second law, much smaller forces or interactions are involved in this stage as compared with the first stage.

When the simple friction law is used, each block stops from nearly the same high velocity in a relatively short time period just like we have seen at the first stage of Figure 13. Obviously, the difference between the instantaneous healing (the simple friction law) and the non-instantaneous healing (the rate and state dependent

friction law) is responsible for the different final stages of fault slip. This is almost intuitively conceivable if we consider the fault as a whole. It is obvious that a fault slip takes a longer time to stop when the slip is stopped by a smaller friction in the case of time dependent healing. The interaction reduction among blocks is just the result of such stopping process elongation. It is this reduction which permits a non-uniform slip along a fault.

About the non-uniform slip along the fault, there is one more possibility that needs to be discussed. We used non-uniform distributions of the characteristic sliding displacement (D) in the simulations. Before, we have indicated that D has the similar meaning with the slip-weakening critical displacement. Our simulation (Cao and Aki, 1984) with the slip-weakening friction law, a heterogeneous distribution of its critical displacement, and a same low spring constant ratio L/C suffered from the smoothing effect, so that the possibility of heterogeneous distribution of D causing non-uniform slip is excluded.

3.6 Discussion and Conclusions

Dynamic slip motion of a single block-spring system (Rice and Tse, 1985) has been extended to a multiple block-spring system following a rate and state dependent friction law which incorporates features observed in rock sliding experiments. Because we have not been able to use this friction law to a more realistic fault model with a large sample of strength distributions as used by Mikumo and Miyatake (1978, 1979, 1983), we could not simulate a great variety

of seismicity patterns observed in situ, but basically two types shown in Figure 9. The first type includes major earthquakes and small earthquakes between those major earthquakes (Figure 9a,b). The second type includes only small earthquakes (Figure 9c, d).

Our seismicity simulations and the analysis of fault slip and stress and strength drops during a major event indicate that the rate and state dependent friction law together with a heterogeneous fault can offer a physical mechanism for the stress deficit roughening process required for the observed stationary magnitude-frequency relation. Since the non-instantaneous healing predicted by the rate and state friction law can reduce the interaction between heterogeneous fault segments, fault slip and stress and strength drops along a fault are heterogeneous too. Therefore, the difficulty in the construction of a model for recurring earthquakes (Andrews, 1978) may be removed by the rate and state dependent friction law.

Because the interaction among fault segments, which are represented by blocks in a discretized one-dimensional fault model, is related to spring constants which characterize the connection of blocks or fault segments, we checked if the spring constants vanish in the limiting case of a continuous fault. We found this does not happen according to Knopoff et al.'s (1973) discussion. Thus, our results are not from fault discretization but hold also for the continuum case.

The simplified form of the rate and state dependent friction law used in this study may require further revision (Okubo, personal

communication). But, the non-instantaneous healing is a fact observed in rock sliding experiments, so that it will remain in the revised forms of the rate and state dependent friction laws. Thus, the main results obtained in this study may not suffer major changes. Of course, further studies are needed considering the fact that only limited number of simulations have been performed.

Our simulations have been performed in a fully dynamic way. The slip process (Figure 13) can be divided into three stages. In the third stage or the arresting stage, the slip velocity of each block varies with time. This result indicates that the quasi-static cut-off velocity procedure used by Dieterich (1981) and Mavko (1983) may not be applicable for studies of stress drop and dynamic slip along a heterogeneous fault.

In summary, we have shown from the numerical simulations of a fault governed by the rate and state dependent friction law that:

1. The rate and state dependent friction law together with a heterogeneous fault simulate non-uniform slip and stress drop along the fault and may provide a physical mechanism for the stress deficit roughening process which is required for an observed stationary magnitude-frequency relation.

2. The physical interpretation for non-uniform slip and stress drop is that the non-instantaneous healing lengthens the time duration for fault slip to stop and reduces the interaction between different fault segments and finally counteracts the smoothing

effect. Here, the interaction is reduced not by reducing the spring constant but by reducing the fault frictional strength due to the time dependent healing. The non-instantaneous healing is described by a state variable in the friction law. When the fault starts to slip quickly, the state variable evolves to a low value and takes a time much longer than the duration of fracture process to be healed up again.

3. Strong patches on the fault may be necessary for the occurrence of large earthquakes. This result is different from the case of using the simple friction law which predicts large events for fault models with or without strong patches (Cao and Aki, 1984).

References

Aki, K., Characterization of barriers on an earthquake fault. J. Geophys. Res., 84, 6140-6148, 1979.

Aki, K., Theory of earthquake prediction with special reference to Monitoring of the Quality Factor of Lithosphere by the Coda Method, Submitted to Proceedings of the U.S.-Japan Symposium on Earthquake Prediction, Tokyo, Nov., 1983.

Aki, K., Asperities, barriers, characteristic earthquakes and strong motion prediction, J. Geophys. Res., 89, 5867-5872, 1984.

Andrews, D.J., From antimoment to moment: plane-strain models of earthquakes that stop, Bull. Seismol. Soc. Am., 65, 163-182, 1975.

Andrews, D.J., Coupling of energy between tectonic processes and earthquakes, J. Geophys. Res., 83, 2259-2264, 1978.

Burridge, R., and L. Knopoff, Model and theoretical seismicity, Bull. Seismol. Soc. Am., 57, 341-371, 1967.

Brune, J. E., Tectonic stress and the spectra of seismic shear waves from earthquakes, J. Geophys. Res., 75, 4997-5009, 1970.

Byerlee, J.D., The mechanics of stick-slip, Tectonophysics, 9, 475-486, 1970.

Byerlee, J.D., Friction of rocks, PAGEOPH, 116, 615-626, 1978.

Cao, T. and K. Aki, Seismicity simulation with a mass-spring model and a displacement hardening-softening friction law, PAGEOPH, vol. 122, 1984.

Cao, T., and K. Aki, Effect of slip rate on stress drop, submitted to J. Geophys. Res., Oct., 1985.

Cohen, S.C., Computer simulation of earthquakes, J. Geophys. Res., 82, 3781-3796, 1977.

Cohen, S., Numerical and laboratory simulation of fault motion and earthquake occurrence, J. Geophys. Res., 17, 61-72, 1979.

Das, S., and K. Aki, Fault planes with barriers: A versatile earthquake model, J. Geophys. Res., 82, 5648-5670, 1977.

Dieterich, J.H., Time-dependent friction as a possible mechanism for aftershocks, J. Geophys. Res., 77, 3771-3781, 1972.

Dieterich, J.H., Modeling of rock friction, 2. Simulation of preseismic slip, J. Geophys. Res., 84, 2169-2175, 1979.

Dieterich, J., Experimental and model study of fault constitutive properties, ASME Appl. Mech. Div., Solid Earth Geophysics and Geotechnology, ed. S. Nemat-Nasser, ASME, New York, 21-29, 1980.

Dieterich, J., Constitutive properties of faults with simulated gouge, Mechanical Behavior of Crustal Rocks, Monograph 24, eds. N.L. Carter, M. Friedman, J.M. Logan, and D.W. Stearns, American Geophysical Union, 103-120, 1981.

Eshelby, J.D., The determination of the elastic field of an ellipsoidal inclusion, and related problems, Proc. Roy. Soc. London, Ser. A, 241, 376-396, 1957.

Gu, J., J.R. Rice, A.L. Ruina and S.T. Tse, Slip motion and stability of a single degree of freedom elastic system with rate and state dependent friction, J. Mech. Phys. Solids, 32, 167-196, 1984.

Kanamori, H., Determination of effective tectonic stress associated with earthquakes faulting, the Tottori earthquake of 1943, Phys. Earth. Plant. Inter., 5, 426-434, 1972.

Kanamori, H., and G.S. Stewart, Seismological aspects of the Guatemala earthquake of February 4, 1976, J. Geophys. Res., 83, 3427-3434, 1978.

Kasahara, K., Earthquake mechanics, Cambridge University Press, pp. 248, 1981.

Knopoff, L., J.O. Mouton, and R. Burridge, The dynamics of a one-dimensional fault in the presence of friction, Geophys. J. Roy. Astron. Soc., 35, 169-184, 1973.

Mavko, G., Large-scale earthquakes from a laboratory friction law, submitted to J. Geophys. Res., Oct., 1983.

Mikumo, T., and Miyatake, T., Dynamical rupture process on a three-dimensional fault with non-uniform frictions, and near-field seismic waves, Geophys. J.R. Astr. Soc., 54, 417-438, 1978.

Mikumo, T., and Miyatake, T., Earthquake sequences on a frictional fault model with non-uniform strengths and relaxation times, Geophys. J.R. Astr. Soc., 59, 497-522, 1979.

Mikumo, T., and Miyatake, T., Numerical modeling of space and time variations of seismic activity before major earthquakes, Geophys. J.R. Astr. Soc., 74, 559-583, 1983.

Ohnaka, M., Experimental studies of stick-slip and their application to the earthquake source mechanism, J. Phys. Earth, 21, 285-303, 1973.

Ohnaka, M., A physical understanding of the earthquake source mechanism, Part II. The fault-slip velocity and acceleration, J. Phys. Earth, 22, 383-394, 1974.

Otsuka, M., A simulation of earthquake occurrence, Phys. Earth Planet. Interiors 6, 311-315, 1972.

Papageorgiou, A.S. and K. Aki, A specific barrier model for the quantitative description of inhomogeneous faulting and the prediction of strong ground motion: Part II, Applications of the model, Bull. Seis. Soc. Am., 73, 953-978, 1983.

Rice, J.R., and J. Gu, Earthquake after-effects and triggered seismic phenomena, PAGEOPH, 121, 187-219, 1983.

Rice, J.R., and J. Gu, Earthquake after-effects and triggered seismic phenomena, PAGEOPH, 121, 187-219, 1983.

Rice, J.R., and A.L. Ruina, Stability of steady frictional slipping, Trans. ASME, J. Appl. Mech., 50, 343-349, 1983.

Rice, J. R., and S. T. Tse, Dynamic motion of a single degree of freedom system following a rate and state dependent friction law, J. Geophys. Res., in press, 1985.

Ruina, A., Friction Laws and Instabilities: A Quasi-static Analysis of Some Dry Friction Behavior, Ph.D. Thesis, Brown University, 1980.

Ruina, A., Slip instability and state variable friction laws, J. Geophys. Res., 1983.

Runia, A., Constitutive relations for frictional slip, Mechanics in Geomaterials, edited by Z. P. Bazant, John Wiley Publishing Co., New York, 1984.

Schwartz, D.P., and K.J. Coppersmith, Fault behavior and characteristic earthquakes: examples from the Wasatch and San Andreas fault zones, J. Geophys. Res., 89, 5681-5698, 1984.

Stuart, W. D., Strain softening prior to two-dimensional strike-slip earthquakes, J. Geophys. Res., 84, 1063-1070, 1979a.

Stuart, W. D., Aging and straining softening model for episodic faulting, Tectonophysics, 52, 613-626, 1979b.

Stuart, W. D., and G. Mavko, Earthquake instability on a strike-slip fault, J. Geophys. Res., 84, 2153-2160, 1979.

Wesson, R.L. and W.L. Ellsworth, Seismicity preceding moderate earthquakes in California, J. Geophys. Res., 78, 8527-8546, 1973.

Wesson, R. L., R. O. Burford and W. L. Ellsworth, Relationship between seismicity, fault creep and crustal loading along the central San Andreas fault, proceeding of conference on tectonic problems of the San Andreas fault system, V, 1973.

Wilson, E.L., and R.W. Clough, Dynamic response by step-by-step matrix analysis. In Symposium on the Use of Computers in Civil Engineering, Lisbon, October 1962, paper 45, pp. 1-14, Laboratorio National de Engenharia Civil, Lisbon, Portugal, 1962.

Yamashita, T., On the dynamical process of fault motion in the presence of friction and inhomogeneous initial stress: Part I, Rupture Propagation, J. Phys., Earth, 24, 417-444, 1976.

Figure Captions

Figure 1. One of the simulated two-dimensional seismicity patterns by Mikumo and Miyatake (1983), which shows the stress deficit smoothing effect. Numbers on the top left of each pattern indicate the time step given in days. Black and outlined areas indicate the shocks that occurred at the indicated time step and ruptured the areas.

Figure 2. A schematic diagram of a discrete fault model (after Burridge and Knopoff, 1967). The blocks representing friction elements are intercontacted by springs to each other and to a moving slab which represents the tectonic driving.

Figure 3. A simulated seismicity pattern using the simple friction law and a spring constant ratio L/C = 1/5. The horizontal scale gives the location of events on the fault, and the vertical scale indicates times of occurrence. A series of horizontally connected solid diamonds represents a single seismic event extended over the connected blocks. Strong stress deficit smoothing effect is obvious.

Figure 4. A simulated seismicity pattern in which only spring constant ratio L/C = 1 is different from in Figure 3. No smoothing effect can be seen.

Figure 5. Friction coefficient vs. slip in hypothetical sliding experiments, after the observations by Dieterich (1979, 1980, 1981). (a) A single degree of freedom spring-slider system. A block of mass m slides distance U with a velocity V and friction τ. The driving force moves distance U_r with a velocity V_r, stressing the block through this spring with stiffness K. (b) When the steady slip rate is switched abruptly from V_1 to V_2 ($V_1<V_2$), we observe an instantaneous increase in friction followed by a gradual decay which happens in a characteristic sliding displacement D (after Mavko, 1983).

Figure 6. A numerical simulation of slip motion of a single block-spring system (Figure 5a) governed by the rate and state dependent friction law. Figures (a) and (b) are first obtained by Rice and Tse (1985). W_1 and W_2 are the welding points between results from quasi-static and dynamic calculations respectively. Friction reaches a maximum value τ_p at point P and a minmum value τ_{w_2} at point W_2. Sliding velocity reaches a maximum value at S. From R to W_2 is the arresting period (Rice and Tse, 1985). In this figure, all the stress and strength are values relative to their corresponding nominal values. (a) Plot of frictional stress versus logarithm of velocity $\ln(V/V_o)$. (b) Plot of frictional stress versus slip distance. (c) Plot of logarithm of slip velocity

$\ln(V/V_o)$ versus time. (d) Plot of frictional stress versus time. (e) Plot of frictional stress due to state variable Θ versus time. (f) Plot of frictional stress versus slip distance, in which everything is the same as in (b) except (A_3-A_2) is larger and one can see that the stress drop $(\tau_p-\tau_{w_2})$ is also larger than in (b).

Figure 7. A schematic comparison of the fault strength and stress between results from the simple friction law and the rate and state dependent friction law. The dashed lines show the evolving spring force. The shaded area on the left side of point S represents the block kinetic energy which is obtained from the excess of spring force over the friction after instability. The healing processes predicted by two friction laws are very different as shown after "arresting" point W_2. The arrows indicate the evolving directions of frictional stress and strength. In the case of the simple friction law, the strength is not continuous, it is plotted by heavy dots (τ_s) and a heavy line (τ_d).

Figure 8. Four fault models used in the simulations. The fault is described by the frictional stress drop which is defined as the difference between maximum and minimum frictional stresses. (A) A fault model with strong patches at blocks 6 and 7. (b) A fault model with strong patches at

blocks 6 and 7 and creeping patchs at blocks 1, 3 and 9. (c) A fault model with creeping patches at blocks 1, 3 and 9 but no strong patches. (d) A fault model with neither strong nor creeping patches.

Figure 9. Simulated seismicity patterns using the rate and state dependent friction law to four fault models shown in Figure 8. The plot is done in the same way as in Figures 3 and 4.

Figure 10. The time changes of stress deficit around event (A) in Figure 9a. The stress deficit is defined as the difference between maximum fault strength τ_p and current fault stress τ. (a) Plots of the stress deficit distribution along the fault length in which the fault stress is a total stress due to $(\theta+A_2\ln(V/V_o))$. (b) Plots of the stress deficit distribution along the fault length in which the fault stress is only a fraction of the total stress due to state variable θ.

Figure 11. Same as Figure 10 but all the plots are for the times before and after event (B) in simulation (a) of Figure 9.

Figure 12. Fault displacement of event (B) in simulation (a) of Figure 9.

Figure 13. Plots of logarithm of velocity $\ln(V/V_o+1)$ versus time for each block. This figure shows that in the arresting stage, the block velocities decrease from their upper limit to near zero within relatively long time periods. The value of $\ln(V/V_o+1)$ has been normalized by $\ln(V_{max}/V_o+1)$, where V_{max} is the maximum velocity reached among all blocks.

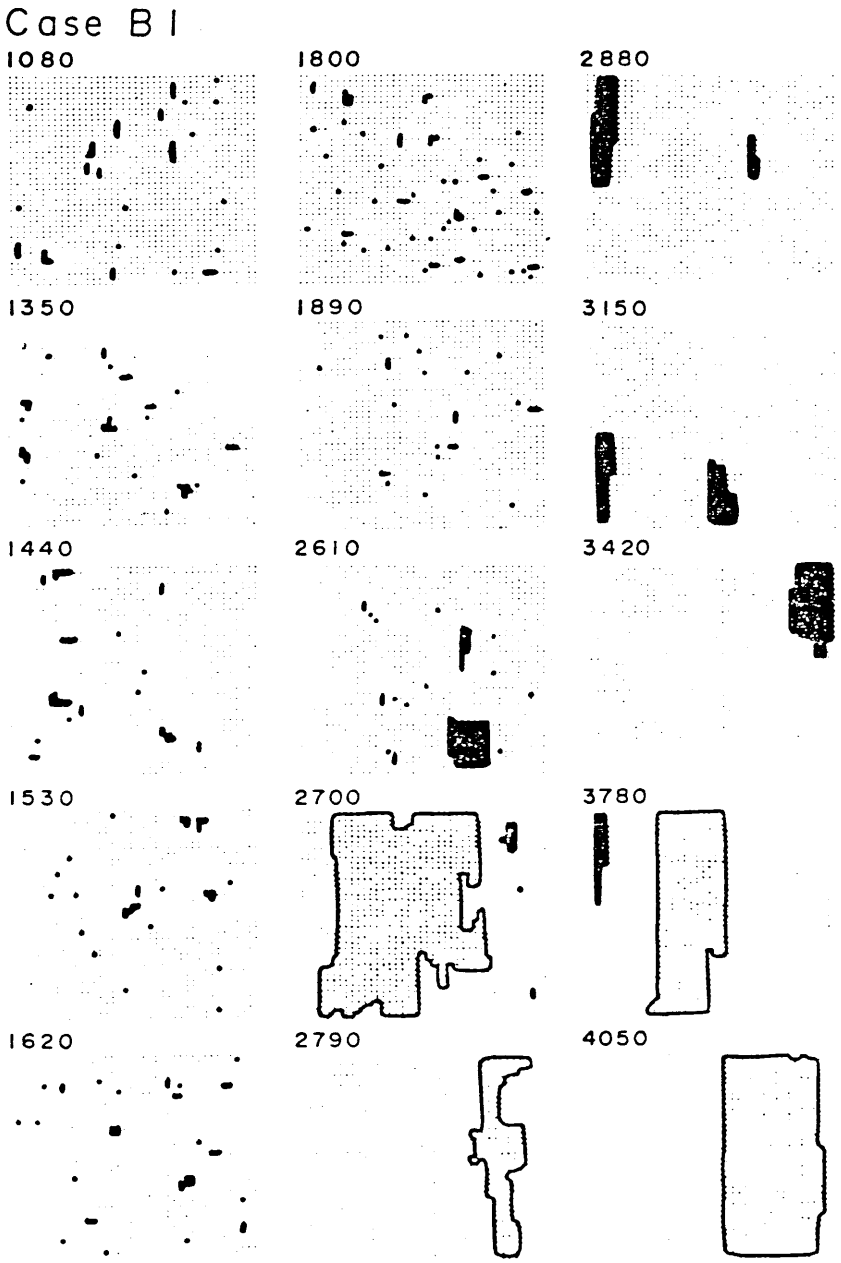
Case B I
1080
1800
2880
1350
1890
3150
1440
2610
3420
1530
2700
3780
1620
2790
4050

Figure 1

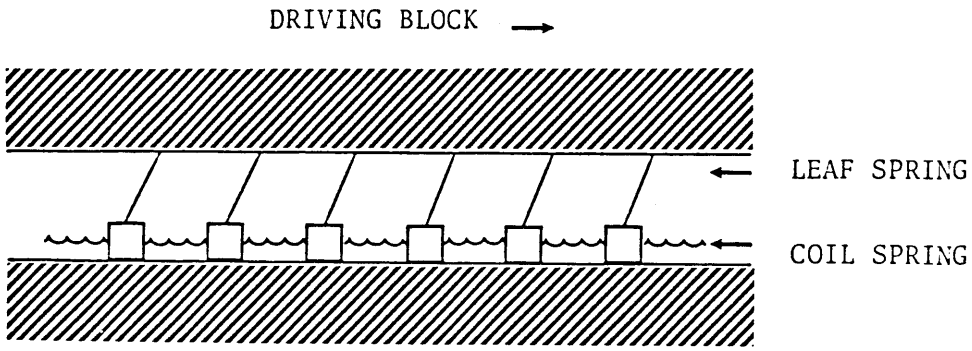

Figure 2

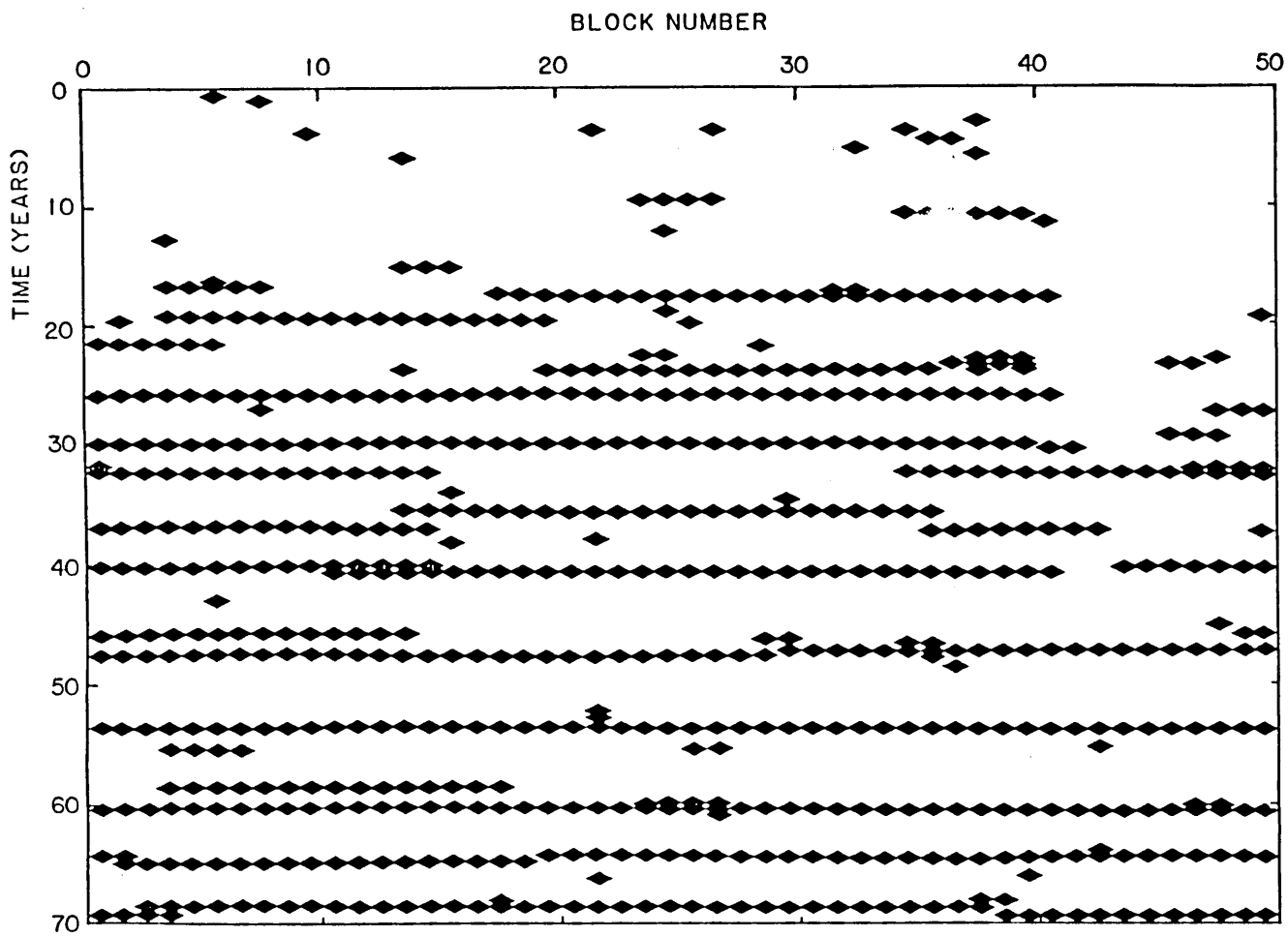

Figure 3

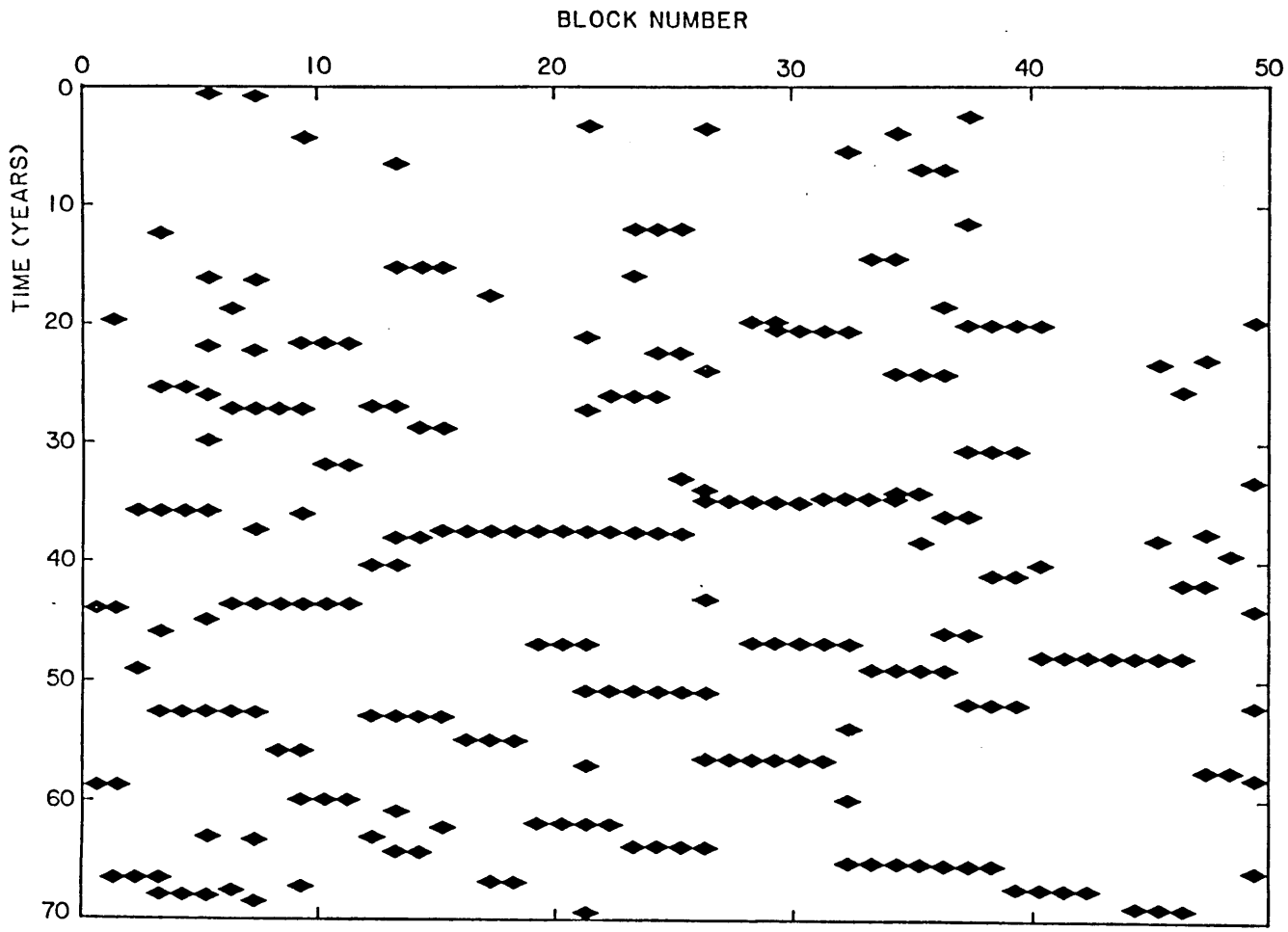

Figure 4

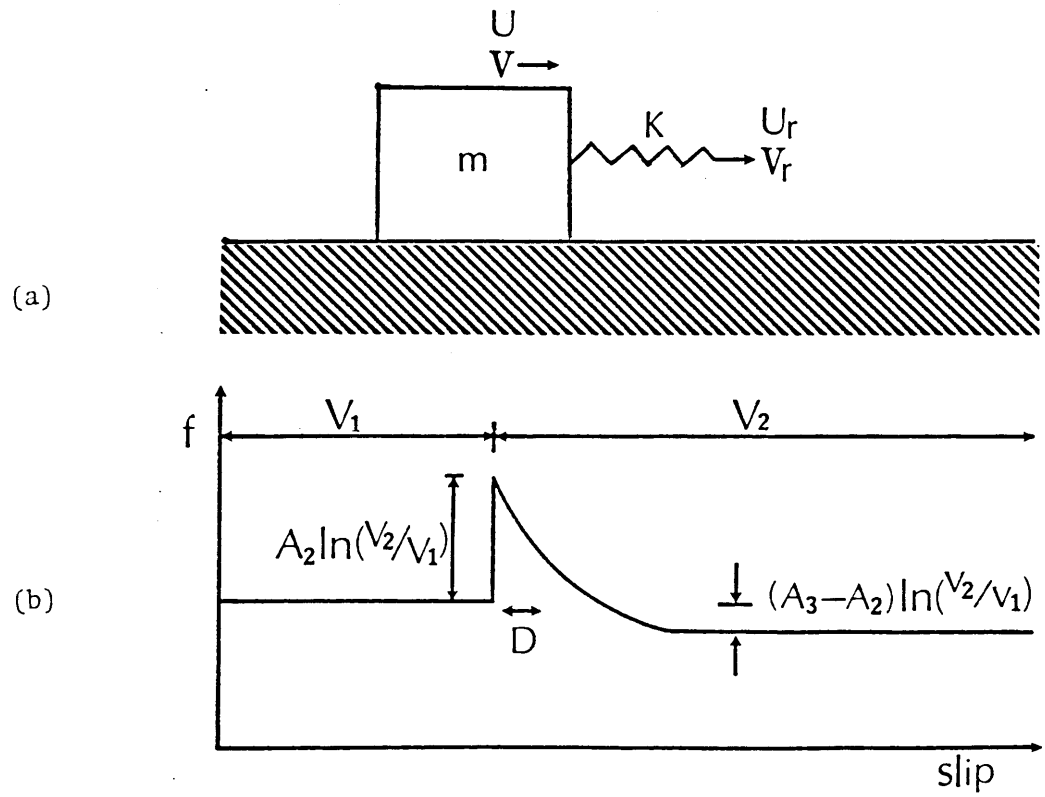

Figure 5

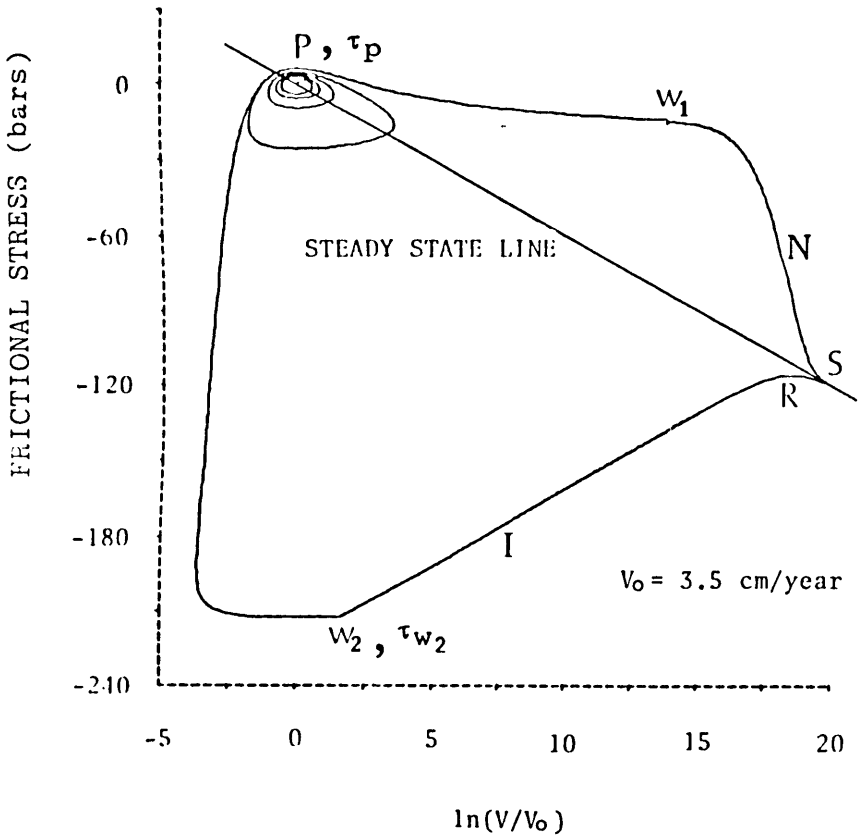

I: INSTANTANEOUS POSITIVE RATE DEPENDENCE
N: NON-INSTANTANEOUS NEGATIVE RATE DEPENDENCE

(a)

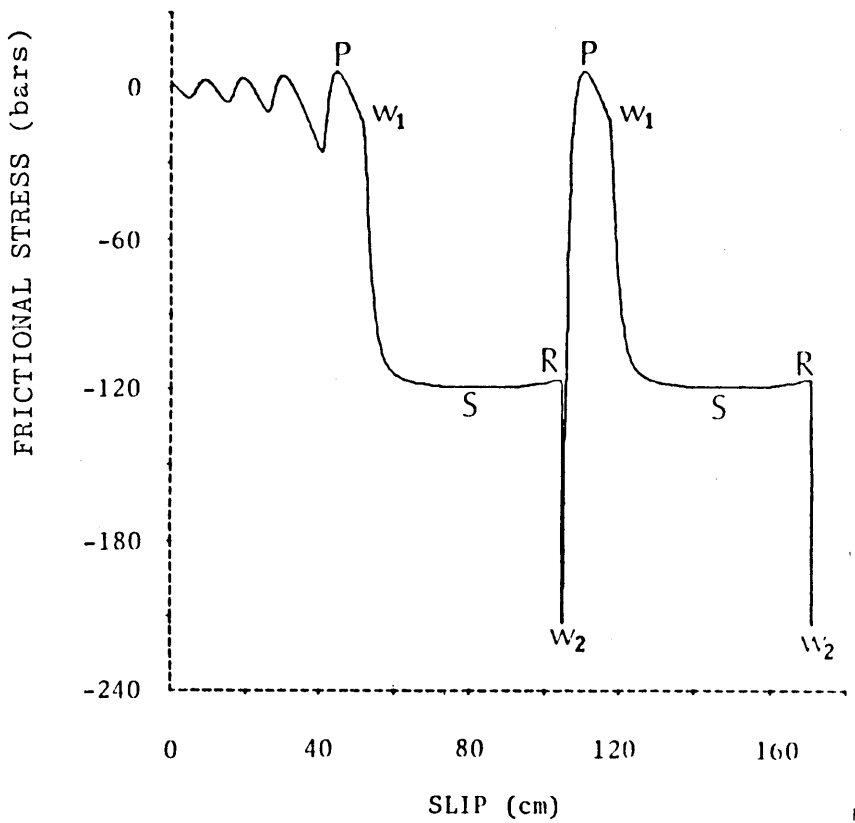

(b)

Figure 6

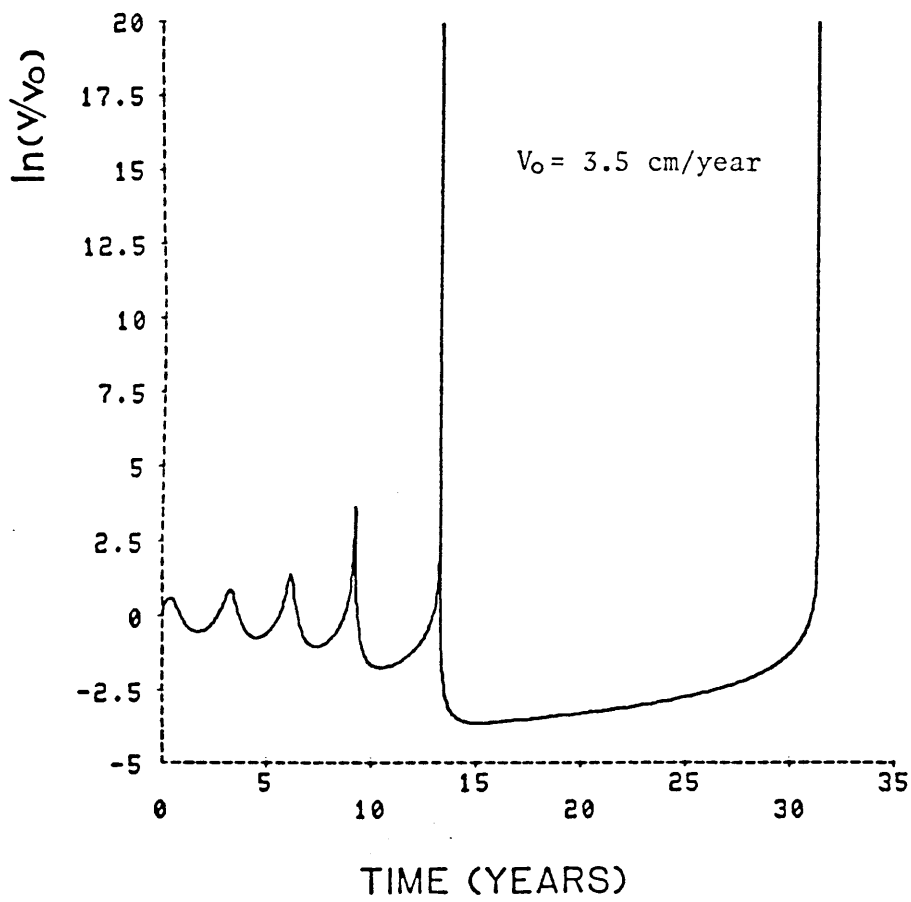
ln(V/Vo)
20
17.5
15
12.5
10
7.5
5
2.5
0
-2.5
-5
0
5
10
15
20
25
30
35
Vo = 3.5 cm/year
TIME (YEARS)

(C)

Figure 6

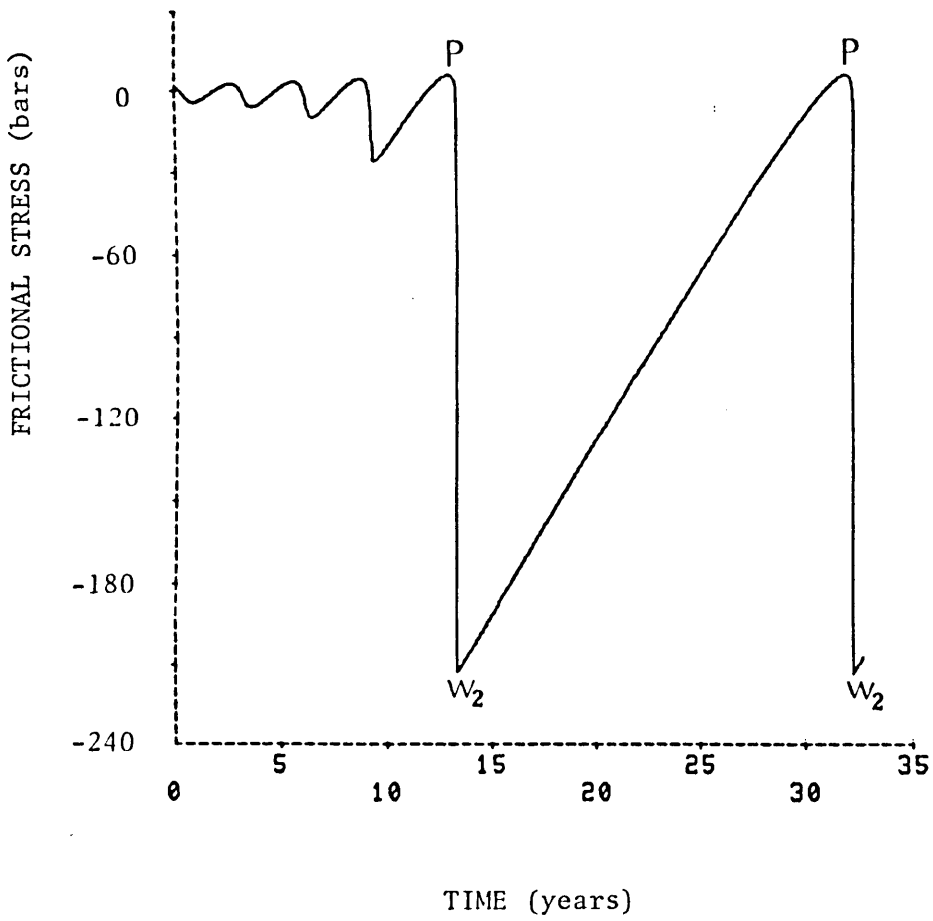
FRICTIONAL STRESS (bars)
0
-60
-120
-180
-240
P
P
W2
W2
0
5
10
15
20
25
30
35
TIME (years)

(d)

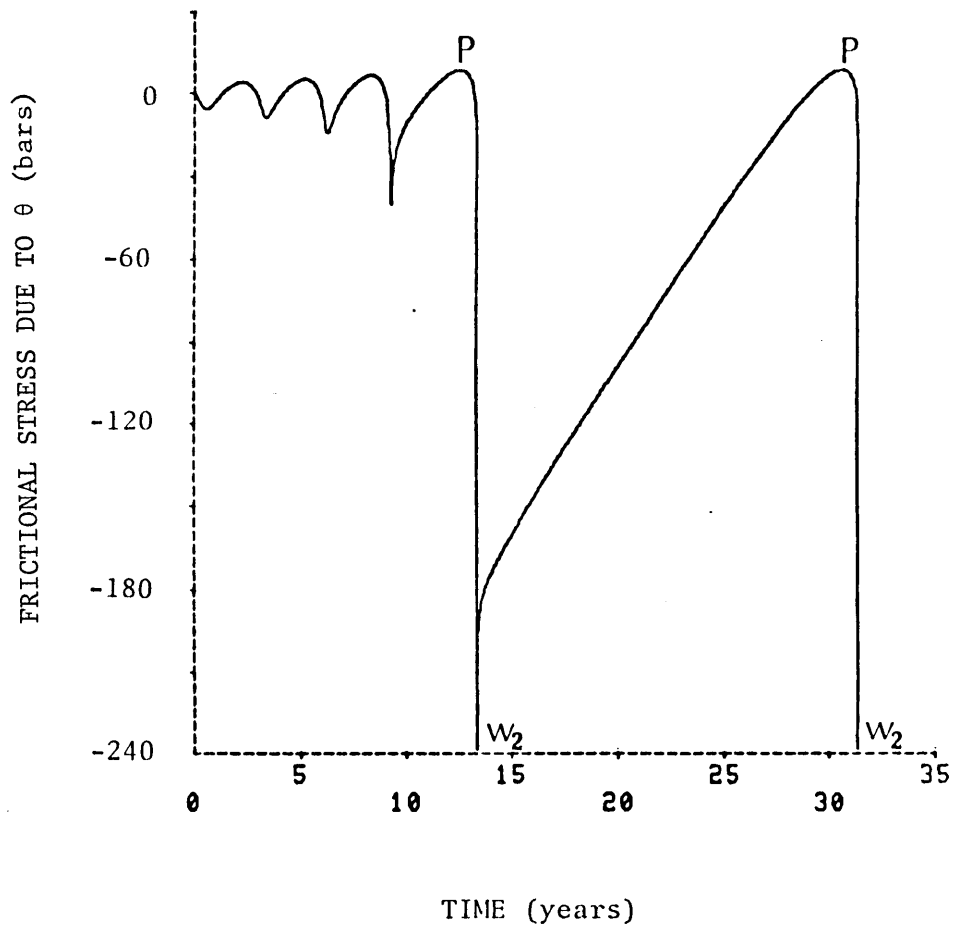
FRICTIONAL STRESS DUE TO θ (bars)
0
-60
-120
-180
-240
P
P
W2
W2
0
5
10
15
20
25
30
35
TIME (years)

(e)

Figure 6

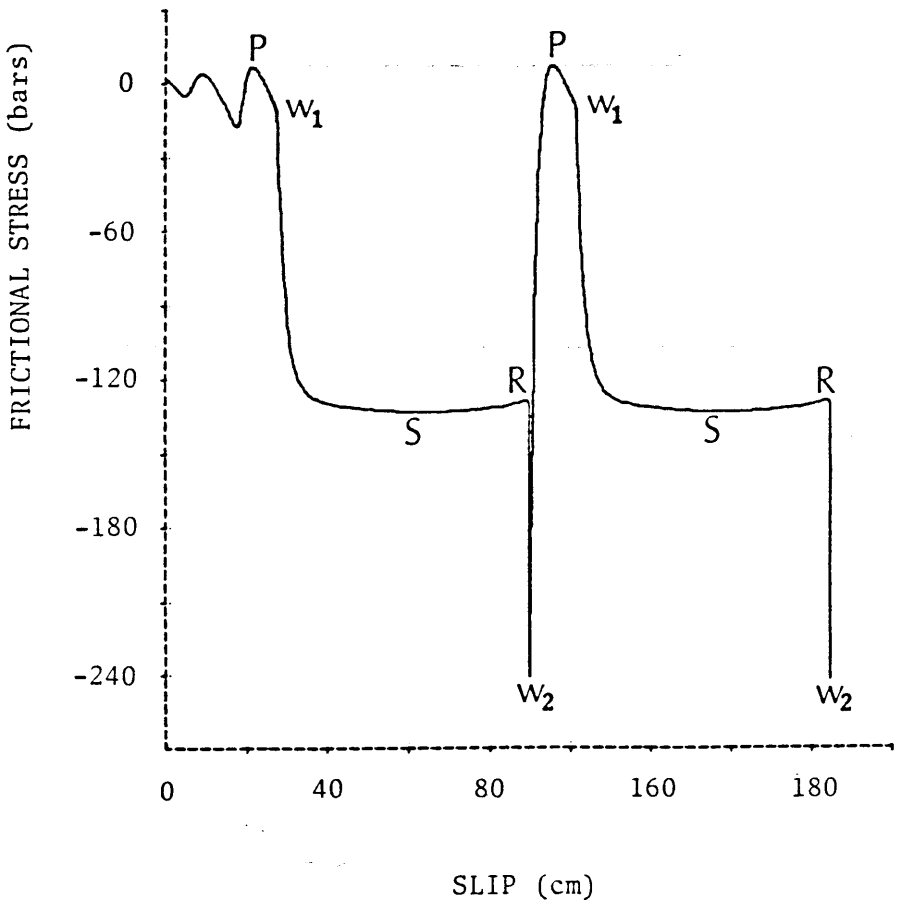
FRICTIONAL STRESS (bars)
0
-60
-120
-180
-240
P
P
W_1
W_1
R
R
S
S
W_2
W_2
0
40
80
160
180
SLIP (cm)

Figure 6 (f)

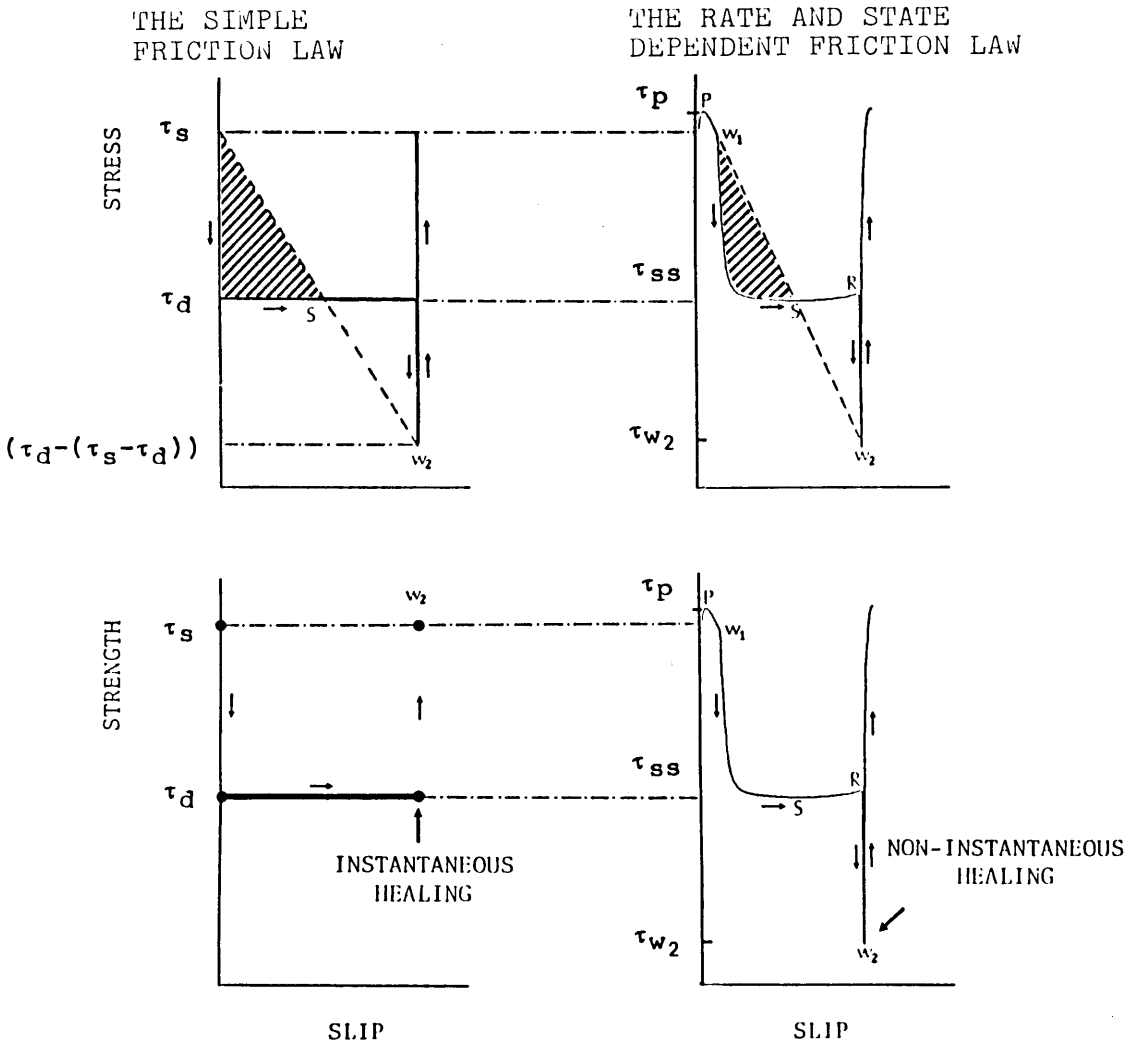
THE SIMPLE FRICTION LAW
THE RATE AND STATE DEPENDENT FRICTION LAW
STRESS
STRENGTH
τ_s
τ_d
$(\tau_d-(\tau_s-\tau_d))$
τ_p
τ_{ss}
τ_{w_2}
P
w_1
R
S
w_2
INSTANTANEOUS HEALING
NON-INSTANTANEOUS HEALING
SLIP
SLIP

Figure 7

FOUR FAULT MODELS

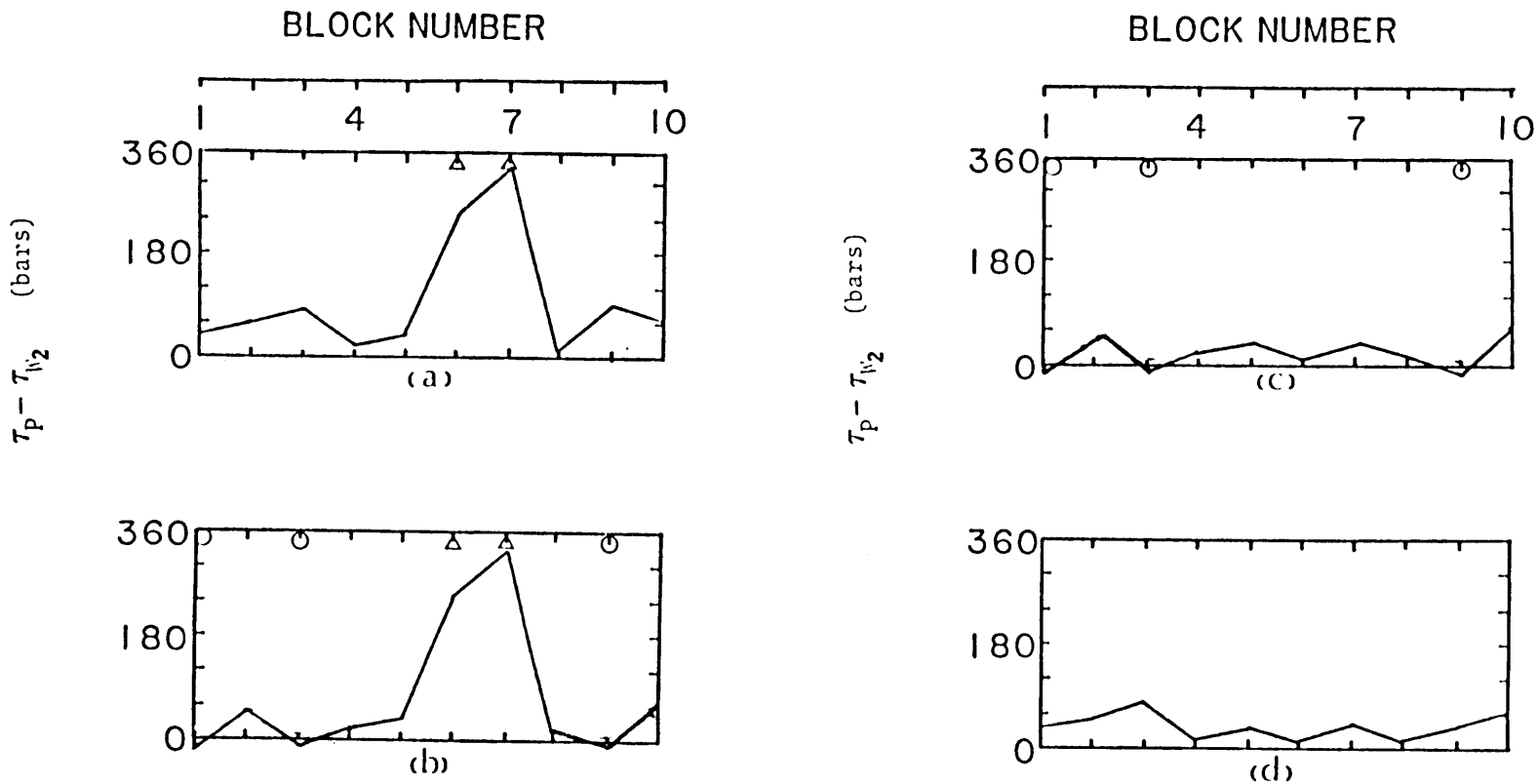

$(\tau_p - \tau_{W_2})$: STRESS DROP

△ STRONG PATCH ○ CREEPING PATCH

Figure 8

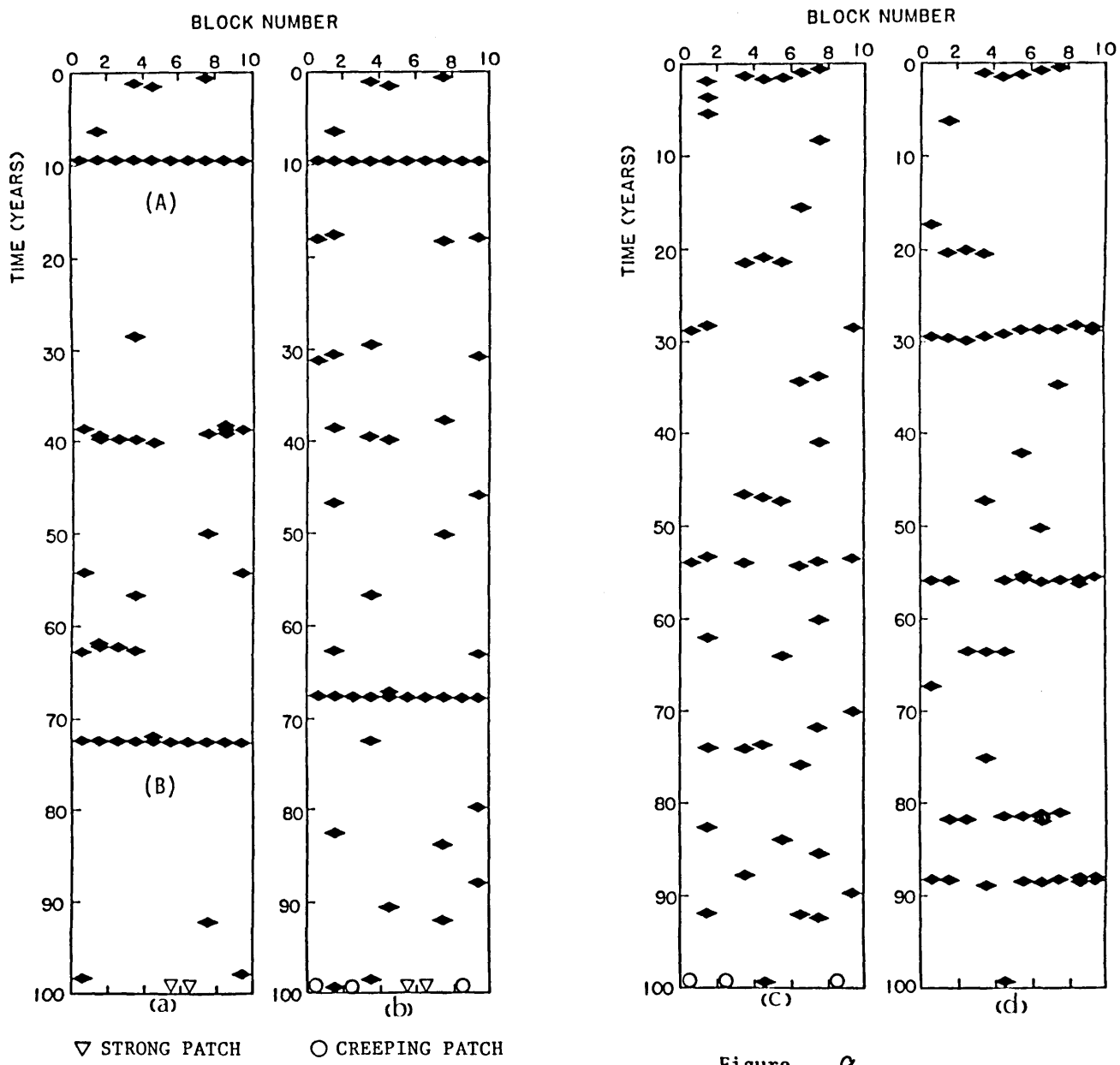
BLOCK NUMBER
TIME (YEARS)
(A)
(B)
(a)
(b)
(c)
(d)
▽ STRONG PATCH
○ CREEPING PATCH

Figure 9

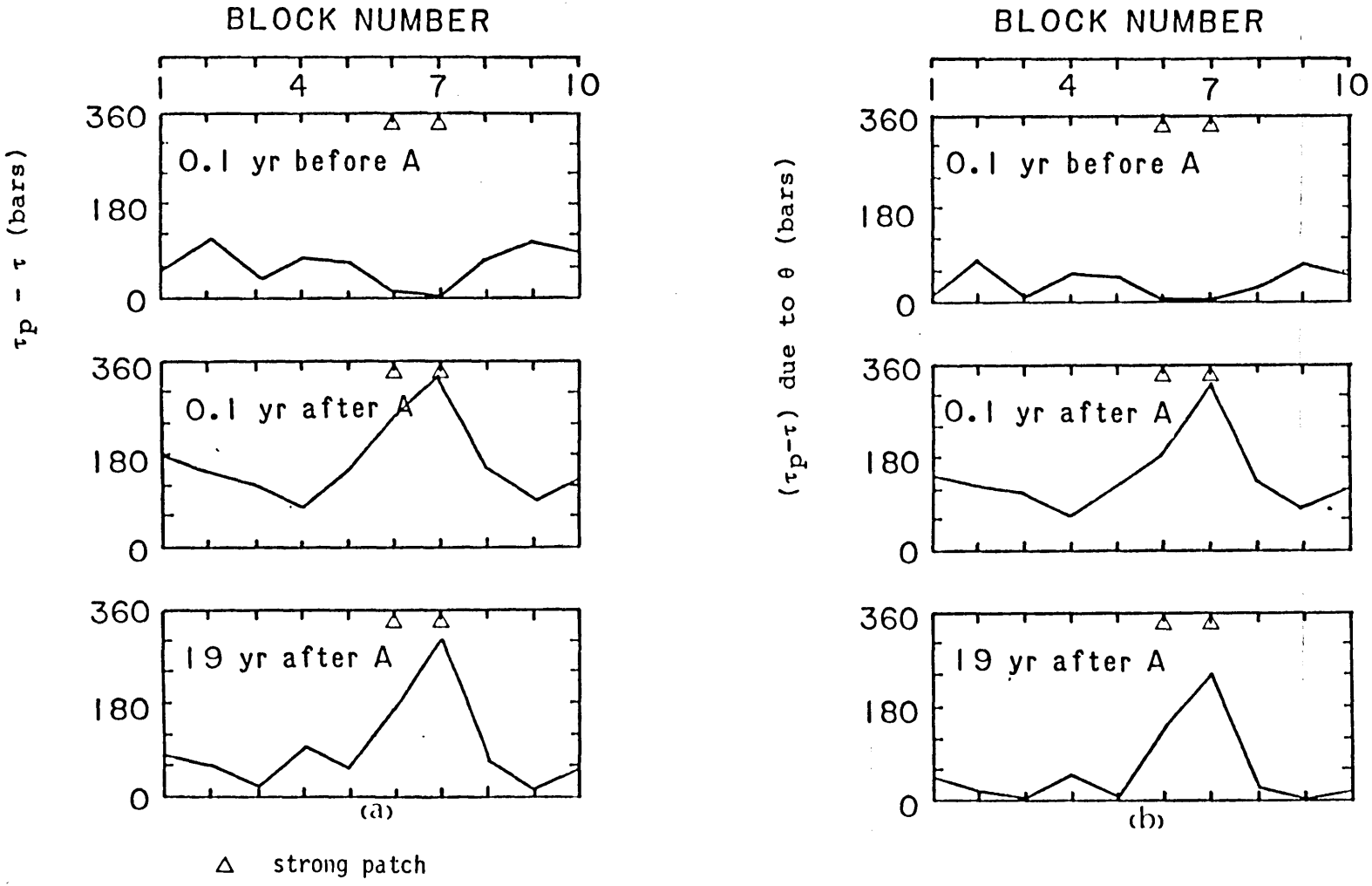
BLOCK NUMBER
1
4
7
10
360
180
0
0.1 yr before A
0.1 yr after A
19 yr after A
$\tau_p - \tau$ (bars)
(a)
BLOCK NUMBER
$(\tau_p - \tau)$ due to θ (bars)
(b)
△ strong patch

Figure 10

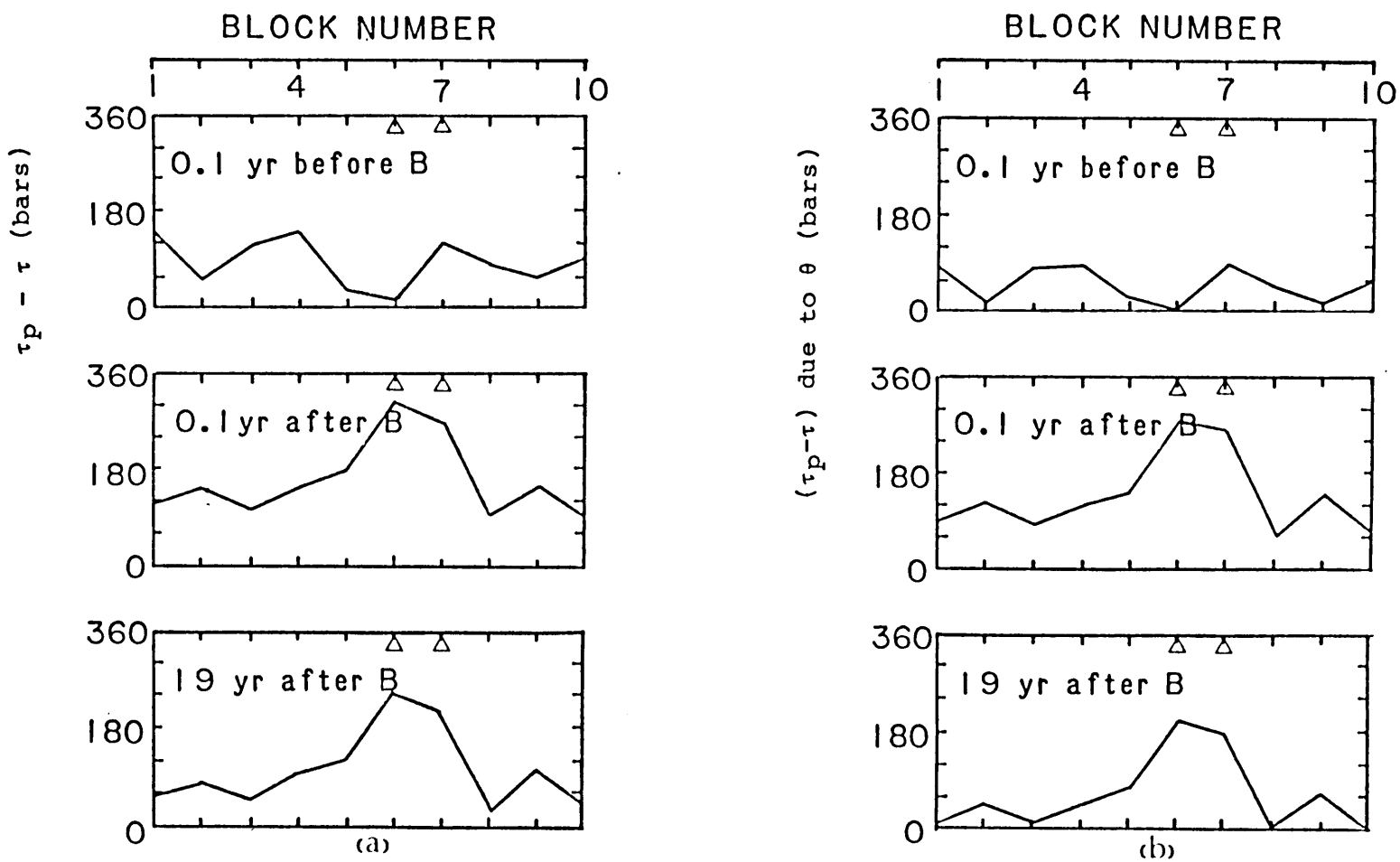

△ strong patch

Figure 11

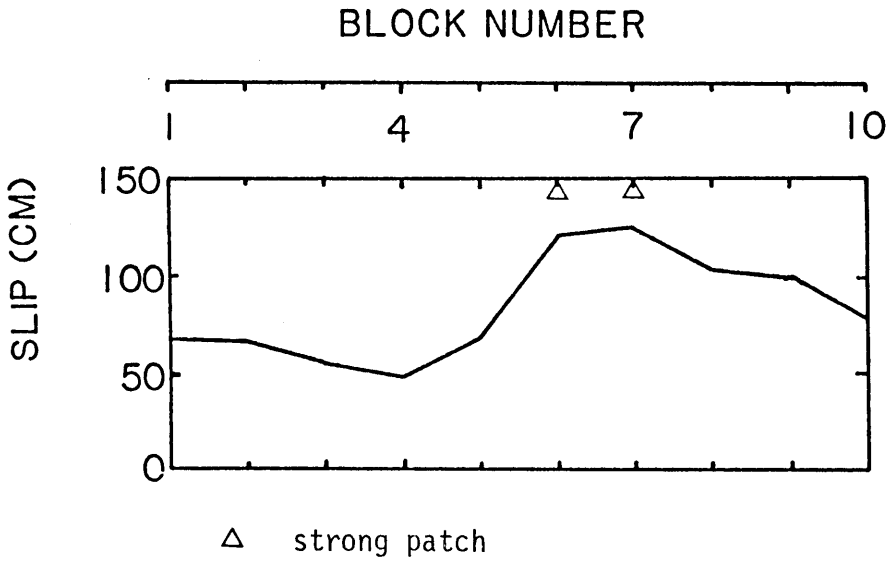

Figure 12

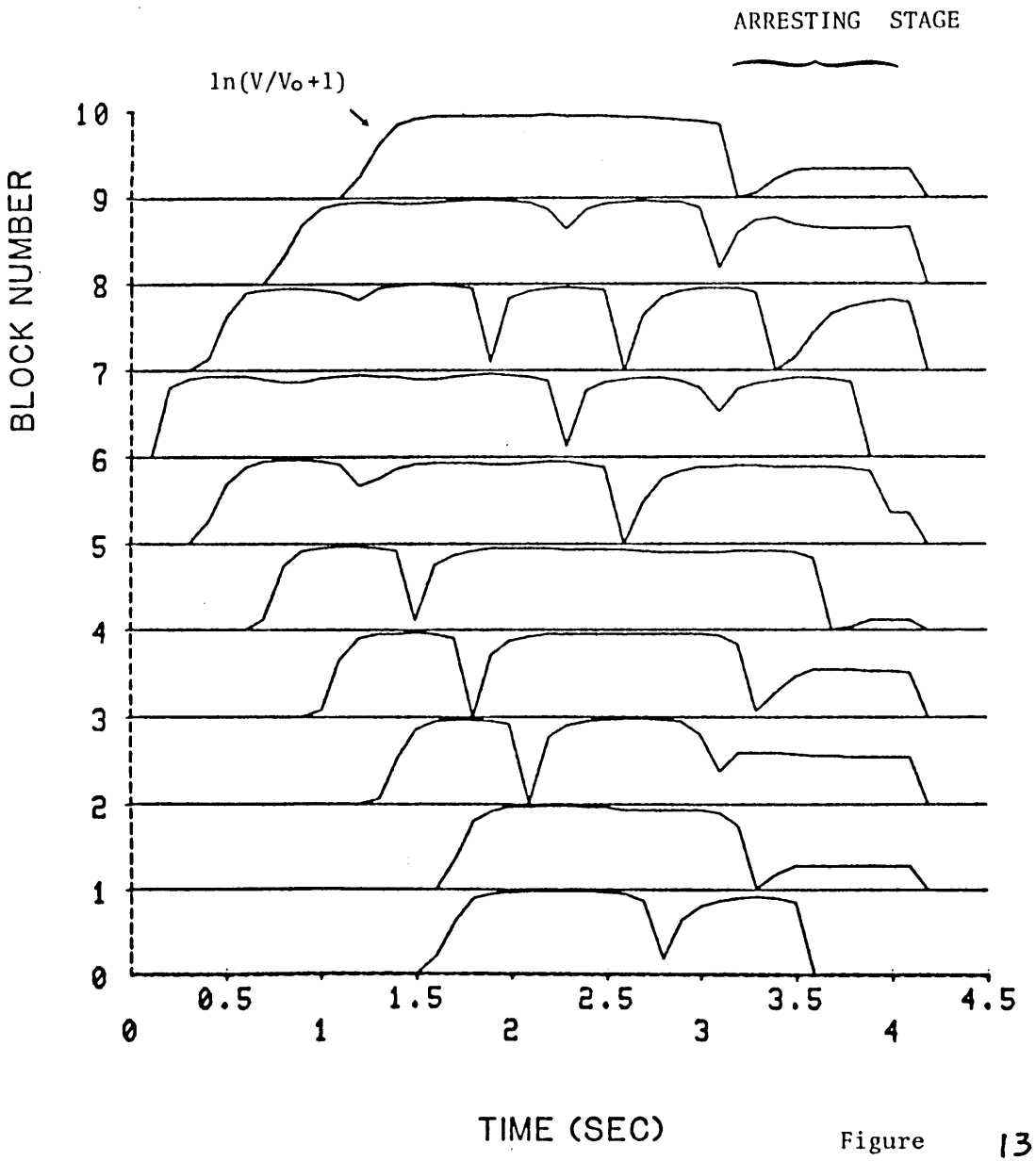
ARRESTING STAGE
ln(V/Vo+1)
BLOCK NUMBER
10
9
8
7
6
5
4
3
2
1
0
0.5
1.5
2.5
3.5
4.5
0
1
2
3
4
TIME (SEC)

Figure 13

Chapter 4

Effect Of Slip Rate On Stress Drop

4.1 Introduction

Recently, Kanamori and Allen (1985) examined the existing data on source parameters for large earthquakes with a broad range of recurrence time and found that earthquakes with longer recurrence times have higher average static stress drops. They considered a model in which a fault which is loaded at a small rate tends to have a larger asperity, and a large slip rate tends to "wear out" the asperity. Since the average static stress drop increases with the ratio of dimensional asperity size to the total area of the fault plane, the model explains why earthquakes with longer recurrence times should have higher average stress drops.

Laboratory experiments also showed that the static friction between rock surfaces increases with time of stationary contact, logarithmically or according to power-law relations (Richardson and Nolle, 1976). However, the specific model discussed by Kanamori and Allen is subject to some questions. First, it is implicitly assumed that the healing process occurs only at an area including the asperity and its periphery. Why does no healing process occur outside the asperity? Secondly, a slow loading rate is taken to imply a long recurrence time. But, a long recurrence time may also be due to a large characteristic slip (Schwartz and Coppersmith, 1984) due to inherently strong asperities. In order to find the relation between slip rate and stress drop, we calculated the

the slip rate as the slip divided by the recurrence interval listed in Kanamori and Allen (1985). The results are shown in Figure 1.

Figure 1 shows that a weak relation between stress drop and slip rate exists. When slip rate increases, stress drop decreases. However, that the data points of stress drop for the same slip rate scatter over a range wider than 100 bars everywhere is clearly evident.

In the present paper, we shall make a theoretical study on the relation between long-term slip rate and average stress drop using a one-dimensional mass-spring fault model controlled by a laboratory inferred rate and state dependent friction law (Ruina, 1980, 1983). Because the healing process is included in this friction law, we can quantitatively study the above relation without making additional assumptions. In the following, we first study the relation for a homogeneous fault which undergoes a wide range of long-term slip rate; then we study the relation for a heterogeneous fault. For the case of heterogeneous fault, we shall compare two sub-cases: one is for a fault with a single asperity and the other is for a fault with multiple asperities.

4.2 Fault Model and Friction Law

We use a one-dimensional discrete array of mass and spring first introduced by Burridge and Knopoff (1967) to simulate seismicity. In this model, equal masses connected by coil springs are placed on a horizontal plane surface. Each mass is also connected to a slab by a leaf spring. The slab moves in the horizontal direction with a constant velocity to simulate the

tectonic loading. The velocity of this movement is the rate of tectonic loading or long term slip rate discussed earlier. The friction between the mass and the plane surface represents the friction acting on an earthquake fault. For boundary conditions, we adopt the assumption of periodicity along a fault (Dieterich, 1972) to avoid abnormal conditions at the ends.

In order to simulate a real fault using a one-dimensional array of masses and springs, we need to follow some scaling relations in choosing spring constants and block masses. These relations were discussed by Yamashita (1976) and used in our earlier seismicity simulations (Cao and Aki, 1984, 1985), where the importance of proper choice of these parameters was discussed.

The fault zone constitutive law used in our modeling is of Ruina's (1980, 1983) form which was originally inferred from laboratory experiments. In this form, the fault strength is described as a frictional coefficient f which is a function of slip rate v and state variable θ:

$$f = A_1 + \theta + A_2 \ln(v/v_o) \tag{1a}$$

$$\dot{\theta} = - [v/D] \; [\theta + A_3 \ln (v/v_o)] \tag{1b}$$

where v_o is an arbitrary constant with velocity dimension, others including A_1, A_2, A_3 and D are all material constants, and v is slip velocity. If velocity v changes abruptly from v_1 to v_2, according to equation (1), f will change by $\Delta f = A_2 \ln (v_2/v_1)$. Therefore, A_2 describes the degree of direct frictional response to a sudden change of slip velocity. A_2 is not very important in the healing process which we are mostly interested in the present study.

According to (1b), θ evolves with time and decreases with increasing slip velocity. In Cao and Aki's (1985) calculation, it has been clearly shown that unstable slip (earthquake) causes significant decrease of f primarily due to the change in θ. After the unstable slip, θ is lowest and negative. Then it increases slowly according to (1b). This is the healing process. From (1b), we see that A_3 and D together characterize the healing process.

As Mavko (1983) discussed based on a quasi-static solution, the stress drop of a uniform fault controlled by the rate and state dependent friction law is given by

$$\Delta\tau = \sigma_n (A_2-A_3) \ln (V_{min}/V_{max}) \tag{2}$$

where σ_n is normal stress, V_{min} and V_{max} are the minimum and maximum fault slip velocities, respectively. We will assume σ_n does not change. Later, we will show that V_{min}/V_{max} does not change much even for a dynamic solution when the loading rate is fixed and (A_3-A_2) changes in a relatively small range. In this case, $\Delta\tau$ and (A_3-A_2) still have an approximate linear relation: When (A_3-A_2) is relatively larger, $\Delta\tau$ increases slower than (A_3-A_2) because of the non-linearity of the rate and state dependent friction law. In the present study, however, we are more interested in investigating $\Delta\tau$ as a function of the loading rate in a dynamic solution in which stress drop is no longer simply represented by equation (2).

Mavko also concluded that the recurrence time of earthquakes on a homogeneous fault, which is governed by a rate and state dependent friction law, depends primarily on (A_3-A_2) and weakly on D. Therefore, when recurrence processes with different recurrence times

are simulated we can change both (A_3-A_2) and D and keep their ratio constant to avoid some complexity. According to Horowitz and Ruina (1985) the dynamics of fault slip affected by this ratio is not well understood.

Let us now consider how to choose material constants in formula (1) in order to simulate a heterogeneous fault. Usually we simulat a heterogeneous fault by specifying a heterogeneous strength distribution along the fault. However, as indicated by Brune (1970), Kanamori (1972) and Yamashita (1976) among others, dynamics of fault rupture are determined by the effective stress which is defined as the static frictional stress minus the sliding frictional stress. In other words, the absolute stress level is irrelevant to the dynamics of fault motion. Therefore, we cannot specify a heterogeneous distribution of A_1 to simulate a recurrence process of a heterogeneous fault. A_1 only affects the absolute stress level but not the stress drop or effective stress as shown by (1a) and (2). A heterogeneous distribution of A_1 will affect the transient period of a simulation but not the dynamic motion of a fault after the first few major events have occurred. Then, the remaining parameters related to strength and stress drop are A_2 and A_3.

As compared in Chapter 3 for the dynamic motion of a single block-spring system, the effective stress is related to the stress drop in a similar way for both the simple friction law and the rate and state dependent friction law. Cohen (1977, 1979) showed that the final stress drop is twice the difference between static friction and dynamic friction or the effective stress. Thus, for

the rate and state dependent friction law we can choose (A_3-A_2) as a parameter which can specify a heterogeneous fault, because (A_3-A_2) determines the stress drop according to (2) and also the effective stress according to the comparison in Chapter 3. A heterogeneous distribution of (A_3-A_2) along a fault defines a heterogeneous fault. A fault segment with higher (A_3-A_2) will have higher effective stress and is stronger in fault dynamics. In the rest of this paper when we say "strong patch of a fault" we mean the area with a higher value of (A_3-A_2).

Now, we are ready to discuss the relation between earthquake recurrence time and average stress drop using a one-dimensional block-spring model which is controlled by the rate and state dependent friction law. We start with homogeneous fault models.

4.3 Homogeneous Fault Models

The quasi-static motion of a homogeneous fault controlled by the rate and state dependent friction law was studied by Mavko (1983) using the laboratory inferred material constants A_1, A_2, and A_3 except D in equation (1). The dynamics of a block-spring system was solved by Rice and Tse (1985). Figure 2 shows the calculated temporal change of frictional coefficient f relative to the nominal value A_1. In the calculation, we have chosen $A_3 = 0.004$, $A_2 = 0.002$, $\sigma_n = 3$ kbars according to the laboratory inferred results (Mavko, 1983). There is a large discrepancy for D between its laboratory inferred values ($1 \sim 50$ μm, Mavko, 1983) and the values (5-25 cm, Mavko, 1983) needed to simulate real seismic faults. We have chosen D = 6.5 cm in Figure 2 in which $A_3-A_2 = 0.002$. This D

value is close to the value inferred from field observations on strong ground motion for a similar fault length to our simulation (Papageorgiou and Aki, 1983; Cao and Aki, 1984). The spring constant for the loading is $K = 3.7 \times 10^6$ dyne/cm^3, v_o and the driving velocity v_r are 3.5 cm/yr.

From Figure 2, we can see that the recurrence process has a fixed period of 86 years and at the beginning there is a transient period which depends on initial conditions. The friction coefficient drops from a maximum value to a minimum value in each cycle. Their difference multiplied by normal stress σ_n gives the stress drop. After the minimum point, a healing process starts until the stress reaches the maximum value again. In Figure 3, we change A_3-A_2 and D to 0.001 and 3.25 cm respectively and keep all other parameters the same as in Figure 2. We find that because of the smaller (A_3-A_2) the recurrence time is much shorter (43 years) and the stress drop is much lower than in Figure 2. This is consistent with our earlier conclusion that we can simulate different stress drops or effective stresses by specifying (A_3-A_2). We are now ready to study the relations among recurrence time, driving slip rate, stress drop, and healing process.

Figure 4 shows that the stress drop increases by 30% when the long term loading rate decreases from ten centimeters per year to one-tenth of a millimeter per year. The increase is much smaller than that was implied in the interpretation of stress drop vs. recurrence time by Kanamori and Allen (1985). Our calculation shows that the stress drop changes only up to 30% for the similar range of recurrence times. In our calculation the material constants are

chosen according to the laboratory experiments and the whole fault is under a healing process. If we limit the healing process only at part of the fault surface, which defines a strong asperity area, as Kanamori and Allen (1985) assumed, we would expect even smaller change in stress drop. In order to examine the possible range of uncertainties about model parameters, we also calculated for the case of A_3-A_2 = 0.001 which is close to the lowest value obtained from existing experimental results (Mavko, 1983). In this case, the stress drop for the corresponding loading rate as in Figure 4 is about half and the stress drop change due to the same loading rate change as in Figure 4 is even less than 30% (Figure 5).

We plotted the calculated stress drop vs. slip rate curve for A_3-A_2=0.0007 in Figure 1. The curve seems to follow the average trend of observed stress drop, although the data points are too scattered to make a strong conclusion. We also tried to change the material constants A_3, A_2, and D in the friction law in order to simulate a more rapid decrease in stress drop with increasing slip rate as suggested by the observations. We did not succeed. For example, to check the effect of A_3 which is a material constant characterizing the healing process, we calculate the stress drop change due to the increase in A_3. According to the laboratory experiments, A_3 increases by about 10% when the gouge size changes from 85 to 250 μm (Mavko, 1983). As shown in Figure 6, with 10% change of A_3 (from 0.004 to 0.0044), a driving rate kept at 3.5 cm/yr, A_2 kept at 0.002, and other parameters kept the same as in Figure 2, the stress drop increases only by 20% and seems to slow

down near 10% increase of A_3. As we indicated before, this is because of the non-linearity of the friction law.

In view of the simplified model configuration and the uncertainties of model parameters, the obtained absolute values of stress drop in Figures 4, 5 and 6 should not be given too much significance. Here we only emphasize the relative change of stress drop due to the changes of loading rate and constant A_3.

We also tried to change material constants in ranges larger than that from the experiments, for example 20% for A_3, we found that the slope of the stress drop vs. slip rate curve in Figure 1 is not sensitive to A_3 or other parameters. This curve predicts a stress drop increase with decreasing slip rate but appears to be too slow to explain the observation. This deficiency suggests that the friction law we used may not be extrapolated to a very low slip rate.

In fact, Shimamoto and Logan (1984) showed that two different empirical laws, a power law and a logarithmic law, which fit the same friction data equally well predict entirely different behavior when extrapolated to very low slip rates. The power law says that the stress drop in frictional experiments is proportional to t^b, where t is the contact time and b is a constant; the logarithmic law says that the stress drop increases with contact time logarithmically. In their Table 1 the long-term predictions for shear stress drop were listed. They found that when the contact time changes from one year to a thousand years, the power law predicts a stress drop change from 916 to 13551 MPa but the

logarithmic law only predicts a change from 25 to 35 MPa. The logarithmic law is an earlier and simpler version of the rate and state dependent friction law. Because a power law predicts a much faster stress drop increase, it will probably fit the observed trend (Figure 1) better than the rate and state dependent friction law. However, more high quality data are needed in order to confirm these suggestions.

In any case, we conclude that Kanamori and Allen's observation on high stress drop for earthquakes with longer recurrence time may not be simply explained by a healing process alone. In order to find a suitable explanation, we shall make some numerical experiments using heterogeneous fault models.

4.4 Heterogeneous Fault Models

We have shown earlier that by specifying different material constant (A_3-A_2) among the fault blocks we can simulate a heterogeneous fault. We use a fault composed of 10 blocks, and choose model parameters in the following way. First, we call ten random numbers of a uniform distribution over 0.001 to 0.003 and assign it to each block randomly as the value of A_3. Second, we replace A_3 values for some blocks in order to have strong patches on a fault. A_2 is fixed to be 0.002. The first fault model (A) has one strong patch at block 6 with A_3 = 0.005. The second fault model (B) has two strong patches at blocks 6 and 7 with A_3 values to be 0.005 and 0.006, respectively. The third fault model (C) has three strong patches at blocks 3, 6, and 7 with A_3 values to be 0.005, 0.006, and 0.005, respectively. All these three models have the

same long term loading rate, 3.5 cm/yr. The fourth model (D) has the same heterogeneity as model (B) but the loading rate is doubled.

From models (A) to (C), the number of strong patch is increasing. The difference of heterogeneity among these fault models is only at the strong patches. The material constant D in formula (1) for each block has been chosen proportional to its (A_3-A_2) value to keep their ratio constant. Same initial conditions are used for all model simulations. Three different heterogeneous fault models are shown in Figure 7 in which the values of (A_3-A_2) are plotted along the fault.

The simulated seismicities using models (A) to (D) are shown in Figure 8. For each model, we simulated 200 years' seismicity which includes enough major events to discuss the recurrence process. Although the recurrence time is not a constant for any fault model, we still can easily find the tendency that recurrence time increases from models (A) to (C) when the fault has more strong patches. It is important to note that this result was obtained under the condition of same loading rate for these three different models. It means that different segments of a fault, which have the same long term loading rate along its entire length, may have different recurrence times dependent upon the fault heterogeneity. This may serve as a model of the San Andreas fault where the recurrence time changes dramatically from segment to segment although the long-term slip rate is the same along the whole fault. Another important thing to note is that the recurrence time is increased not by

increasing the strength of strong patches but only the number of strong patches on each fault. The loading rate also affects the recurrence time as can be seen from the simulation of fault model (D), which has the same heterogeneity as model (B) but much faster loading rate. In this case, the recurrence time is much shorter as shown in Table 1.

Because the first major event in the model simulation may be affected by the initial conditions, we plot stress drops of three consecutive major events starting from the second major event in each model simulation as shown in Figure 9. These events are denoted with a, b, and c in Figure 8 and their stress drops are denoted with Aa, Ab, and Ac for three events from model A and the like for models B, C, and D in Figure 9. Similar to the uniform fault model, we used 3 Kbar as the normal stress and the stress drops are proportional to this value. Again, the absolute values of stress should not be given too much significance. We are mostly interested in the differences among models.

As can be seen in all the stress drop curves along the faults (Figure 9), high stress drop always occurred at strong patches with high (A_3-A_2) values. Average stress drops of these 12 events are listed in Table 1 and plotted in Figure 9 using dotted lines. The average stress drop for events from the same model in the same row of Figure 9 is roughly the same. Average stress drops in the same column of Figure 9 increase significantly from model A to C. In Table 1, we averaged the stress drops from each model. The results show that fault models with two and three strong patches have stress

drops 54% and 99%, respectively, higher than model A with one strong patch. Model D has the same heterogeneity as model B but higher loading rate. The average stress drops are almost the same for these two models (Table 1). In summary, we found that:

1) The loading slip-rate naturally affects the recurrence time, but only slightly affects the average stress drop along a heterogeneous fault.
2) An increase in the number of strong patches with similar strength on a fault lengthens the recurrence time and increases the average stress drop significantly.

4.5 Conclusions and Discussion

Much of the motivation for the present study stemmed from Kanamori and Allen's (1985) observational result about earthquake recurrence time and average stress drop. In order to explain this result they proposed a model in which the asperity increases its size due to the healing process and was responsible for higher average stress drop during earthquakes. To test their model quantitatively, we used a laboratory inferred friction law with the laboratory determined parameters except for the constant D which was inferred from field data.

Although Kanamori and Allen's observational result was about the relation between recurrence time and stress drop, their explanation was to attribute the stress drop difference to the long-term slip rate difference. We first checked the observational relation between stress drop and slip rate using the data set of Kanamori and Allen (1985), and found only a weak relation between

stress drop and long-term slip rate exists. Our simulation result for a homogeneous fault model based on the rate and state dependent friction law showed also a very weak relation. Therefore, the healing of a single asperity alone does not seem to be able to explain the observed variation of stress drop by two orders of magnitude. The result for heterogeneous faults (model B and D) also showed very weak effect of slip-rate on stress drop. Our calculation also suggests that for a slow loading, the power law may better explain observations than the rate and state dependent friction law at least for strike-slip fault.

The simulations for heterogeneous fault models characterized by the number of strong patches with similar strength on a fault show that both the recurrence time and average stress drop are affected by this number. In our simulation, the stress drop was doubled by increasing the strong patch number from one to three. A fault may have more than one strong patch as implied by many studies such as Rudnicki and Kanamori (1981) and Rundle and Kanamori (1984) among others. Therefore, our conclusion is that the inherent difference of fault strength may be primarily responsible for both the longer recurrence time and higher stress drop.

Shimamoto and Logan (1984) found that two different empirical friction laws, which equally fit the available data, predict entirely different results when extrapolated to slow deformation occurring in nature. They suggested that long-term experiments, lasting up to a few years, would be necessary to test the validity of friction laws. From this point of view, the friction law we used also need to be confirmed for long-term extrapolation.

Figure Captions

Figure 1. The stress drop vs. long-term slip rate relation. The slip rates are calculated from observational seismic moments and recurrence times compiled by Kanamori and Allen (1985). The stress drops are also from Kanamori and Allen's paper. The curve is obtained from a homogeneous fault model using the rate and state dependent friction law with A_3-A_2 = 0.0007.

Figure 2. The time change of coefficient of friction f relative to the nominal value A_1 for a homogeneous one-dimensional fault model in which the material cosntants are A_2 = 0.002, A_3 = 0.004, D = 6.5 cm, and the loading rate V_r = 3.5 cm/yr. There is transient period at the beginning of the simulation.

Figure 3. Same as Figure 2 except A_3 = 0.003 and D = 3.25 cm. We see that the range of friction coefficient change is much smaller than in Figure 2 and the recurrence time is also much shorter due to the smaller difference of (A_3-A_2) as compared with Figure 2.

Figure 4. The stress drop as a function of the driving velocity for a homogeneous fault model with all the material constants chosen from laboratory experiment (A_3-A_2 = 0.002) except D. Here, the driving velocity has covered the possible tectonic loading rate over three orders of magnitude but the stress drop changes only by up to 30%. The corresponding recurrence time changes by more than two orders of magnitude.

Figure 5. Same as Figure 4, but A_3-A_2 = 0.001. The stress drops are almost half of the values in Figure 4.

Figure 6. The stress drop as a function of A_3 which characterizes the healing process. When A_3 increases, the stress drop increases too. The increase of stress drop tends to be slow down as A_3 increases by 10%. The stress drop change is within 20%.

Figure 7. Three hetergenous fault models which are represented by a distribution of (A_3-A_2) along the fault. Those high peak values of (A_3-A_2) represent the strong patchs.

Figure 8. The simulated seismicities for four heterogeneous fault models. The block numbers denote the block locations along a fault. Each solid triangle represents a unstable event. If many triangles line up at a time, it represents a larger event. If all ten triangles line up, it is a major event. Capital characters A, B, C, and D on the up-right side of each sub-figure indicate the different models as described in the text. Small characters a, b, and c indicate the events and their stress drops are shown in Figure 9. Model A has one strong patch at block 6; model B has two strong patches at blocks 6 and 7; model C has three strong patches at blocks 3, 6, and 7. These are shown in Figure 7. Model D has the same heterogeneity as model B but is loaded with a faster rate, 7 cm/yr. The average recurrence times for each model are listed in Table 1.

Figure 9. The stress drop distributions along the faults. Here, we only plotted stress drops for three major events (events a, b, and c in Figure 8) from each model. We see that the high stress drops occur at the strong patches. The average stress drop increases when the number of strong patches on a fault increases. The details of stress drop related to strong patch number are shown in Table 1. The capital characters A, B, C, and D and the small a, b, and c on up-right corner of each sub-figure have the same meaning as in Figure 8. They indicate the models and events, respectively.

References

Burridge, R., and L. Knopoff, Model and theoretical seismicity, Bull. Seismol. Soc. Am. 57, 341-371, 1967.

Brune, J. E., Tectonic stress and the spectra of seismic shear waves from earthquakes, J. Geophys. Res., 75, 4997-5009, 1970.

Cao, T., and K. Aki, Seismicity simulation with a mass-spring model and a displacement hardening-softening friction law, PAGEOPH, 122, 10-24, 1984/85.

Cao, T., and K. Aki, Seismicity simulation with a rate and state dependent friction law, submitted to J. Geophys. Res., 1985.

Cohen, S. C., Computer simulation of earthquakes, J. Geophys. Res., 82, 3781-3796, 1977.

Cohen, S. C., Numerical and laboratory simulation of fault motion and earthquake occurrence, J. Geophys. Res., 17, 61-72, 1970.

Dieterich, J. H., Time-dependent friction as possible mechanism for aftershocks, J. Geophys. Res., 77, 3771-3781, 1972.

Horowitz, F.G., and A. Ruina, Slip patterns generated in a spatially homogeneous fault, manuscript for the 5th Ewing Symosium on Earthquake Source Mechanics, 1985.

Kanamori, H., Determination of effective tectonic stress associated with earthquakes faulting, the Tottori earthquake of 1943, Phys. Earth Plant. Inter., 5, 426-434, 1972.

Kanamori, H., and C. R. Allen, Earthquake repeat time and average stress drop, manuscript for the 5th Ewing Symposium on Earthquake Source Mechanics, 1985.

Mavko, G. M., Large-scale earthquakes from a laboratory friction law, submitted to J. Geophys. Res., 1983.

Papageorgiou, A., and K. Aki, A specific barrier model for the quantitative description of inhomogeneous faulting and the prediction of strong ground motion, II, Applications of the model, Bull. Seismol. Soc. Am., 73, 953-978, 1983.

Richardson, R. S. H., and H. Nolle, Surface friction under time-dependent loads, Wear, 37, 87-101, 1976.

Rice, J. R., and T. Tse, Dynamic motion of a single degree of freedom system following a rate and state dependent friction law, J. Geophys. Res., in press, 1985.

Rudnicki, J. W., and H. Kanamori, Effects of fault interaction on moment, stress drop and strain energy release, J. Geophys. Res., 86, 1785-1793, 1981.

Ruina, A., Friction laws and instabilities: a Quasi-static analysis of some dry friction behavior, Ph.D. Thesis, Brown University, 1980.

Ruina, A., Slip instability and state variable friction laws, J. Geophys. Res., 88, 10359-10370, 1983.

Rundle, J. B., H. Kanamori, and K. C. McNally, An inhomogeneous fault model for gaps, asperities, barriers, and seismicity migration, J. Geophys. Res., 89, 10219-10231, 1984.

Schwartz, D. P., and K. J. Coppersmith, Fault behavior and characteristic earthquakes: examples from the Wasatch and San Andreas fault zones, J. Geophys. Res., 89, 5681-5698, 1984.

Shimamoto, T., and J. M. Logan, Tectonophysics, 109, 165-175, 1984.

Yamashita, T., On the dynamical process of fault motion in the presence of friction and inhomogeneous initial stress: part I, Rupture propagation, J. Phys., Earth, 24, 417-444, 1976.

Table 1 Stress drop and recurrence time

fault model	driving rate (cm/yr)	average stress drop (bars)			average stress drop (bars) (a+b+c)/3	increase of stress drop (%)	recurrnce time (yr)
		a	b	c			
A	3.5	41.5	32.4	60.0	44.6	0	40
B	3.5	58.3	91.1	56.9	68.8	54	55
C	3.5	83.1	94.6	88.8	88.8	99	65
D	7.0	61.8	47.0	94.7	67.8	52	37

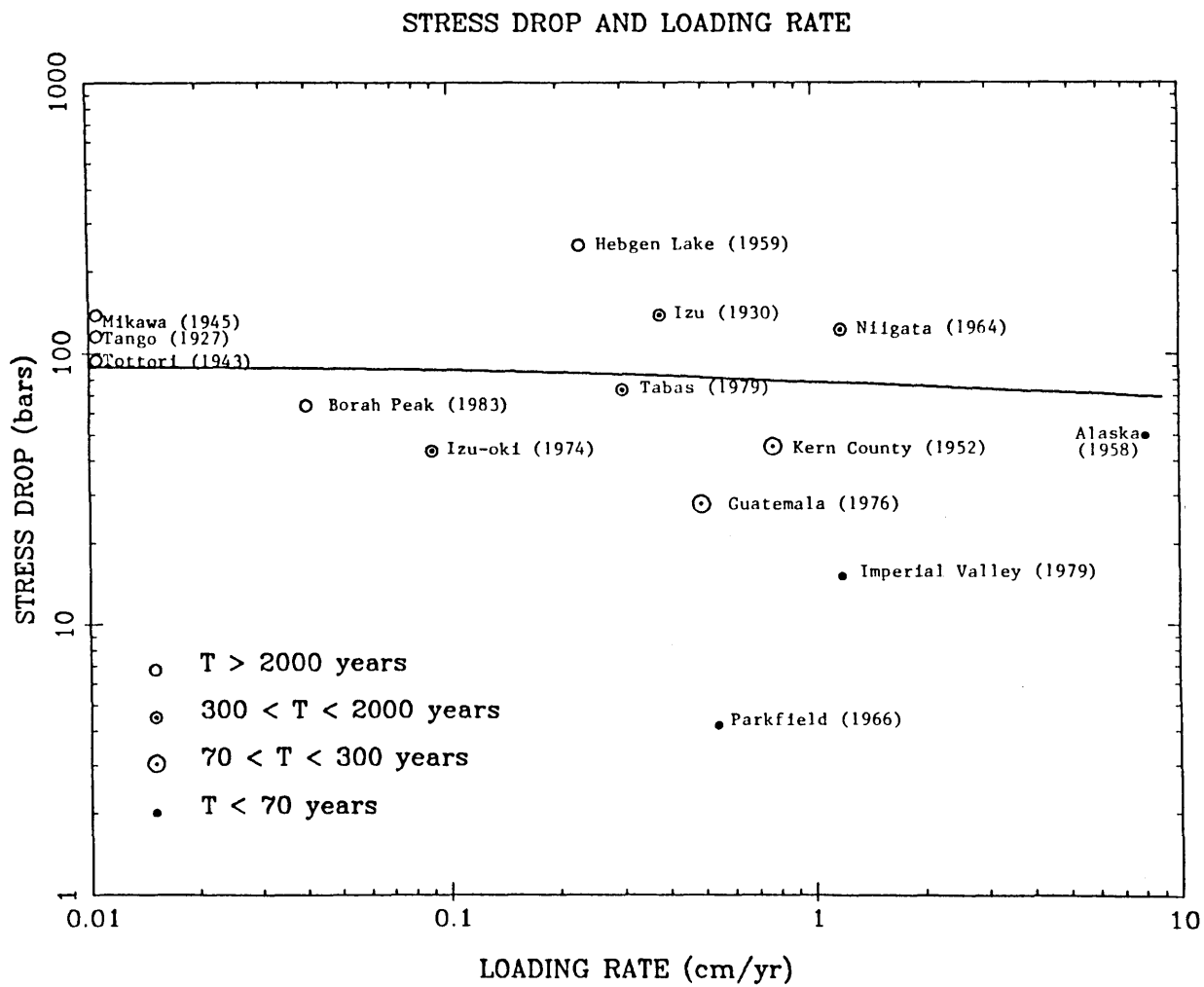
STRESS DROP AND LOADING RATE
STRESS DROP (bars)
1000
100
10
1
0.01
0.1
1
10
LOADING RATE (cm/yr)
Hebgen Lake (1959)
Izu (1930)
Niigata (1964)
Mikawa (1945)
Tango (1927)
Tottori (1943)
Tabas (1979)
Borah Peak (1983)
Izu-oki (1974)
Kern County (1952)
Alaska (1958)
Guatemala (1976)
Imperial Valley (1979)
Parkfield (1966)
T > 2000 years
300 < T < 2000 years
70 < T < 300 years
T < 70 years

Fig. 1

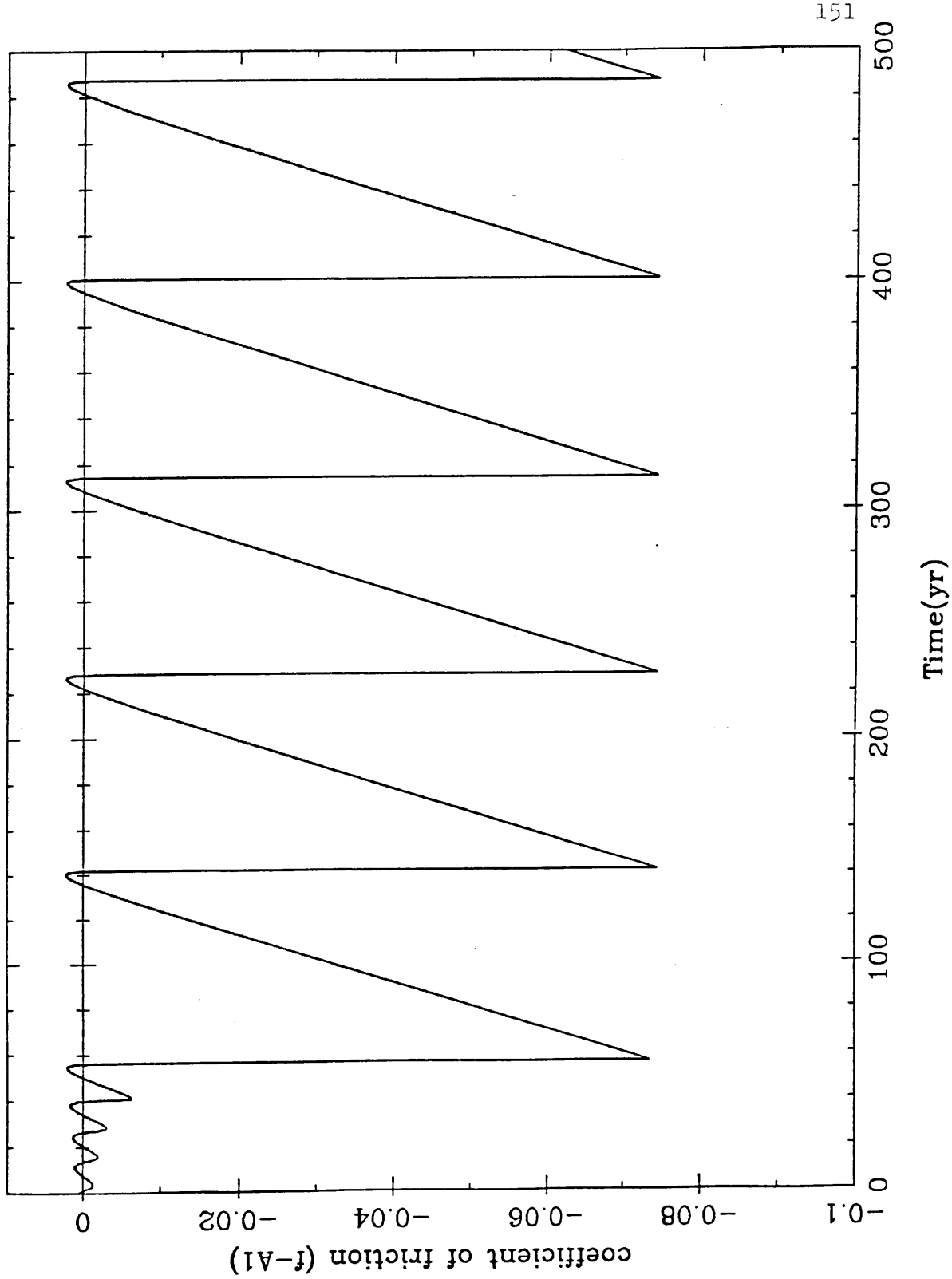
coefficient of friction (f−A1)
0
−0.02
−0.04
−0.06
−0.08
−0.1
0
100
200
300
400
500
Time(yr)

Fig. 2

coefficient of friction (f−A1)
−0.1
−0.08
−0.06
−0.04
−0.02
0
Time(yr)
0
100
200
300
400
500

Fig. 3

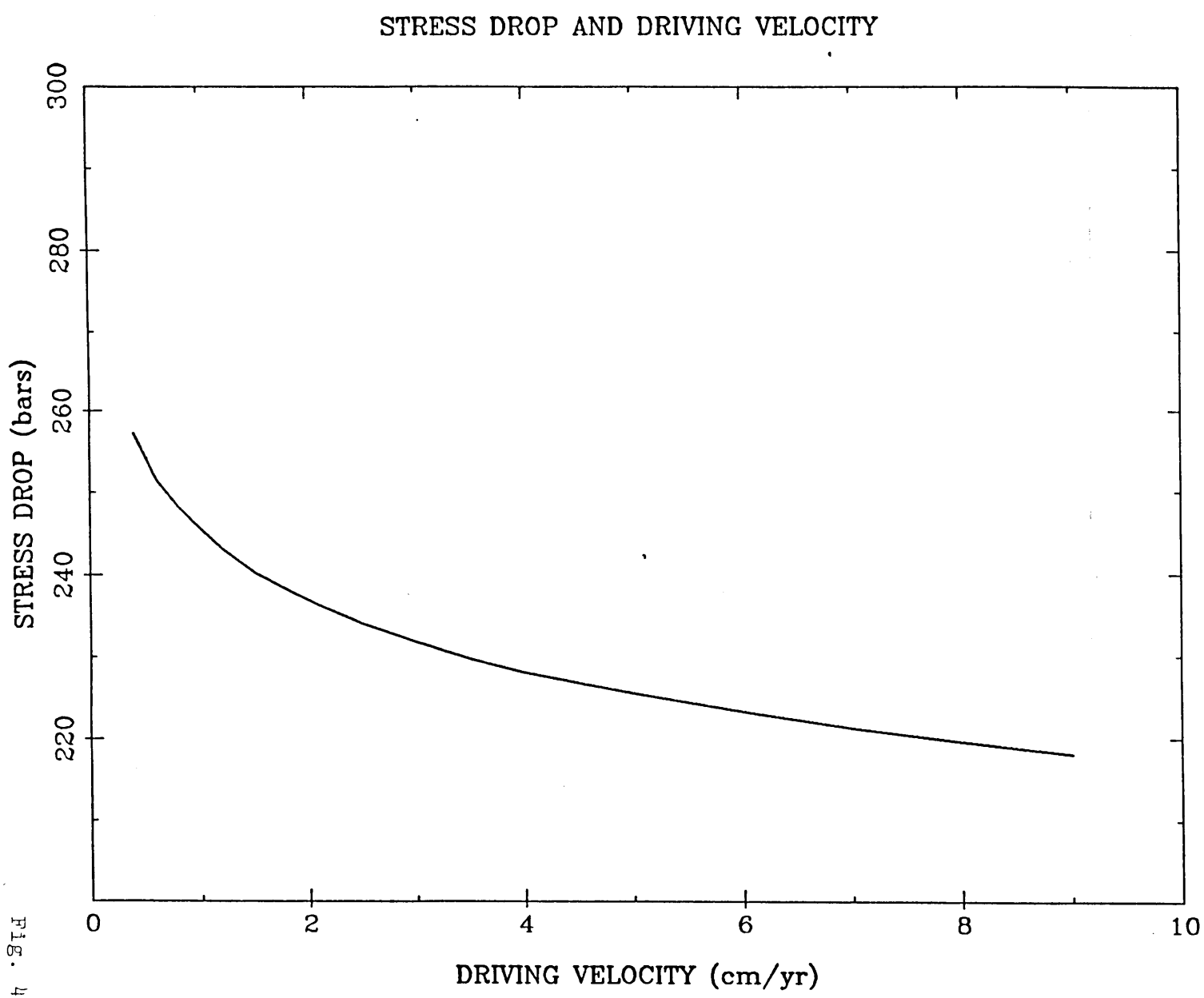
STRESS DROP AND DRIVING VELOCITY
STRESS DROP (bars)
300
280
260
240
220
0
2
4
6
8
10
DRIVING VELOCITY (cm/yr)

Fig. 4

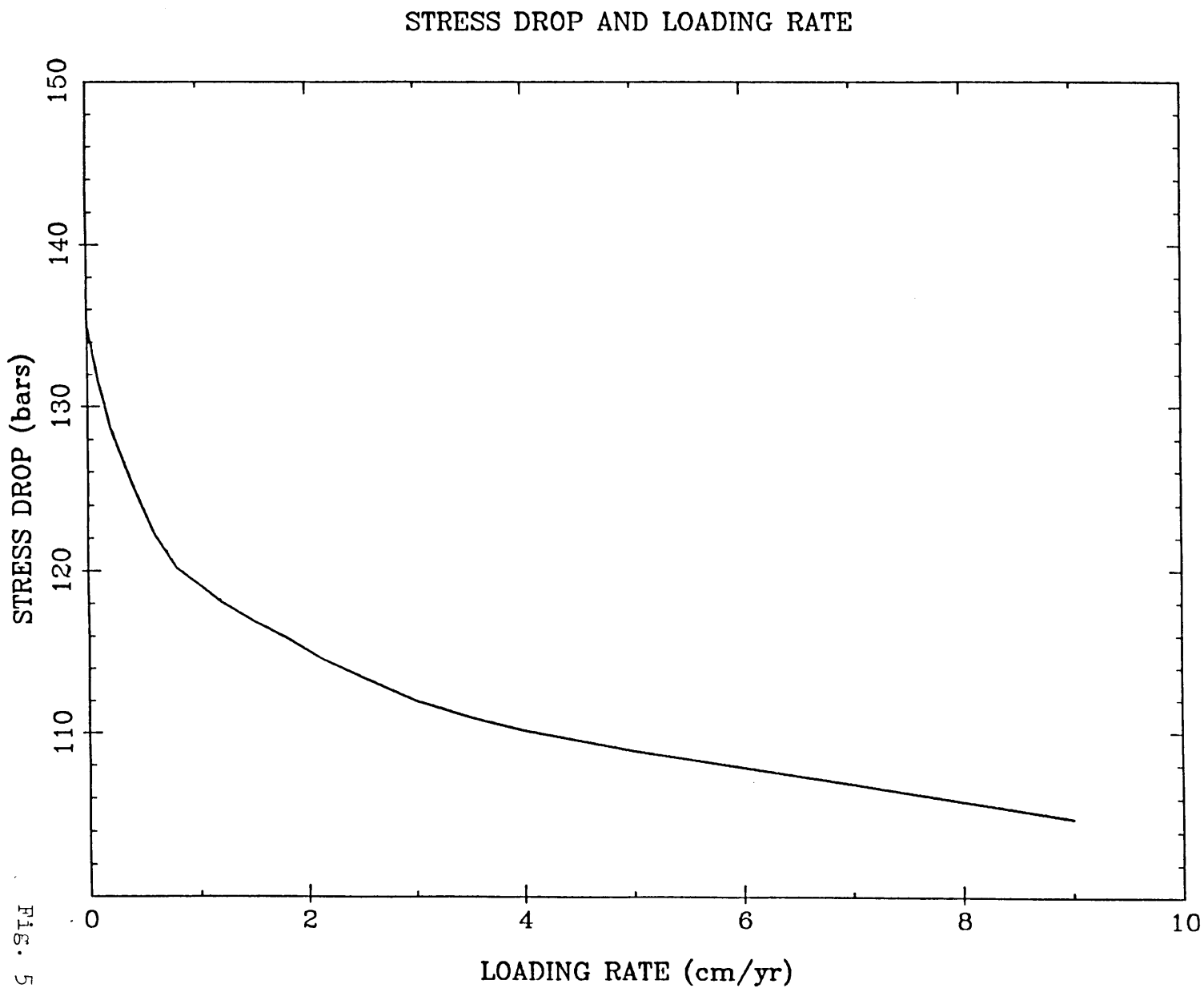
STRESS DROP AND LOADING RATE
STRESS DROP (bars)
150
140
130
120
110
0
2
4
6
8
10
LOADING RATE (cm/yr)

Fig. 5

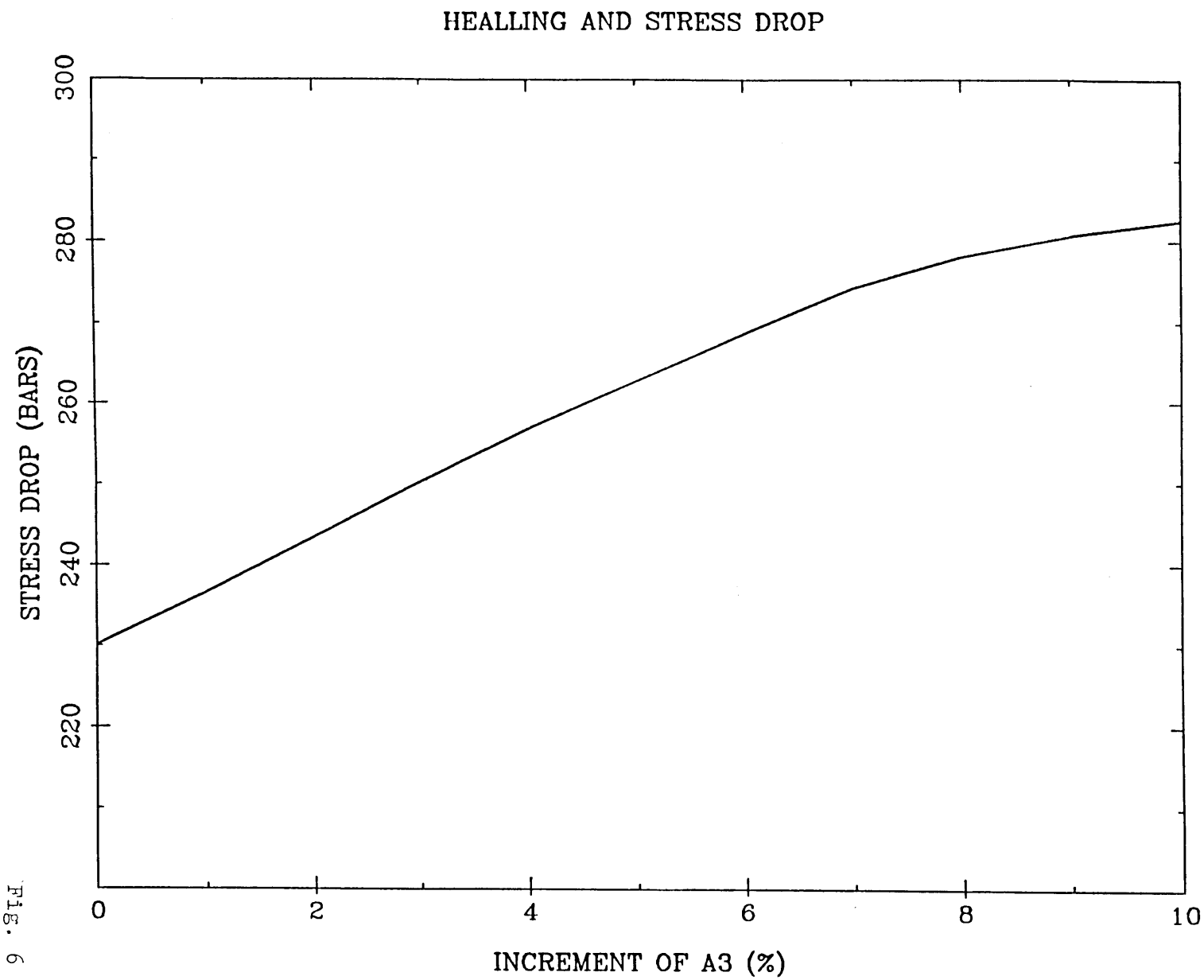
HEALLING AND STRESS DROP
STRESS DROP (BARS)
300
280
260
240
220
0
2
4
6
8
10
INCREMENT OF A3 (%)

Fig. 6

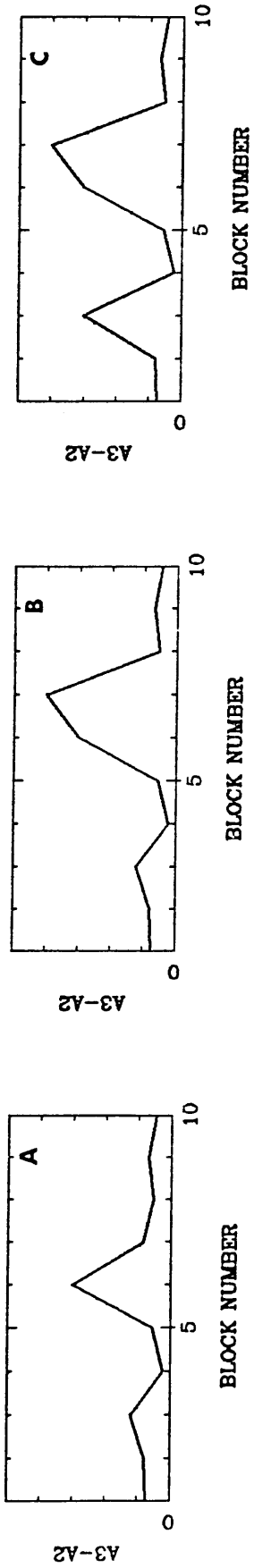

Fig. 7

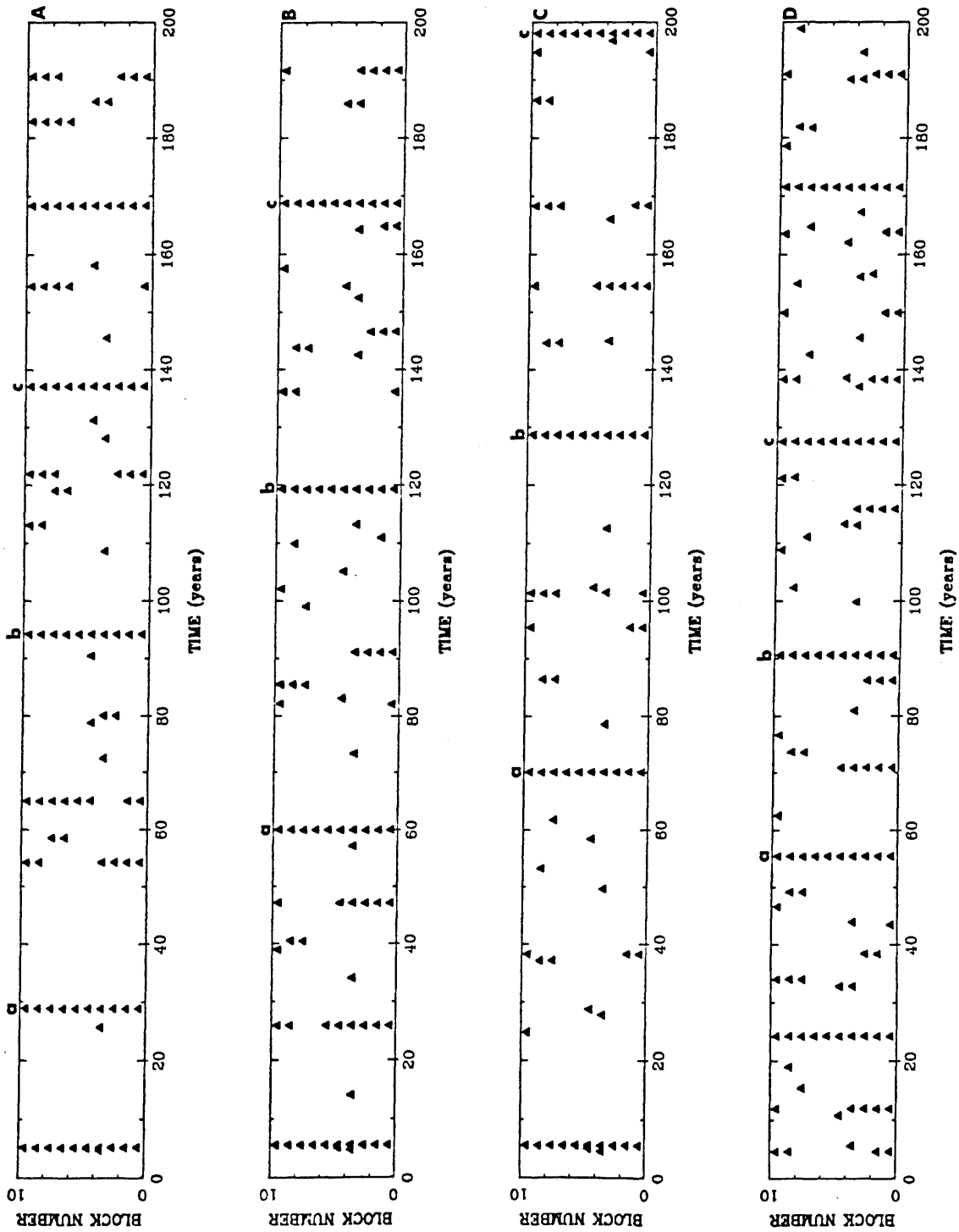
A
B
C
D
a
b
c
BLOCK NUMBER
TIME (years)
0
10
20
40
60
80
100
120
140
160
180
200

Fig. 8

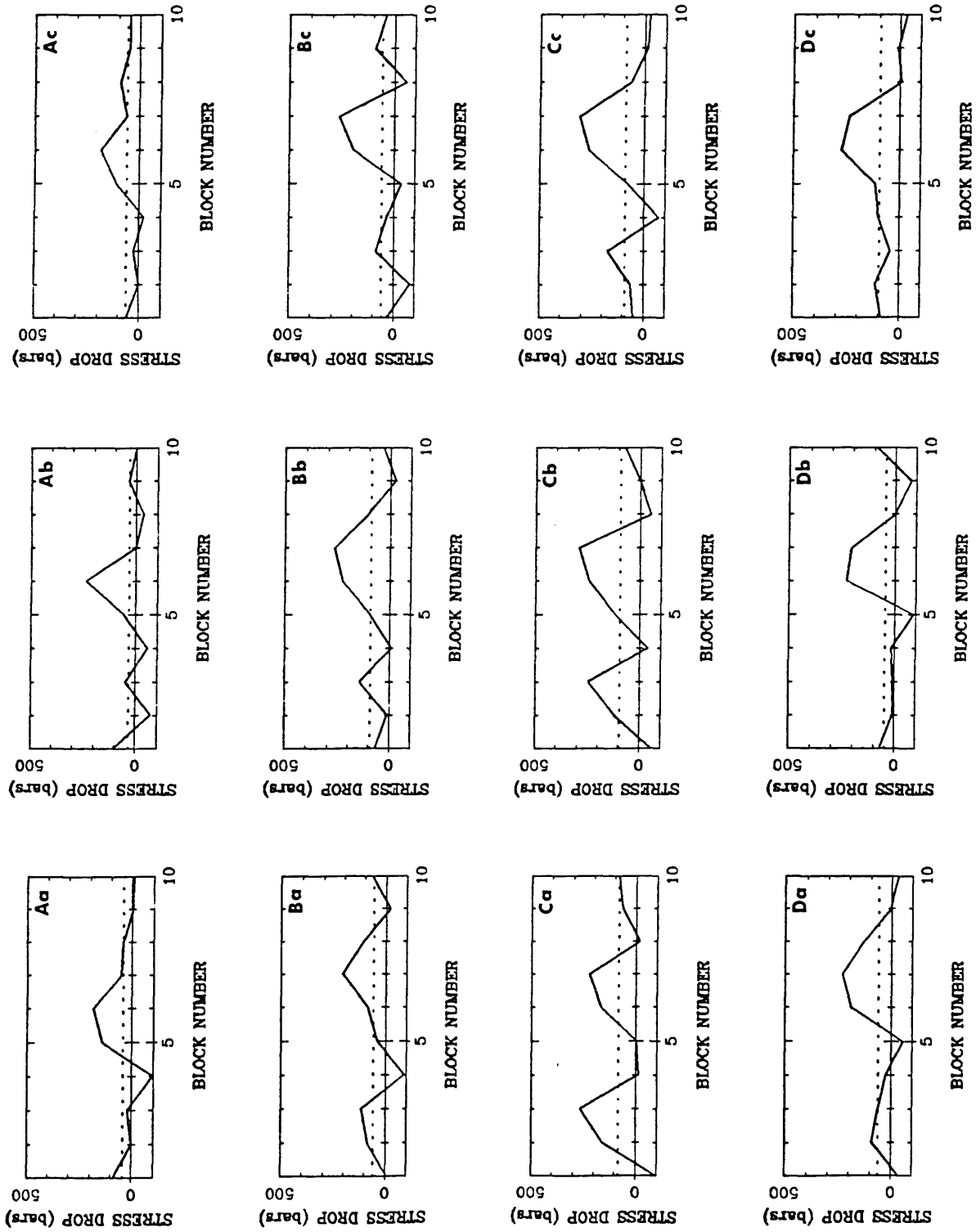
Ac
Ab
Aa
Bc
Bb
Ba
Cc
Cb
Ca
Dc
Db
Da
STRESS DROP (bars)
500
0
BLOCK NUMBER
5
10

Fig. 9

Chapter 5

Summary and Proposed Future Research Directios

In this thesis, we tried to relate some of the observed seismic phenomena to the constitutive relations between fault slip and frictional stress with special reference to important potential precursors of earthquakes. We studied the mechanism of seismic quiescence; the relation between seismicity pattern and the critical displacement of fault slip; the mechanism of stress deficit roughening process; and the effect of slip rate on stress drop. Our results are new but preliminary and further studies are needed. The following is a summary of our results and the directions for further investigations.

1. The mechanism of seismic quiescence

By comparing the simulated seismicities for fault models with the same heterogeneous strength and initial stress distributions but different constitutive relations, we showed that seismic quiescence can be produced by introducing the displacement hardening-softening friction law to a heterogeneous fault, on which the strength is distributed randomly with a uniform probability between given limits. Examining various aspects of the modeling results, we arrived at the following explanation. When the average stress along a fault reaches a certain high level before the occurrence of a large earthquake, many parts of the fault start aseismic slip and reduce the probability of occurrence of small events causing seismic quiescence. A similar explanation was speculated by Wyss and Habermann (1979).

Our explanation suggests a new diretion of research in which we may investigate the seismicity and fault displacement together. Such a research will enable us to test three existing explanations, namely, Kanamori's bimodal explanation based on fault heterogeneity itself; Ohnaka's explanation based on stress corrosion process; and the one presented in this thesis. Kanamori's explanation does not require a concurrent aseismic slip and can be easily distinguished from the others.

2. The relation between seismicity pattern and the critical displacement

In our numerical seismicity simulations of fault recurrence process with a slip weakening friction law we found that only when we choose the critical slip-weakening displacement comparable to that obtained by the interpretation of strong motion data using the specific barrier model (Papageorgiou and Aki, 1983), we obtain the realistic seismicity pattern. By a realistic pattern we mean that consists of main events, enough small events to assure a realistic magnitude-frequency relation, aseismic slip, and quiescence before main events. Our result about critical slip-weakening displacement was confirmed by Stuart's (1985) more detailed simulation of earthquakes along the San Andreas fault from Parkfield to Salton Sea. But why magnitude-frequency relation is affected by the critical slip-weakening displacement is not well understood. As shown in our simulations, the larger critical displacement gives less small events. Probably, the critical displacement may be related to fault ductility.

The critical displacement estimated by Papagiorgiou and Aki (1983) for several California earthquakes ranges from 0.4 to 3 m which roughly agrees with the range 10 cm to 1 m obtained by the numerical experiments on recurrence process. On the other hand, the critical displacement ranges from 5×10^{-4} to 25×10^{-4} cm for the laboratory experiments with a 2 m long rock sample (Okubo and Dieterich, 1984). This several orders of magnitude difference in critical displacement, however, is consistent with equally large differece in the apparent Griffith energy between laboratory estimates on rock samples and earthquakes (Ida, 1972; Aki, 1979).

3. The mechanism of stress deficit roughening process

The Gutenberg-Richter magnitude-frequency relation is still the most fundamental observation on seismicity, although the idea of characteristic earthquakes may modify this relation for earthquakes associated directly with certain fault segments (Schwartz and Coppersmith, 1984). In order to simulate this relation, a stress deficit roughening process is required to counteract the smoothing effect due to the interaction among fault segments.

Our simulations showed that the rate and state dependent friction law together with a heterogeneous fault predicts non-uniform slip and stress drop along the fault and may provide a physical mechanism for such a roughening process. The non-instantaneous healing predicted by the rate and state dependent friction law lengthens the time duration for fault slip to stop and reduces the interaction among fault segments and finally allows

non-uniform slip and stress drop along a heterogeneous fault. Here the interaction is reduced not by reducing the connecting spring constants but by reducing the frictional strength and lengthening the interaction time due to the time dependent healing. The heterogeneous distribution of the critical displacement alone does not produce stress deficit ruoghening process as shown earlier for the friction laws which do not include time dependent healing.

Another interesting result from the rate and state dependent friction law is that strong patches are necessary for the occurrence of large earthquakes.

We have not studied quantitatively the effects of fault heterogeneity and the changes of parameters in the rate and state dependent friction law on magnitude-frequency relation. We have neither studied the simulation of characteristic earthquakes which will be directly relevant to deterministic predictions of earthquake occurrence and strong motion.

4. The effect of slip rate on stress drop

So far, we have discussed the cases in which the parameters controlling the tectonic loading are constant. We varied the loading rate and found that only a weak relation exists between stress drop and tectonic loading rate. We found that the increase of stress drop due to the decrease of loading rate is roughly in agreement with Kanamori and Allen's observational results. The healing of a single asperity alone, however, cannot explain the observed variation of stress drop by up to two orders of magnitude.

By numerical simulations we showed that the variability of stress drop may be due primarily to the different distribution of fault strength. Our simulation also suggests that the power law can explain the observed stress drop vs. slip rate relation better than the logarithmic law which is an earlier and simpler version of the rate and state dependent friction law.

A model with the above features may be used to simulate realistic fault behavior. The observed recurrence time, tectonic loading rate (long-term slip rate), seismic and aseismic slip, and seismicity patterns all can be used to constrain the model parameters and in turn, by changing the model parameters within their estimated uncertainties, we can obtain a probability for the time of occurrence of the next predicted earthquake.

Toward the ultimate goal of reliable earthquake prediction, we have been working along two lines of approaches. One is the theoretical deterministic approach by physical modeling of recurrence behavior of earthquakes on a heterogeneous fault using laboratory-inferred friction laws as discussed in this thesis and the other is the empirical statistical approach by assigning probabilities of earthquake occurrence according to observed precursors.

Following the procedure pioneered by Utsu (1979) and using the idea of probability gain proposed by Aki (1981), we (see appendix) assigned the probability gain of various precursors for four large Chinese earthquakes that occurred in the 1970's. From this study we

learned the following lessons which are important for probability assignment.

(1) It is possible to collect enough precursory data and reach a probabilistic assignment close to 1, for large ($M > 7$) earthquakes in China.

(2) The Chinese success was largely due to their reliance on intermediate and short-term precursors, even though these precursors have very low success rate.

(3) In order to estimate the success rate for each precursor, a long historical record, which includes many cycles of large earthquake recurrence, is needed. (The success rate is needed to compute the probability gain.)

These lessons from the Chinese experience, however, are not applicable to predicting earthquakes on the San Andreas fault because of the lack of data on intermediate and short-term precursors. This fact has forced us to switch to another approach for California earthquakes, namely, the deterministic physical modeling as mentioned earlier. Here, although the modeling itself is deterministic, the results contain uncertainty because of uncertainties in model configuration and model parameters. If the modeling is constrained by some well-observed parameters and data, such as the tectonic loading rate and recurrence times of large earthquakes, and some less well determined parameters and data, we can always obtain optimal estimates of model parameters according to the theory of stochastic inverse (e.g., Tarantola and Valette, 1982). In the framework of the stochastic inverse theory, both data

and model are considered as stochastic processes, and the stochastic inverse operator will be optimal for the a priori probability distribution of the model parameters. As new data are introduced, the model parameters will be revised by the application of the inverse operator to the data, and the a posteriori probability distribution of the model parameters can be estimated. Such a modeling can contribute directly to the probabilistic approach to earthquake prediction.

Thus the probabilistic approach can be improved by incorporating a physical model, especially for an area like the San Andreas fault zone, where the most important elements for a numerical model - the tectonic loading rate, the constitutive relation of fault slip, and the fault heterogeneity - are known with some uncertainty. Stuart et al. (1985), studied an earthquake instability model including preseismic and coseismic changes of fault slip and ground deformation. By applying their model to the Parkfield segment of the San Andreas fault, they were able to predict the recurrence interval. In their modeling the information from seismicity has not been used. Our heterogeneous fault model, however, can accommodate the information from both seismicity and fault deformation.

One thing we feel important is that all simulations obtained from a discrete model need to be checked carefully for scale dependence. We only checked the effect of spring constant ratio. Our results are very preliminary at this point.

REFERENCES

Aki, K., Characterization of barriers on an earthquake fault, J. Geophy. Res., 84, 6140-6148, 1979.

Aki, K., A probabilistic synthesis of precursory phenomena, in Earthquake Prediction, An International Review, edited by D. W. Simpson and P. G. Richards, 680 pp., AGU, Washington, D. C., 1981.

Ida, Y., Cohesive force across the tip of a longitudinal shear crack and Griffith's specific surface energy, J. Geophys. Res., 77, 3796-3805, 1972.

Okubo, P. G., and J. H. Deterich, Effects of physical fault properties on frictional instabilities produced on simulated faults, J. Geophys. Res., 89, 5815-5827, 1984.

Papageorgiou, A. S., and K. Aki, A specific barrier model for the quantitative description of inhomogeneous faulting and the prediction of strong ground motion: Part II, Applications of the model, Bull. Seis. Soc. Am., 73, 953-978, 1983.

Schwartz, D. P., and K. J. Coppersmith, Fault behavior and characteristic earthquakes: examples from the Wasatch and San Andreas fault zones, J. Geophys. Res., 89, 5681-5698, 1984.

Stuart, W. D., R. J. Archuleta, and A. L. Lindh, Forecast model for moderate earthquakes near Parkfield, California, J. Geophys. Res., 90, 592-604, 1985.

Tarantola, A., and B. Valette, Generalized nonlinear inverse problems solved using the least-squares criterion, Rev. Geophys. Space Phys., 20, 219-232, 1982.

Utsu, T., Calculations of the probability of success of an earthquake pre-diction (in the case of Izu-Oshima-Kinkai earthquake of 1978), Rep. Cood. Comm. for Earthquake Prediction, 21, 164-166, 1979.

Wyss, M., and E. Habermann, Seismic quiescence precursory to a past and a future Kuriles islands earthquake, PAGEOPH, 117, 1195, 1979.

APPENDIX

Assigning Probability Gain for Precursors of Four Chinese Earthquakes

by

Cao and Aki

JOURNAL OF GEOPHYSICAL RESEARCH, VOL. 88, NO. B3, PAGES 2185–2190, MARCH 10, 1983

Assigning Probability Gain for Precursors of Four Large Chinese Earthquakes

TIANQING CAO[1] AND KEIITI AKI

Department of Earth and Planetary Sciences, Massachusetts Institute of Technology, Cambridge, Massachusetts 02139

We extend the concept of probability gain associated with a precursor (*Aki*, 1981) to a set of precursors which may be mutually dependent. Making use of a new formula, we derive a criterion for selecting precursors from a given data set in order to calculate the probability gain. The probabilities per unit time immediately before four large Chinese earthquakes are calculated. They are approximately 0.09, 0.09, 0.07 and 0.08 per day for 1975 Haicheng (M = 7.3), 1976 Tangshan (M = 7.8), 1976 Longling (M = 7.6), and Songpan (M = 7.2) earthquakes, respectively. These results are encouraging because they suggest that the investigated precursory phenomena may have included the complete information for earthquake prediction, at least for the above earthquakes. With this method, the step-by-step approach to prediction used in China may be quantified in terms of the probability of earthquake occurrence. The ln P versus t curve (where P is the probability of earthquake occurrence at time t) shows that ln P does not increase with t linearly but more rapidly as the time of earthquake approaches.

INTRODUCTION

We are still at the rudimentary stage in trying to predict the occurrence of an earthquake. At this stage, in addition to our effort for understanding the physics of earthquake failure, we need to pursue statistical approaches based on empirical data. The basic difficulties in using a probabilistic model are the lack of an adequate physical theory and the lack of suitable data [*Rikitake*, 1976]. However, as *Vere-Jones* [1978] indicated, 'Despite these difficulties, there may be already sufficient knowledge of precursory phenomena to achieve modest but not trivial reductions in the losses due to earthquake damage.' During the last 15 years, many precursory phenomena before large earthquakes have been documented in China (Reports for Hsingtai, Bohai, Donghai, Luhuo, Yongshan-Daguan, Haicheng, Longling, Tangshan, and Songpan earthquakes; these reports will be abbreviated as 'Reports for Chinese Earthquakes' in the following, except where explicit references are made.) Several major earthquakes were predicted on the basis of empirical relations between large earthquakes and their precursory phenomena, but none of these predictions had a quantitative estimate of the probability of their occurrence. For the Tangshan earthquake, an intermediate-term prediction was made, but the attempt to make an imminent prediction failed. It might have been helpful if we had had an objective quantitative measure for the probability of earthquake occurrence. After the Tangshan earthquake many people including seismologists were very shocked that false predictions were made for many areas, and hundreds of millions of people living in various provinces of China were forced to live outdoors for longer than one month. This underlines the need for an objective quantitative measure for the probability of earthquake occurrence both before and after a large earthquake. The fact that several major earthquakes have been predicted in China shows that we have received some real information about the earthquake occurrence, although the data are contaminated with noise. It may be possible to establish an objective earthquake prediction method, if we assume that these anomalies recognized by Chinese seismologists are reflecting the physical state of the earth preparing for an earthquake.

Kagan and Knopoff [1976, 1977] introduced the concept of predictive ratio $P(\Delta|I)/P(\Delta)$, where Δ denotes a region in the five-dimensional space (latitude, longitude, depth, time, and magnitude) in which an earthquake is going to occur and $P(\Delta|I)$ is the conditional probability of occurrence given information I. They did not give a practical risk formula which can synthesize all of the precursors. *Utsu* [1979] and *Rhoades and Evison* [1979] obtained a formula for probability calculation using independent precursors. Later, *Aki* [1981] reduced the formula into an extremely simple form by introducing the concept of probability gain for each precursor. This concept is similar to that of predictive ratio [*Kagan and Knopoff*, 1976, 1977]. All of these results encounter two difficulties. First, we do not have sufficient data. Second, these formulas apply only to independent precursors, while we do not know if our precursors are independent or dependent.

In this paper we will modify the above formula to apply to mutually dependent precursors. Although our new formula also suffers from the first difficulty, it enables us to select precursors which are independent. Following this approach, we calculate the probability gain for four Chinese large earthquakes. We will also discuss a variety of problems which we encountered in our approach.

CONDITIONAL PROBABILITY FOR MUTUALLY DEPENDENT PRECURSORS

We first introduce a few definitions following *Aki* [1981]. If in a specified area an earthquake is predicted to occur, the average frequency of occurrence of earthquakes with a certain magnitude range in that area is $P_0 = N(M)/T$. Here, $N(M)$ is the number of earthquakes with a magnitude equal to or greater than M recorded during the total time period T. For a short time interval τ, then, the unconditional probability of occurrence of an earthquake with magnitude equal to or greater than M in that area is $P(M) = P_0\tau$. We divide the time axis into consecutive segments with a constant interval τ (Figure 1). The interval τ is taken short enough so that each segment contains, at most, one earthquake.

[1]On leave of absence from the Seismological Bureau of Liaoning Province, Shenyang, China.

Copyright 1983 by the American Geophysical Union.

Paper number 2B1951.
0148-0227/83/002B-1951$05.00

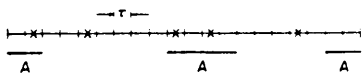

Fig. 1. This is the time axis divided into consecutive segments with the constant interval τ. The precursor A occurs in time intervals marked A. The crosses indicate the occurrence of an earthquake with magnitude equal to or greater than M.

Consider those segments during which the precursor A exists. Of these segments, let the number of segments containing an earthquake be n_A, and the number of segments containing no earthquake be $\bar{n}_A$. Then, the conditional probability $P(M|A)$ of occurrence of an earthquake within a time interval τ is given by

$$P(M|A) = \frac{n_A}{n_A + \bar{n}_A} \tag{1}$$

Since, for small τ, $P(M|A)$ is proportional to τ, we may put

$$P(M|A) = P_A \tau \tag{2}$$

where P_A is the probability of an earthquake occurrence per unit time under the condition that the precursor A is existing. Let $B, C, \cdots$ designate the other precursors, and we define similarly n_B, $\bar{n}_B$, and P_B for precursor B, and so on. For simplicity, we shall discuss the case of two precursors A and B in the following. The results can be easily extended to include any number of precursors.

For any precursors A and B, we can write

$$P(A, B|M) = \alpha P(A|M)P(B|M) \tag{3}$$

and

$$P(A, B|\bar{M}) = \beta P(A|\bar{M})P(B|\bar{M}) \tag{4}$$

where α and β are two constants and $\bar{M}$ means the nonoccurrence of an earthquake. If A and B are conditionally independent, $\alpha = 1$ and $\beta = 1$.

For $\alpha < 1$ or $\beta < 1$, A and B given M or $\bar{M}$ are less likely to occur simultaneously than the independent case. For $\alpha > 1$ or $\beta > 1$, A and B given M or $\bar{M}$ are more likely to occur simultaneously than the independent case. According to Bayes' theorem,

$$P(M|A, B) = \frac{P(A, B|M)P(M)}{P(A, B|M)P(M) + P(A, B|\bar{M})P(\bar{M})} \tag{5}$$

Putting the equations (3) and (4) into (5), we obtain

$$P(M|A, B) = \frac{\alpha P(M)P(A|M)P(B|M)}{\alpha P(M)P(A|M)P(B|M) + \beta P(\bar{M})P(A|\bar{M})P(B|\bar{M})} \tag{6}$$

Following the same procedure as used by *Aki* [1981], for a small time interval τ we can write (6) as

$$P(M|A, B) \approx P\tau \tag{7}$$

where

$$P = \frac{\alpha}{\beta} P_0 \frac{P_A}{P_0} \frac{P_B}{P_0} \tag{8}$$

In the above formula, P_A/P_0 and P_B/P_0 are the probability gains due to A and B, respectively. Their product is the total probability gain. When $\alpha = 1$, $\beta = 1$, this formula becomes the same as *Aki*'s [1981]. In principle, this formula can be used for any precursors if we have enough data to estimate the coefficients α and β. For example, we can take all seismicity patterns (periodicity, enhancement, migration, swarm, foreshock, etc.) as precursors and calculate their α, β, and the total probability gain. Here, we encounter again the difficulty that the data are not enough. We shall get around this difficulty by an appropriate selection of precursors.

How to Select Precursors

Before we give the selection criterion, it is useful to recall some basic facts about the precursory phenomena. These facts are well known in China after many prediction practices [Reports for Chinese Earthquakes; *Ma*, 1979; *State Seismological Bureau*, 1979]. They are as follows:

1. Before a large earthquake, we observe precursors with different precursor times. They can be roughly classified into long-term, intermediate-term, short-term, and imminent precursors. By using these precursors, a step-by-step approach to prediction can be made. According to our past experience, precursors with similar precursor times often have different success rates in earthquake predictions (the details are given in the next section). Having similar precursor times means that they occur roughly simultaneously before earthquakes.

2. With the present accuracy of precursor observation, we have found more precursory phenomena before larger earthquakes than before smaller earthquakes. Some precursors, such as anomalies of radon content and animal behavior, almost always appeared before earthquakes with $M \geq 7.0$, but not always before earthquakes with $M < 7.0$.

The fact (1) means that our data set includes many dependent precursors. If we use all these precursors as independent events, we will overestimate the probability. Therefore, the first step is to select precursors with different precursor times.

A close look at equation (3) tells us that if $P(A|M) = 1$, then $P(A, B|M) = P(B|M)$ and $\alpha = 1$. For more precursors, if all of the conditional probabilities of the selected precursors $P(A|M)$, $P(B|M)$, $\cdots$ are equal to 1 except for one of them, then we have $\alpha = 1$. This is a very special condition. With the fact (2), we can raise the magnitude of the predictive earthquakes and find precursors which satisfy or are close to this special condition (shown in the next section). Therefore, the selected precursors satisfy $\alpha = 1$. Thus our criterion for selecting a set of independent precursors is either they always precede an earthquake ($P(A|M) = 1$, $P(B|M) = 1$, etc.), or they always precede an earthquake with one exception. In these two cases, it can be assured that at least $\alpha = 1$. With $\alpha = 1$, it seems reasonable to assume that these precursors occur independently when there are no earthquakes, or $\beta = 1$. This is based on the physical consideration that all anomalies not followed by large earthquakes may be caused by some random sources and are independent.

Classification and Selection of Precursors

According to the Chinese experience with earthquake prediction, precursors with different precursor times are classified into four types, namely, long-term, intermediate-term, short-term, and imminent precursors. Now we give the details about these types and our selection method.

The first type includes long-term alternation or seismically

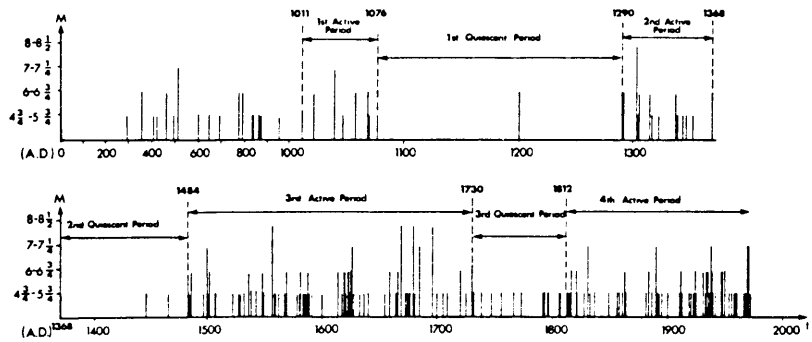

PERIODIC VARIATION OF SEISMICITY IN NORTH CHINA

Fig. 2. The periodic variation of seismicity in North China.

active and quiescent periods and migration of large earthquakes ($M \geq 6.0$) in a seismic region. According to the precursor time, they are the long-term anomalies. The time scale of the alternation is about 100 to 300 years in North China and Southwest China [*Savarensky and Mei*, 1959; *Mei*, 1960; *Chu*, 1976; *Lee and Brillinger*, 1979]. The *M-t* diagram of North China (Figure 2) shows that all earthquakes with $M \geq 7.0$ occurred in active periods. Thus it satisfies our selection criterion.

The second type of precursors includes enhancement of seismicity of moderate-sized earthquakes ($4\frac{3}{4} < M < 7$), swarms, temporal change of relative elevation along a short base line (about several hundred meters long), gravity anomaly, etc. One example of the synchronous change of seismicity and relative elevation is given in Figure 3 from *Gu and Cao* [1980]. According to many observations in China, their precursor times are approximately several years (Reports for Chinese Earthquakes). We will select the seismicity enhancement of intermediate earthquakes as their representation and call it the intermediate-term anomaly. This is the only selected anomaly which does not always appear before large earthquakes, but it appeared before all of the four earthquakes we are discussing.

The third type of precursors, so-called short-term anomaly, includes radon content in groundwater, earth current, resistivity, etc. Their precursor times are about several months (Reports for Chinese Earthquakes). Among them, data on radon content are most abundant. It is selected to represent this type of precursors.

The fourth type of precursors is the imminent precursors which includes anomalies of ground water (changes in level, color, taste, etc.), anomalous animal behavior, earth light, etc. We call them macro-anomalies or imminent anomalies. Their precursor times are about several days [*Jiang*, 1980]. We select anomalous animal behavior as the representation of this type of precursors. It has the best data set compared with other macro-anomalies. In China many historical records exist on precursory animal behavior [*Academia Sinica*, 1956]. It played a very important role in the Chinese predictions and was confirmed before every large earthquake in the past 15 years.

The fact that a certain type of precursors has a relatively stable precursor time is a basis of earthquake prediction. This makes the conditional probability, obtained according to the past experience, a meaningful quantity which can be used in the future prediction.

According to *Utsu* [1979], the conditional probability of an earthquake occurrence per unit time given an individual precursor is its success rate divided by the precursor time $m\tau$. If $\hat{P}(M|A)$ is the success rate of precursor A, then the conditional probability per unit time is

$$P_A = \hat{P}(M|A)/m\tau \tag{9}$$

ASSIGNMENT OF PROBABILITY GAIN

Now, we are ready to assign the probability gain for four large Chinese earthquakes. They are Haicheng earthquake and Tangshan earthquake in region I; Longling earthquake and Songpan earthquake in region II, as shown in Figure 4. Regions I and II are, according to the historical seismicity, independent seismic areas [*Li*, 1957]. In our case, each specified area is about one sixth of region I or II (Figure 4). The size of specified area approximately corresponds to the extent of precursor distribution (long-term precursor excluded).

We designate the long-term anomaly as A, intermediate-term anomaly as B, short-term anomaly as C, and imminent anomaly as D and the probability gain for A, B, C, and D as G_A, G_B, G_C, and G_D.

The historical seismicity in North China (region I) has shown alternation of active periods and quiescent periods for more than one thousand years (Figure 2). Because of the incompleteness of historical records, the frequency of earth-

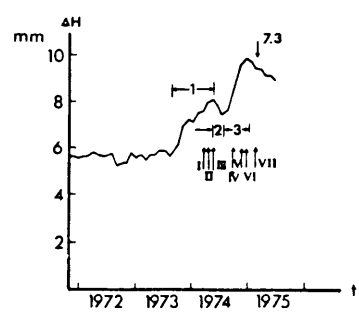

Fig. 3. Synchronization between seismicity of small earthquakes and ground deformation. The curve represents the changes in relative elevation ΔH as a function of time t for 1972–1976 along a short level line across the Jinzhon fault in Liaoning Province. I~VII are swarms that occurred before Haicheng earthquake. All the swarms occurred in segments 1 and 3 of the curve corresponding to the rapid changes of the relative elevation.

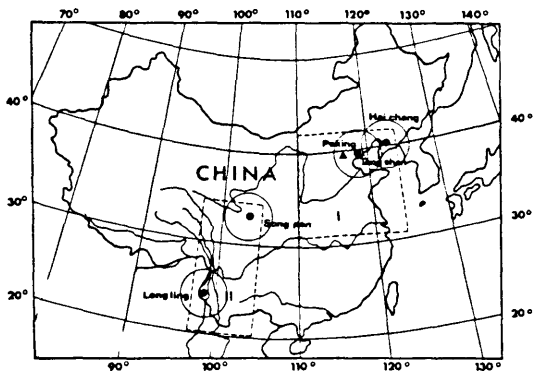

Fig. 4. Location of region I, II, and epicenters of the Haicheng earthquake, Tangshan earthquake, Songpan earthquake, and Longling earthquake. Circles surrounding the epicenters indicate the specified areas for these earthquakes.

quake occurrence for $4\frac{3}{4} \leq m \leq 5\frac{3}{4}$ in first and second active periods is lower than in third quiescent period. Our calculation is for $M \geq 7.0$, the effect of the incompleteness may be neglected. The alternation of active and quiescent periods has repeated 4 times during the period from 1011 A.D. to present. Total of 14 large earthquakes ($M \geq 7.0$) occurred in this period. The long-term average rate of earthquake occurrence P_0^{I} ($M \geq 7.0$) for each of the specified area in region I (Figure 4) is therefore about $14/[(1975-1011) \times 365 \times 6] \approx 6.7 \times 10^{-6}$ per day. The superscript I notes for the specified area in region I. Here, we have assumed the specified areas are large enough so that the average rates of earthquake occurrence in these areas are approximately proportional to their size. The factor 6 in the denominator is the area ratio between region I and the specified area for the Haicheng or the Tangshan earthquakes. All these 14 large earthquakes occurred in four active periods, 1101–1076; 1290–1368; 1484–1730; and 1812–1975. Therefore the conditional probability P_A^{I} ($M \geq 7.0$) of earthquake occurrence during active periods is

$$14/\{[(1076-1011) + (1368-1290) + (1730-1484) + (1975-1812)] \times 365 \times 6\} \approx 1.2 \times 10^{-5}$$

per day and $G_A^{\mathrm{I}} = P_A^{\mathrm{I}}/P_0^{\mathrm{I}} \approx 1.7$. This result is applicable to the Haicheng earthquake as well as to the Tangshan earthquake.

A similar calculation can be performed for the Longling and the Songpan earthquakes. Historical records in region II are shorter than in region I. They are relatively complete after 1515 A.D. for $M \geq 6.0$ earthquakes. During 460 years from 1515 to 1975, twenty earthquakes with $M \geq 7.0$ occurred (aftershocks excluded) in this region. The long-term average rate of earthquake occurrence (in a specified area) P_0^{II} ($M \geq 7.0$) is $20/[(1975-1515) \times 365 \times 6] \approx 1.0 \times 10^{-5}$ per day. The superscript II notes for the specified area in region II. Among these earthquakes, 16 occurred in an active period from 1733 to 1975. We obtain the conditional probability P_A^{II} ($M \geq 7.0$) $= 16/[(1975-1733) \times 365 \times 6] \approx 1.5 \times 10^{-5}$ per day with $G_A^{\mathrm{II}} = P_A^{\mathrm{II}}/p_0^{\mathrm{II}} \approx 1.5$. This result is applicable to the Songpan and the Longling earthquakes, although $P^{\mathrm{II}}(A|M) = 16/20 = 0.8 \approx 1$ meets our precursor selection criterion approximately, though not perfectly.

The enhancement of seismicity of intermediate earthquakes ($4\frac{3}{4} < M < 7$) before large earthquakes ($M \geq 7.0$) in North China was studied by *Wang et al.* [1981] using the pattern recognition method [*Gelfand et al.*, 1972, 1976]. In this work, the recognized objects D (dangerous) are (1) the number of earthquakes with $M \geq 5.5$ in 20 years preceding a large earthquake is greater than or equal to 5 and (2) the number of earthquakes with $M \geq 5.0$ in the preceding ten years is greater than or equal to 3. The recognition rate or, in our words, the conditional probability is about 0.67 for the whole region I and $\bar{P}(M|B) = 0.67/6 \approx 0.11$ for a specified area in region I. According to Wang's results and the fact that the seismicity has enhanced since the 1966 Hsingtai earthquake in North China, we take ten years as the precursor time, then according to formula (9) $P_B^{\mathrm{I}} = 0.11/(10 \times 365) \approx 3.1 \times 10^{-5}$ per day and $G_B^{\mathrm{I}} = P_B^{\mathrm{I}}/P_0^{\mathrm{I}} = 4.6$. The historical records in region II are very incomplete especially for intermediate earthquakes. We take the conditional probability 0.11 for a specified area in region I as the approximate value for region II. In Songpan region, the enhancement of seismicity of moderate earthquakes began in 1966 with the Nanping earthquake (November 7, 1966, $M = 4.8$, 32.9°N, 104.3°E), then the Renshon earthquake (January 24, 1967, $M = 5.5$, 30°15′N, 104°08′E). The precursor time is also 10 years [*State Seismological Bureau*, 1977, p. 1; *Seismological Bureau of Szechuan Province*, 1979]. In Longling region, it is again 10 years. During 1966–1976, seismicity of earthquakes with $M \geq 4.0$ enhanced surrounding the Longling region [*Chen and Zao*, 1979, p. 2]. Therefore the precursor times of the enhancement of moderate earthquakes are the same for these four earthquakes.

The history of instrumental recording of radon content is much shorter than that of seismicity. The recording began in 1973 in the Haicheng area. We count the number of anomalies during the past 10 years, except one which appeared just before the Haicheng earthquake, then we can calculate the total number expected during the average recurrence time of large earthquakes in a specified area. According to the suggestion of seismologists who worked on the earthquake prediction in the Haicheng area using radon data, the data from Panshan station (about 50 km northwest of the epicenter of the Haicheng earthquake) has the best quality and longest record. It is selected to calculate the success rate of radon anomalies. We calculated the standard deviation for ten years data and found that the observed radon contents exceeded twice the standard deviation over 2 month's duration 5 times (around 1973.9, 1974.6, 1975.1, 1976.1, 1976.9). One of them (1975.1) appeared just before the Haicheng earthquake. The average recurrence time of a large earthquake in this area is $1/P_0^{\mathrm{I}} \approx 409$ years. Therefore, we may expect $(5-1) \times 409/10 \approx 163$ anomalies without earthquakes. The success rate is approximately $1/163 \approx 0.006$. Obviously, this value is a rough approximation. We will use this success rate for regions I and II. In selecting the precursor times for radon anomalies, we used a method different from the method used by some Chinese seismologists. Usually, the Chinese seismologists consider that radon content can show imminent and short-term anomalies as well as intermediate-term ones (Reports for Chinese Earthquakes). But, we find the period of recorded data are too short to identify the reliable intermediate-term anomalies. We therefore prefer to consider the radon anomaly as a short-term anomaly. Then, the precursor times of radon anomalies for Hiacheng, Tangshan, Longling, and Songpan earthquakes are 60, 60, 75, and

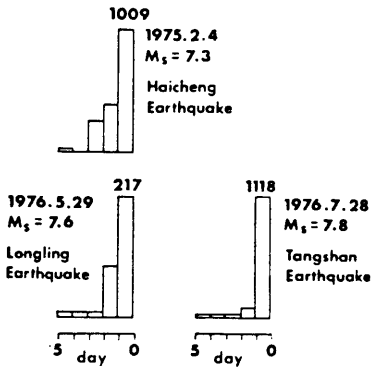

Fig. 5. The number of occurrences of anomalous animal behavior as a function of its appearane time before three large Chinese earthquakes [from *Jiang*, 1980].

45 days [*Seismological Bureau of Liaoning Province*, 1975, vol. 3, p. 85; *Tangshan Earthquake Team*, 1977, pp. 36–37; *Chen and Zao*, 1979, pp. 48–49; *Seismological Bureau of Szechuan Province*, 1979, pp. 31–32]. These are approximate values representing the most reliable observations.

For anomalous animal behavior, we use the same method as for radon anomaly. The number of anomalies in Haicheng area (similarly in Songpan area) is seven in the past ten years, most of them occurred in a time period about six weeks long before the large earthquakes. The success rate is $10/[409 \times (7-1)] \approx 0.004$. The precursor times for anomalous animal behavior have been studied by many people [*Rikitake*, 1976; *Jiang*, 1980]. We simply quote Jiang's results for Haicheng, Tangshan and Longling earthquakes (Figure 5). They are all 5 days. For the Songpan earthquake, the precursor time is 7 days [*Seismological Bureau of Szechuan Province*, 1979, p. 62].

According to formula (9), we divide the success rates of radon anomaly and anomalous animal behavior by their precursor times to obtain P_c, P_D, respectively. With precursors A, B, C, and D, and $\alpha/\beta \approx 1$, formula (8) becomes

$$P = P_0 \frac{P_A}{P_0} \frac{P_B}{P_0} \frac{P_c}{P_0} \frac{P_D}{P_0} \tag{10}$$

By using this formula, we can calculate the total probability gain and final probability for the four large Chinese earthquakes. All the results are listed in Table 1.

These results show that the probability gain may be useful in estimating the hazard rate of earthquake occurrence. The calculated probabilities immediately before these earthquakes are about 0.1 per day. This suggests that Chinese observations of precursory phenomena may have included complete information about an earthquake occurrence. The total probability gain is about 10^4 for all four cases.

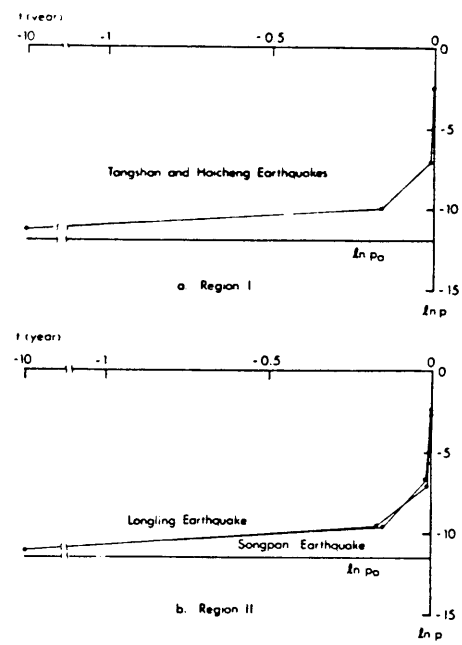

Fig. 6. The conditional probability P of earthquake occurrence as a function of time t before the four Chinese earthquakes.

STEP-BY-STEP APPROACH TO PREDICTION

A step-by-step approach has been used for many years in China, but without a quantitative estimation for the hazard rate of earthquake occurrence. The prediction practice showed that it was successful especially for intermediate-term prediction or even short-term prediction, but sometimes not for imminent prediction. On the other hand, because we didn't have a quantitative estimate at that time, many false alarms were made. Now some may be avoided. For example, in the southern part of region I some false predictions were made just because some macrophenomena appeared. There, some fruit trees which usually bloom once a year flowered a second time and some cracks appeared on the earth's surface. But no other precursory phenomena such as the enhancement of seismicity, radon anomalies, etc., occurred. If one had calculated the probability gain at that time, one would have found that it was very small and did not increase with time because no other precursory phenomena occurred subsequently.

If we plot the natural logarithm of the probability of earthquake occurrence per day against the time t before the earthquake occurrence as shown in Figure 6, the relation between ln P and t is nonlinear. It is interesting to compare

TABLE 1. Total Probability Gain and Final Probability for Four Chinese Earthquakes

Earthquake and Magnitude, M	Average Rate per day, P_0	Periodicity of Seismicity, P_A	Enhancement of Seismicity			Radon Concentration			Anomalous Animal Behavior			Total Probability Gain	Final Probability, per day
			$\hat{P}(M\|B)$	T_B	G_B	$\hat{P}(M\|C)$	T_C	G_C	$\hat{P}(M\|D)$	T_D	G_D		
Haicheng, 7.3	6.7×10^{-6}	1.2×10^{-5}	0.11	3650	4.6	0.006	60	15	0.004	5	119	1.4×10^4	0.09
Tangshan, 7.8	6.7×10^{-6}	1.2×10^{-5}	0.11	3650	4.6	0.006	60	15	0.004	5	119	1.4×10^4	0.09
Longling, 7.6	1.0×10^{-5}	1.5×10^{-5}	0.11	3650	4.6	0.006	75	12	0.004	5	80	6.6×10^3	0.07
Songpan, 7.2	1.0×10^{-5}	1.5×10^{-5}	0.11	3650	4.6	0.006	45	20	0.004	7	57	7.9×10^3	0.08

this relation to *Mogi*'s [1962] empirical relation for rock failure $\mu(t) = \mu_0 \exp(\beta\sigma)$, where $\mu(t)$ is the hazard rate, σ is the applied stress, and we get $\ln \mu(t) = \ln \mu_0 + \beta\sigma$. If Mogi's equation applies to actual earthquake occurrence we find that σ doesn't vary linearly with time, but the nearer to the earthquake occurrence, the more rapidly it increases. On the other hand, at the time when the long-term and intermediate term precursors occur, σ increases slowly. This nonlinear behavior of increase in probability gain has an important practical implication for the earthquake prediction.

The imminent precursors to be used in the last step are very variable and erratic from one earthquake to another so that the imminent prediction remains most difficult.

DISCUSSION

Earthquake prediction, especially the synthetical prediction using all the obtained precursory data and making a decision for prediction, will have to be a trial and error process for a while. Because of the complexity of precursory phenomena, a quantitative estimate of the hazard rate is difficult to obtain. Nevertheless, the concept of probability gain provides a feasible and promising method to synthesize the complex precursory phenomena. In this paper, we use the data from four large Chinese earthquakes to test the effectiveness of this concept in practical use. We have not paid much attention to the identification of precursors and assumed that the observation was complete. Actually, the precursory phenomena are so variable from one earthquake to another and from one region to another that we will always encounter the problem of how to recognize the anomalies. The normal background against which anomalies are recognized may also vary from place to place, making our problem even more difficult. The best known phenomenon is foreshock. We still don't have an unequivocal method for distinguishing foreshocks from swarms, so it is hard to use foreshocks for risk estimate especially for those regions where swarms often occur. Of course, at the last moment when the probability of earthquake occurrence has approached 0.1 per day, the foreshocks can indicate the rough time and location and even magnitude of the coming earthquake. But we cannot wait for them forever because they may never happen as in the case of the Tangshan earthquake. This is why we have not used foreshocks to estimate the probability gain. As a first approximation, we selected only those precursors which appear frequently and are easy to recognize.

In spite of these limitations, we feel that the probability gain assigned to each stage of precursory phenomena of four earthquakes shown in Table 1 adequately express the increase of grade of concern experienced by Chinese scientists for earthquake occurrence at each stage.

Acknowledgments. The authors are grateful to Steve Ellis for helpful discussion. This work was supported by the U.S. Geological Survey under contract 14-08-0001-19150.

REFERENCES

Academia Sinica, Seismological Committee, *Chronological Tables of Earthquake Data of China* (in Chinese), 2 volumes, 1653 pp., Science Press, Peking, China, 1956.

Aki, K., A probabilisitc synthesis of precursory phenomena, in *Earthquake Prediction, An International Review*, edited by D. W. Simpson and P. G. Richards, 680 pp., AGU, Washington, D.C., 1981.

Chen, L. D., and W. C. Zao, *The Nineteen Seventy-Six Longling Earthquake* (in Chinese), Earthquake Press, Peking, China, 1979.

Chu, F. M., Review of prediction, warning and disaster prevention in the Haicheng earthquake (M = 7.3), in *Proceedings of the Lectures by the Seismological Delegation of the People's Republic of China* (in Japanese), pp. 15–26, Seismological Society of Japan, Tokyo, 1976.

Gelfand, I. M., Sh. A. Guberman, V. I. Keilis-Borok, L. Knopoff, F. Press, E. Ya. Ranzman, I. M. Rotwain, and A. M. Sadovsky, Criteria of high seismicity determined by pattern recognition, *Tectonophysics*, *13*, 415–422, 1972.

Gelfand, I. M., et al., Pattern recognition applied to strong earthquakes in California, *Phys. Earth Planet. Inter.*, *2*(3), 227–283, 1976.

Gu, H. D., and T. Q. Cao, Precursory earthquake swarm and the polarization of S-wave, *Acta Seismol. Sinica*, *2*(4), 343–355, 1980.

Jiang, J. C., Animal abnormal behavior in an earthquake short-term precursor (in Chinese), *Acta Seismol. Sinica*, *2*(3), 304–313, 1980.

Kagan, Ya., and L. Knopoff, Statistical search for non-random features of the seismicity of strong earthquakes, *Phys. Earth Planet. Inter.*, *12*, 291–318, 1976.

Kagan, Ya., and L. Knopoff, Earthquake risk prediction as a stochastic process, *Phys. Earth Planet. Inter.*, *14*, 97–108, 1977.

Lee, W. H. K., and D. R. Brillinger, On Chinese earthquake history—An attempt to model an incomplete data set by point process analysis, *Pure Appl. Geophys.*, *117*, 1229–1257, 1979.

Li, S. B., Chinese seismic regionalization and its illustration, *Acta Geophys. Sinica*, *6*(2), 1957.

Ma, Z. J., Step-by-step approach to prediction and the discussion on three theoretical problems (in Chinese), internal report, State Seismological Bureau, Peking, China, 1979.

Mei, S. R., Chinese seismicity, *Acta Geophys. Sinica*, *9*(1), 1960.

Mogi, K., Study of elastic shocks caused by the fracture of heterogeneous material and its relation to earthquake phenomena, *Bull. Earth. Res. Inst. Univ. Tokyo*, *40*, 125–173, 1962.

Rhoades, D. A., and F. F. Evison, Long-term earthquake forecasting based on a single predictor, *Geophys. J. R. Astron. Soc.*, *59*, 43–46, 1979.

Rikitake, T., *Earthquake Prediction*, Elsevier, New York, 1976.

Savarensky, E. F., and S. R. Mei, About the Chinese seismicity, *Acta Geophys. Sinica*, *8*(2), 1959.

Seismological Bureau of Liaoning Province, The Haicheng earthquake, internal report, Shanyang, China, Earthquake Press, Peking, China, 1975.

Seismological Bureau of Szechuan Province, *The Nineteen Seventy-Six Songpan Earthquake* (in Chinese), Earthquake Press, Peking, China, 1979.

State Seismological Bureau, The Hsingtai earthquake (in Chinese), internal report, Peking, China, 1966.

State Seismological Bureau, The Bohai earthquake (in Chinese), internal report, Peking, China, 1969.

State Seismological Bureau, The Donghai earthquake (in Chinese), internal report, Peking, China, 1970.

State Seismological Bureau, The Luhuo earthquake (in Chinese), internal report, Peking, China, 1973.

State Seismological Bureau, The Yongshan-Daguan earthquake (in Chinese), internal report, Peking, China, 1974.

State Seismological Bureau, *The Catalog of Chinese Earthquakes*, Earthquake Press, Peking, China, 1977.

State Seismological Bureau, The annual report of earthquake prediction of 1978 (in Chinese), internal report, Peking, China, 1979.

Tangshan Earthquake Team, The short-team and imminent precursor data of the Tangshan earthquake (in Chinese), Earthquake Press, Peking, China, 1977.

Utsu, T., Calculation of the probability of success of an earthquake prediction (in the case of Izu-Oshima-kinkai earthquake of 1978), report, pp. 164–166, Coord. Comm. for Earthquake Predict., Japan, 1979.

Vere-Jones, D., Earthquake prediction—A statistician's view, *J. Phys. Earth*, *26*, 129–146, 1978.

Wang, B., et al., Pattern recognition of seismic activity before large earthquakes, *Acta Seismol. Sinica*, *4*(2), 105–115, 1982.

(Received September 17, 1981;
revised November 2, 1982;
accepted December 17, 1982.)